SANDIA REPORT
SAND2009-4484
Unlimited Release
July 2009

Spent Fuel Sabotage Test Program, Characterization of Aerosol Dispersal: Technical Review and Analysis Supplement

E.R. Lindgren and S.G. Durbin

Prepared by
Sandia National Laboratories
Albuquerque, New Mexico 87185 and Livermore, California 94550

Sandia is a multiprogram laboratory operated by Sandia Corporation,
a Lockheed Martin Company, for the United States Department of Energy's
National Nuclear Security Administration under Contract DE-AC04-94AL85000.

Approved for public release; further dissemination unlimited.

Issued by Sandia National Laboratories, operated for the United States Department of Energy by Sandia Corporation.

NOTICE: This report was prepared as an account of work sponsored by an agency of the United States Government. Neither the United States Government, nor any agency thereof, nor any of their employees, nor any of their contractors, subcontractors, or their employees, make any warranty, express or implied, or assume any legal liability or responsibility for the accuracy, completeness, or usefulness of any information, apparatus, product, or process disclosed, or represent that its use would not infringe privately owned rights. Reference herein to any specific commercial product, process, or service by trade name, trademark, manufacturer, or otherwise, does not necessarily constitute or imply its endorsement, recommendation, or favoring by the United States Government, any agency thereof, or any of their contractors or subcontractors. The views and opinions expressed herein do not necessarily state or reflect those of the United States Government, any agency thereof, or any of their contractors.

Printed in the United States of America. This report has been reproduced directly from the best available copy.

Available to DOE and DOE contractors from
U.S. Department of Energy
Office of Scientific and Technical Information
P.O. Box 62
Oak Ridge, TN 37831

Telephone: (865) 576-8401
Facsimile: (865) 576-5728
E-Mail: reports@adonis.osti.gov
Online ordering: http://www.osti.gov/bridge

Available to the public from
U.S. Department of Commerce
National Technical Information Service
5285 Port Royal Rd.
Springfield, VA 22161

Telephone: (800) 553-6847
Facsimile: (703) 605-6900
E-Mail: orders@ntis.fedworld.gov
Online order: http://www.ntis.gov/help/ordermethods.asp?loc=7-4-0#online

SAND2009-4484
Unlimited Release
July 2009

Spent Fuel Sabotage Test Program, Characterization of Aerosol Dispersal: Technical Review and Analysis Supplement

E.R. Lindgren and S.G. Durbin
Dept. 6774 – Advanced Nuclear Fuel Cycle Technologies
Sandia National Laboratories
P.O. Box 5800
Albuquerque, New Mexico 87185-MS0747

Abstract

This project seeks to provide vital data required to assess the consequences of a terrorist attack on a spent fuel transportation cask. One such attack scenario involves the use of conical shaped charges (CSC), which are capable of damaging a spent fuel transportation cask. In the event of such an attack, the amount of radioactivity that may be released as respirable aerosols is not known with great certainty. Research to date has focused on measuring the aerosol release from single short surrogate fuel rodlets subjected to attack by a small CSC device in various aerosol chamber designs. The last series of three experiments tested surrogate fuel rodlets made with depleted uranium oxide ceramic pellets in a specially designed double chamber aerosol containment apparatus. This robust testing apparatus was designed to prevent any radioactive release and allow high level radioactive waste disposal of the entire apparatus following testing of actual spent fuel rodlets as proposed.

DOE and Sandia reviews of the project to date identified a number of issues. The purpose of this supplemental report is to address and document the DOE review comments and to resolve the issues identified in the Sandia technical review.

ACKNOWLEDGEMENTS

The authors would like to express their appreciation to Alex Thrower, Lee Finewood, and Jay Thompson of the US Department of Energy for exceptional programmatic and technical guidance. Internal, technical reviews provided by Charles Morrow, Marlin Kipp, and Ron Dykhuizen of Sandia National Laboratories (SNL) are also gratefully recognized. The individual efforts of Mike Gregson and Will Wente of SNL to help transfer prior institutional knowledge are deeply appreciated. Finally, the authors thank Herb Pluemer of PVC Inc. for locating technical drawings of the experimental test chambers.

CONTENTS

FIGURES

TABLES

1 INTRODUCTION

1.1 Background

The overall objective of this project is to provide vital data required to assess the consequences of a terrorist attack on a spent fuel transportation cask. Spent fuel transportation casks are presently in use for over-the-road transport. Conical shaped charges (CSC) are known to be capable of damaging a spent fuel transportation cask. The dose of radioactivity that would be released in case of such an attack is still in question. The amount of radioactivity available for release as respirable aerosols is the focus of this experimental program. These particles have the potential for the greatest human health risk.

Almost all testing to date has been done using fresh surrogate ceramic (*e.g.* CeO_2 or depleted UO_2) as fuel pellets. The release of respirable aerosols from spent fuel may be significantly different from fresh fuel because of the presence of intradispersed decay products and the mechanical degradation of the ceramic fuel pellets. The spent fuel ratio is the ratio of the respriable aerosol released from explosively disrupted spent fuel rods to the respirable aerosols released from surrogate fuel rods. The mass of respirable aerosol is typically normalized by the disrupted rod mass, termed the respirable or release fraction (RF). Whether spent fuel would release more or less respirable aerosols than fresh fuel (*i.e.* whether the spent fuel ratio is greater or less than one) is subject to debate. From the very limited testing done to date, disruption of spent fuel rods would release somewhere between 0.5 to over 5 times the respirable aerosols of surrogate fuel.[1, Section 1.3]

The goal of this project is to measure the spent fuel ratio with greater accuracy and precision. Determination of the spent fuel ratio would allow more meaningful interpretation of larger scale tests previously conducted by others using surrogate fuel. Testing to date under this project includes single surrogate spent fuel rod segments that were disrupted by a small CSC inside of a specially designed reusable aerosol sampling chamber. Most recently, three of six depleted uranium oxide rod segments were tested. In the proposed final phase of this project, actual spent fuel segments would be tested in single use chambers. With the testing of actual spent fuel the spent fuel ratio is expected to be determined with significantly greater accuracy and precision than in the previous experiments.

1.2 Technical Review

The last project report written on this topic was SAND2007-8070, "Spent Fuel Sabotage Test Program, Characterization of Aerosol Dispersal: Interim Final Report" by Dr. Martin A. Molecke *et al.* March 2008.[1] A DOE review of this report identified a number of issues.[2] In summary, the findings were:

1. The statistical analysis of the existing respirable fraction data set is limited.
2. Known aerosol losses are not taken into account in the data analysis.
3. There is not a complete technical basis presented for evaluating the merits of the proposed Phase-4 experiments.

In order to address these issues, a detailed technical review of the project was undertaken by Sandia. The focus of the review was specifically on the apparatus and respirable aerosol

measurements and calculations required to determine the spent fuel ratio. The technical review identified the following additional issues in the project reports.

1. The dimensional description of the aerosol test chambers is incomplete especially for the more recent double chamber designs. The aerosol chamber volume used to calculate the RF was 40% larger than actual.
2. The data analysis methodology used inherently makes two erroneous assumptions. First, there is an inherent assumption that the sample gas temperature is the same as the aerosol chamber temperature at the time of sampling. The average aerosol chamber temperature was approximately double the sample gas temperature. Second, the previous analysis assumes that all of the aerosols initially generated remain in the aerosol chamber throughout sampling. Since this is a double chamber apparatus, a significant amount of gas can and does flow from the upper chamber into the lower chamber during the sampling interval.
3. There is no discussion of experimental errors or the effects of experimental error on the RF results.

The purpose of this supplemental report is to address and document the DOE review comments and correct the issues identified in the Sandia technical review. Familiarity by the reader with the last project report is assumed.[1] A new conceptual model for the double chamber experiment was developed that allows for a more accurate determination of RF. The new analytic model is inherently independent of both the aerosol chamber temperature and particle-laden gas flow from the upper chamber into the lower chamber during the sampling activity.

1.3 Testing Apparatuses

A brief overview of the hardware used to collect aerosol data for release fraction calculations is presented in this section. This review is intended only to re-familiarize the reader with these apparatuses. Details of these devices are referenced in the last project report.[1]

The resulting data from three distinct vessels are presented in this report. These aerosol chamber designs are shown in Figure 1.1. The “Tweety Bird” and “Grandma” designs are double-chamber, closed vessels. The “Tweety Bird” design was used exclusively in the Phase 3, depleted uranium tests and also in Phase 2 Tests 2-9A and 2-9B. The “Grandma” vessel was used in Phase 2 Tests 2-5E, 2-5G, 2-6A, 2-6B, 2-8C, and 2-8D. The third vessel pictured in the figure shows the single, open-chamber design used in Tests 2-10B, 2-10C, and 2-10D.

Four parallel, aerosol-sampling devices are evident at the top of each vessel design in Figure 1.1. The data reexamined in this report was taken using Marple 298 impactors. These devices are designed to collect aerosols ranging in aerodynamic equivalent diameters of 0.4 to 21 μm. The Marple impactor consists of eight aluminum stages with substrate collection filters. Figure 1.2 shows pictures of the assembled and disassembled Marple impactor and a typical collection filter.

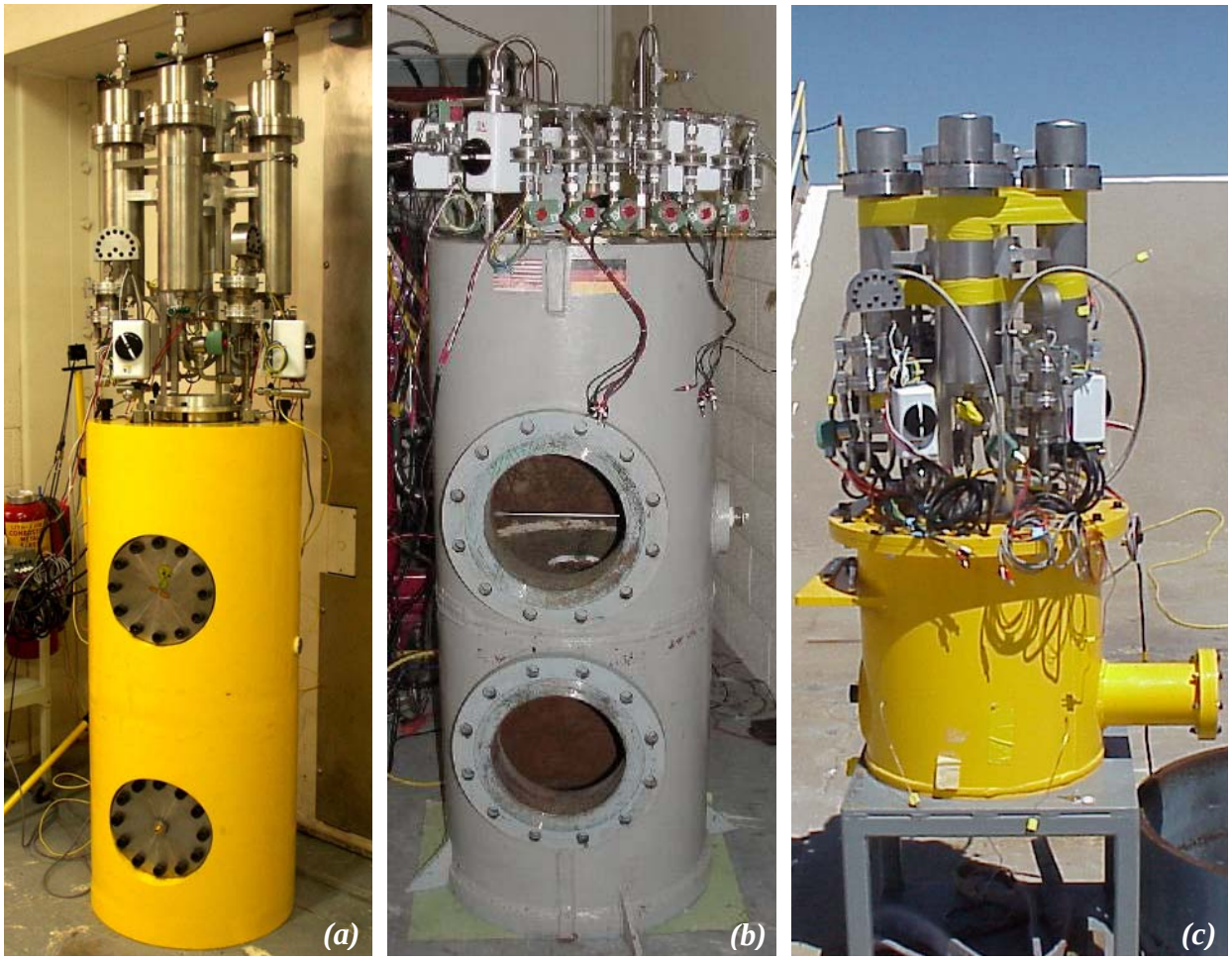

Figure 1.1 Three chamber designs were used in the collection of respirable fraction data – *a*) "Tweety Bird", *b*) "Grandma", and *c*) the single, open-chamber design.

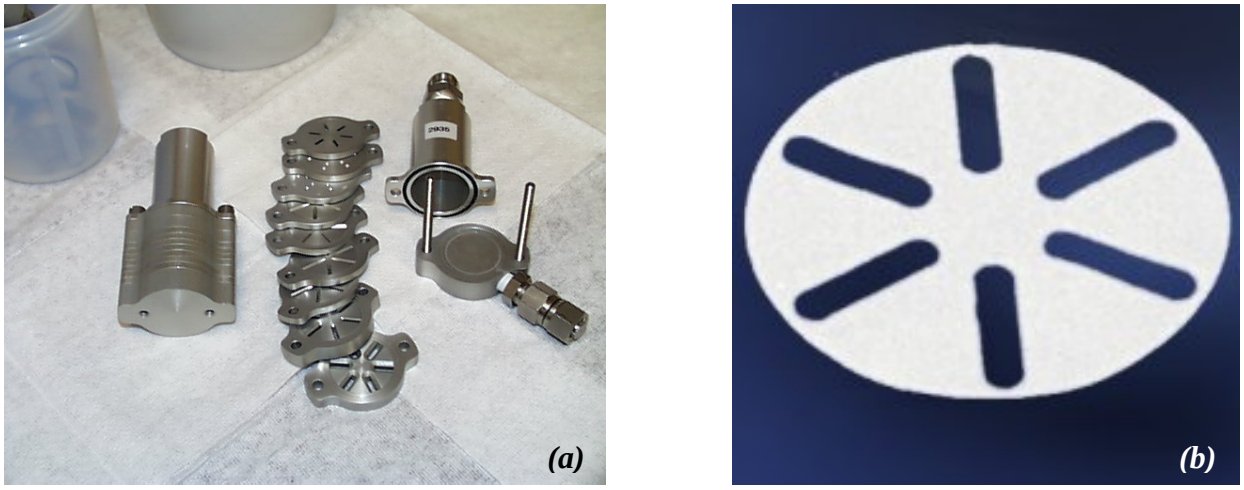

Figure 1.2 Pictures of *a*) the Marple 298 impactor and *b*) a typical stage collection filter.

This page intentionally blank

2 ANALYTIC METHODOLOGY

2.1 Molar Basis

2.1.1 Conceptualization of Experiment

The previous conceptual model inherently assumed all of the aerosols were generated and contained in a single chamber without the possibility of loss. Essentially, the method calculated the aerosols contained in the aerosol chamber at the time of sampling, which required knowledge of the chamber gas temperature. However, the aerosol chamber temperature was not measured. Furthermore, with the double chamber apparatus a significant amount of aerosol-laden gas flows from the upper aerosol chamber into the lower chamber before and during the sample collection period. The movement of these aerosols was not accounted for in the previous methodology. A more intricate conceptual model has been developed that overcomes the limitation of the previous approach in that the aerosol chamber temperature is not required, and the method does not require the assumption that the aerosols are all contained in a single chamber with no possibility of outflow. The elimination of these conditions is made possible by instead determining the initial moles of gas into which the generated aerosols are mixed.

Figure 2.1 illustrates the new conceptualization of the experiment progression that guides the determination of the initial moles of gas present in the upper aerosol chamber at the time of aerosol generation and mixing. This parameter is vital for determining the release fraction using the double chamber experimental apparatus. Once the initial moles are determined assuming a well-mixed gas, the aerosol concentration is fixed and the outflow of aerosol-laden gas will not cause a change. Knowledge of the chamber gas temperature during sampling is not required.

Initially as shown in Figure 2.1a, the gas in the upper and lower chambers is at the same temperature and pressure. The moles of gas in each chamber are easily calculated with the ideal gas law. When the conical shaped charge (CSC) is detonated in the lower chamber, energy and gas are released in the amounts of E_{csc} and n_{csc} respectively as illustrated in Figure 2.1b. The chemical reaction is represented by:

$$C_{1.42}H_{2.66}N_{2.57}O_{2.57}F_{0.1} \Rightarrow 1.33H_2O(g) + 1.285N_2(g) + 0.62CO_2(g) + 0.8C(s) + 0.05F_2(g) \quad 2.1$$

Part of the energy released is focused into a projectile with energy E_{ke}, which is injected into the upper chamber and shatters the target fuel rod. This action generates the aerosols in the upper chamber. Part of the kinetic energy will heat the gas in the upper chamber and part will be lost to the chamber wall (E_{loss}). The remainder of the energy release is assumed to heat the gas in the lower chamber. The unequal heating in the two chambers and the presence of explosive product gases results in a significantly higher pressure in the lower chamber relative to the pressure in the upper chamber. The time scale for this step is on the order of 100 μs.

The pressure differential developed across the 25.4 mm (1 in.) diameter hole between the chambers is sufficient for a sonic flow jet to develop. The resulting violent flow of gas will mix the aerosols and gas in the upper chamber. The flow continues until the pressures are equilibrated as depicted in Figure 2.1c. The pressure equilibration is treated as an isentropic expansion where energy is carried from the gas in the bottom chamber, and the same amount of energy is added to the gas in the upper chamber. All the gas flowing into the upper chamber is

assumed to enter at the average temperature of the gas in the lower chamber after correction for the isentropic expansion. After the pressure equilibration is complete, the pressure in both chambers is equal at a value greater than the initial post-detonation pressure of the upper chamber and less than the initial post detonation pressure of the lower chamber. The temperature of the gas in the lower chamber is cooled by the isentropic expansion. The gas temperature of the upper chamber equilibrates to a temperature less than the gas temperature in the lower chamber and greater than the initial post detonation gas temperature in the upper chamber. In the short time period over which these events occur, heat transfer to the walls is neglected. The moles of gas contained in the upper chamber after pressure equalization are assumed to homogeneously contain all of the aerosols generated in the disruption of the fuel rod. The time scale for this step is on the order of 10 ms.

The time scale for the final step is on the order of seconds so the system is no longer considered adiabatic. Since the lower chamber was heated to ~500K higher temperature than the upper chamber, the lower chamber will cool faster than the upper chamber. This results in a flow reversal in order to maintain pressure equilibrium as depicted in Figure 2.1d. Because the gas and aerosols in the upper chamber are well mixed, the flow of aerosol-laden gas from the upper chamber into the bottom chamber does not change the molar-based concentration of aerosols in the upper chamber. The aerosol sample is collected at this time. The moles of gas removed during sampling are an order of magnitude less than the moles of gas flowing from the upper chamber into the lower chamber. This means that sampling will not change the direction of flow between the chambers, which would dilute the sample.

Because the new method determines the initial moles of well mixed, aerosol-laden gas, the method is not affected by the out flow of aerosol-laden gas before and during gas sampling. The method also does not require measurement of the aerosol chamber temperature. The new method determines the initial moles of aerosol-laden gas by utilizing information about the energy and gaseous release of the explosive device used. Utilization of this new information introduces new errors but allows the elimination of larger errors in the original analysis. The experimental error of following the new method for recalculating the RF is the subject of Chapter 3. In Chapter 4, experimental improvements are discussed. This discussion includes an approach to measure the moles of initial aerosol-laden gas directly.

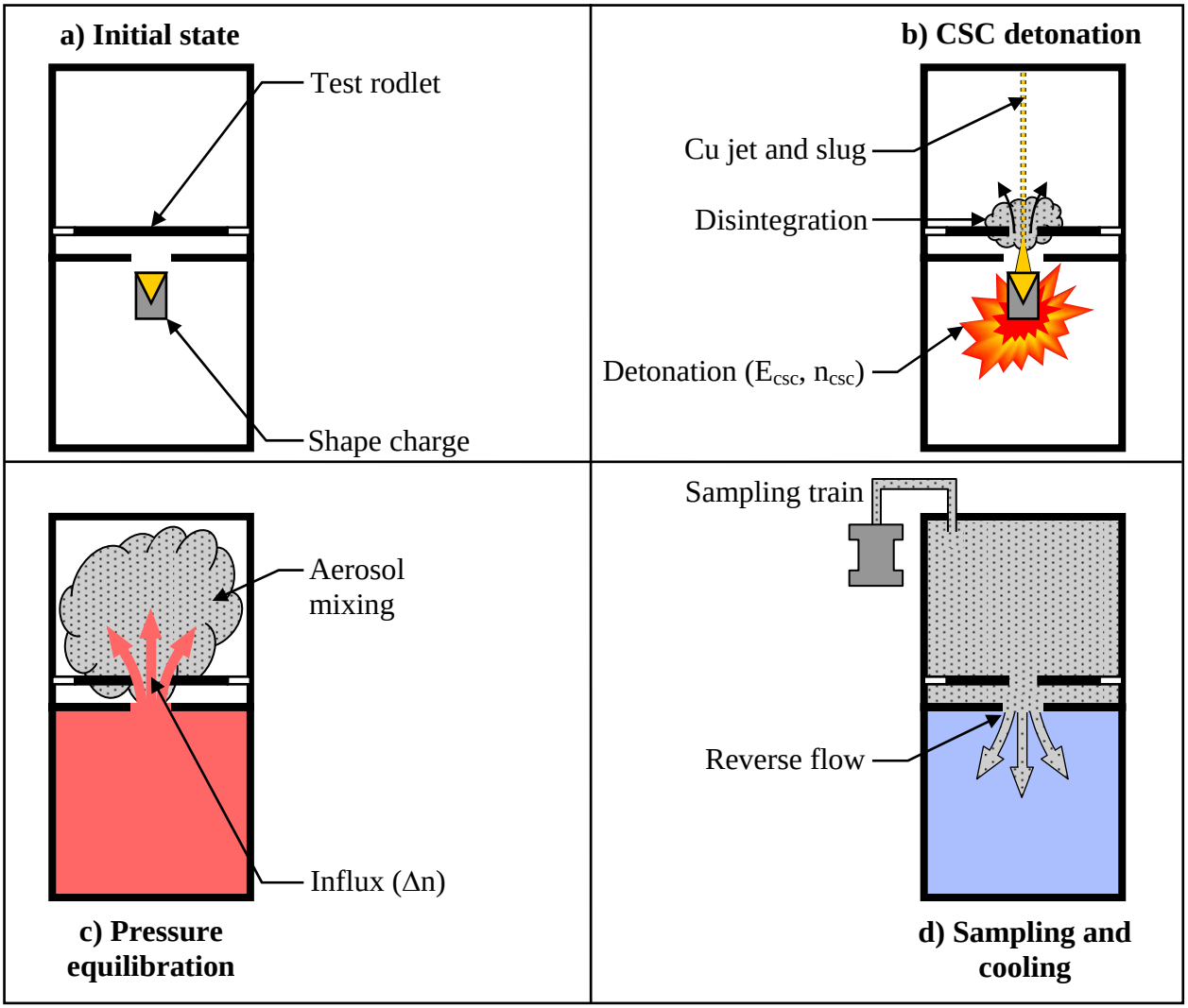

Figure 2.1 Sequencing of events in the release fraction measurement experiments.

2.1.2 Governing Equations

The equations for calculating the release fraction following the new conceptual model are summarized below. The details of the equation derivation and parameter definitions are given in Appendix A.

$$\mathrm{RF} = \frac{n_{chamber} R T_{avg}}{m_{tot} Q t_{sample} P_{avg}} \sum_i \frac{m_{stage,\,i}}{\eta_{stage,\,i} \eta_{loss,\,i}} = \frac{n_{chamber}}{n_{sample}} \frac{\sum_i \frac{m_{stage,\,i}}{\eta_{stage,\,i} \eta_{loss,\,i}}}{m_{tot}} \qquad 2.2$$

The moles of gas sampled from the upper chamber are expressed in Equation 2.3.

$$n_{sample} = \frac{R T_{avg}}{Q t_{sample} P_{avg}} \qquad 2.3$$

The moles of gas in the upper chamber during aerosol generation and mixing are defined as:

$$n_{chamber} = n_1 + \Delta n - n_{\text{condense}} \tag{2.4}$$

The initial moles of gas in the upper chamber, *i.e.* before detonation, are given as n_1.

$$n_1 = \frac{P_i V_1}{\mathrm{R} T_i} \tag{2.5}$$

The number of moles entering the upper chamber from the lower due to the detonation of the explosive is given as Δn.

$$\Delta n = \frac{V_1\left[\frac{(E_{\text{csc}} - E_{ke} - E_{PV})}{c_v} + T_i \cdot n_{\text{csc}}\right] - V_2 \frac{\left(E_{ke} - E_{loss} + E_{PV}\right)}{c_v}}{\left[\frac{(E_{\text{csc}} - E_{ke} - E_{PV})/c_v}{\left(\frac{P_i V_2}{R T_i}\right) + n_{\text{csc}}} + T_i\right]\left(V_2 + V_1\right)} \tag{2.6}$$

Finally, the dew point of the sample gas is estimated to be 319 K based on the stoichiometry of the reaction and the moles of gas exchanged between the chambers. Since the gas sample temperature was measured to be about 300 K, a significant amount of water vapor can be expected to condense out of the sample stream. A correction must be made for the change in moles of gas resulting from this condensation.

The number of moles of water condensing in the upper chamber is given in Equation 2.7.

$$n_{\text{condense}} = \Delta n \frac{n_{H2O}}{n_2 + n_{\text{csc}}} - \left(n_1 + \Delta n\right)\frac{P_{sat}}{P_{avg}} \tag{2.7}$$

2.2 Example Calculations

2.2.1 Molar Model

With the new approach the release fraction is given by Equation 2.8 (reiteration of Equation 2.2).

$$\mathrm{RF} = \frac{n_{chamber} \mathrm{R}\, T_{avg}}{m_{tot} Q\, t_{sample} P_{avg}} \sum_i \frac{m_{stage,\,i}}{\eta_{stage,\,i}\eta_{loss,\,i}} = \frac{n_{chamber}}{n_{sample}} \frac{\sum_i \frac{m_{stage,\,i}}{\eta_{stage,\,i}\eta_{loss,\,i}}}{m_{tot}} \tag{2.8}$$

For example the calculation of the DU release fraction for test 3/2A and Marple 1

$n_{chamber}$ = 5.063 moles (for aerosol chamber volume of 99.1 liters) initial moles of aerosol-laden gas in upper aerosol chamber

P_{avg} =1.93×10^5 Pa average sample pressure

T_{avg} = 299.8 K average sample temperature

Q = 1.920 lpm = 0.0320 lps sample flow rate

t_{sample} = 8.99 sec sample collection time

m_{total} = 26.36 g of DU total mass of fuel rod component (*e.g.* U, Zr, Cs or Ru) disrupted by the CSC projectile

R = 8.314 J/(mol·K) universal gas constant

$\sum_i m_{stage,\,i}$ = 1.0276×10^{-3} g of DU mass of aerosol component collected

$\eta_{stage,\,avg}$ = 0.955 impactor collection efficiency

$\eta_{loss,\,i}$ = 0.7 sample train transport efficiency

RF = 0.0133

2.2.2 Volumetric Model

2.2.2.1 Previous Analytic Approach

The previous analysis took an approach appropriate for sampling aerosols at ambient conditions where the aerosol chamber and the sampling device are at the same temperature and pressure (like sampling diesel soot in a train station). These conditions are typical of many sampling situations in aerosol science. This approach is not applicable for the more complicated situation where the aerosols to be measured are located in a gas with a temperature significantly higher than the gas metered through the aerosol impactor. The calculation below is presented as it was performed to produce the results given in the previous project reports. The same values are used even though they are now known to be erroneous in order to duplicate the previous result.

For the same example of test 3/2A and Marple 1

$$\mathrm{RF}_{\mathrm{previous}} = \frac{V_1}{m_{tot} Q t_{sample}} \sum_i m_{stage,\,i} = \frac{V_1}{V_{sample}} \frac{\sum_i m_{stage,\,i}}{m_{tot}} \qquad 2.9$$

V_1 = 139 liters

Q = 1.909 lpm = 0.03182 lps

t_{sample} = 10 sec

m_{tot} = 26,360 mg

$\sum_i m_{stage,\,i}$ = 1.03 mg

$\mathrm{RF}_{\mathrm{previous}}$ = 0.0171

In Appendix A, the calculation is repeated with the errors corrected using the best available information and estimates. If known errors in chamber volume, sample volume and sample time are corrected, the corrected RF for the previous methodology is 25% lower than the RF calculated by the new methodology. This is due to the flow of aerosol-laden gas from the upper chamber into the lower chamber prior to and during aerosol sampling.

3 RESULTS

More extensive statistical evaluations of the molar-based and previously determined results were undertaken to assist in the appropriate interpretation of release fractions. The statistical methods and definitions used in this chapter were taken from a standard engineering statistics text.[3] The error propagation analyses (EPA) were derived using widely accepted methods and definitions from an engineering handbook.[4] Two types of confidence intervals are presented, one derived from statistical population bounds (*i.e.* product of *t*-statistic and standard deviation) and the other based on the experimental uncertainty limits predicted from EPA. All confidence intervals (CI) cited in this chapter refer to 95% levels unless otherwise noted. As will be demonstrated in this chapter, these confidence intervals are significantly large in comparison to the experimental measurements they describe and raise questions concerning the validity of any conclusions drawn from the release fraction data sets.

3.1 Phase 3

Phase 3 testing used depleted uranium oxide pellets inside Zircaloy tubing as a surrogate for spent nuclear fuel. The 3-1C test also included dopants of cesium and ruthenium to simulate decay products. All tests were conducted in the "Tweety Bird" closed, double-chamber vessel. These tests represent an important milestone in the determination of the spent fuel ratio (SFR). This section examines the Phase 3 results using standard statistical treatments and error propagation methods to assist in interpreting the release fraction data.

3.1.1 Depleted Uranium

3.1.1.1 Statistical Treatment of Test Samples

An analysis of variance (ANOVA) was conducted for the depleted uranium release fraction (RF) results determined by the molar methodology for tests 3-2A, 3-5B, and 3-1C. This analysis examines the null hypothesis that the means of each test are equal. The sample populations within each test are assumed to be independent representations of an overall population and normally distributed. If the null hypothesis of the ANOVA is accepted, the test samples are assumed to be from the same overall population and will be analyzed together.

Explicitly, the ANOVA tests the following null hypothesis (H_o) and offers an alternate hypothesis (H_a).

H_o: $\mu_{3\text{-}2A} = \mu_{3\text{-}5B} = \mu_{3\text{-}1C}$

H_a: At least two of the means are not equal.

The ANOVA P-value was determined using MINITAB® 15.1.30.0. The null hypothesis is accepted with a P-value of 0.999. For the purposes of this report, P-values greater than 0.1 will be used to accept the null hypothesis. Values of 0.01 to 0.1 are considered inconclusive, and values less than 0.01 reject the null hypothesis. The ANOVA also indicates that the variance within each test is significantly large enough to preclude the determination of variation introduced between tests. Therefore, the RF values from the three tests are treated as samples from a single population for the remainder of this report.

Next, the samples were examined to determine if the data follow a normal or lognormal distribution. Figure 3.1 shows the normal probability plots for the depleted uranium (DU) RF results with 95% confidence intervals around the fit. Similarly, Figure 3.2 gives the lognormal probability plot of the same RF data and 95% confidence intervals. Both of these probability tests indicate that either distribution could represent the data with P-values of 0.621 and 0.360 for normal and lognormal, respectively. For ease of analysis, the data will be assumed to follow a normal distribution. Therefore, the appropriate *t*-distribution statistics will be applied to determine the 95% confidence interval on the overall population.

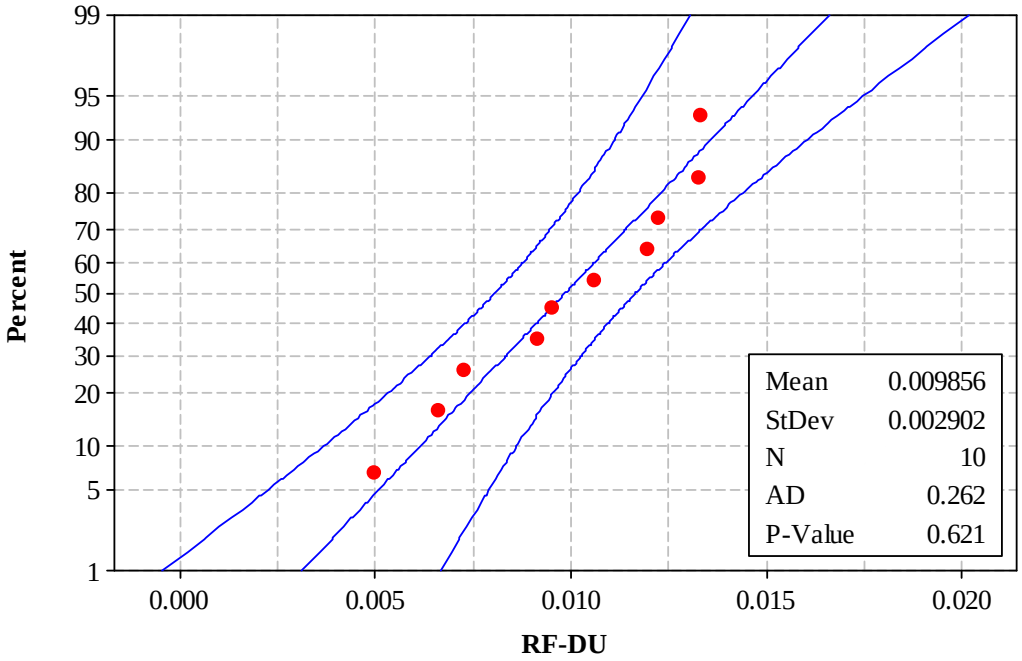

Figure 3.1 Normal probability plot of the depleted uranium RF values for the Phase 3 tests.

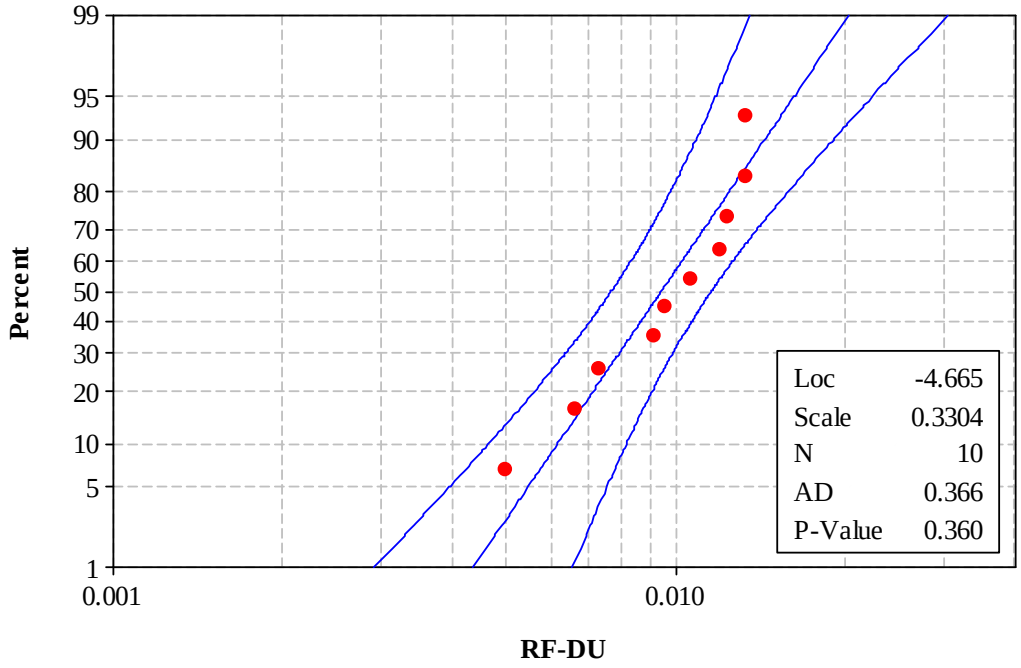

Figure 3.2 Lognormal probability plot of the depleted uranium RF values for the Phase 3 tests.

Table 3.1 gives the statistical values of all of the Phase 3 tests and an "Overall" entry. The overall values assume that the ANOVA is adequate to group all the Marple samples into one population for analysis. The average of the three tests are within 1.2E-4 of each other, but the standard deviations vary up to 7.5E-4 between tests. The 95% statistical bounds of the individual test populations predicted by the product of the appropriate *t*-statistic and the standard deviation indicate that the RF varied between negative values (nonphysical) and over twice the reported value. However, combining the samples together as justified in the ANOVA gives a 95% CI of 6.56E-3. Assuming that twelve additional samples may be obtained through additional testing and that the standard deviation does not change appreciably, the overall confidence interval would decrease by a factor of 0.92 due to the decreased value of the *t*-statistic ($t_{0.025,\ 9}$ = 2.262 *vs.* $t_{0.025,\ 21}$ = 2.080). The standard deviation would also likely change due to an increase in the number of samples but cannot be estimated in the absence of the new data.

Table 3.1 Statistical values of depleted uranium for tests 3-2A, 3-5B, and 3-1C.

Test	Average	Std Dev.	95% CI	Avg + 95% CI	Avg - 95% CI
3-2A	9.87E-03	3.08E-03	1.33E-02	2.31E-02	-3.40E-03
3-5B	9.90E-03	3.65E-03	1.16E-02	2.15E-02	-1.72E-03
3-1C	9.78E-03	2.90E-03	1.25E-02	2.22E-02	-2.68E-03
Overall	9.86E-03	2.90E-03	6.56E-03	1.64E-02	3.29E-03

3.1.1.2 Consideration of Experimental Error

An error propagation analysis (EPA) was performed to determine the uncertainty in the experimentally determined RFs based on widely accepted practices.[4] These error analyses

consider the errors, or uncertainties, in the underlying measurements used to determine the release fraction. The equation for the RF by the molar methodology is repeated in Equation 3.1.

$$\mathrm{RF} = \frac{\left(n_1 + \Delta n - n_{cond}\right)\mathrm{R}T_{avg}}{m_{tot} Q\, t_{sample} P_{avg}} \sum_i \frac{m_{stage,\,i}}{\eta_{stage,\,i}\eta_{loss,\,i}} \qquad 3.1$$

Table 3.2 gives an example of the error analysis results for Marple 1 of Test 3-2A. The standard uncertainty for each measurement is analogous to the standard deviation of a population and describes the bounds to which the measurement is known. These measurements and their associated uncertainties are assumed to behave normally. Therefore, the 95% expanded uncertainty, U_{RF}, of each measurement is twice the standard uncertainty. The factor of two on the standard uncertainty is rounded up from 1.96 for the purposes of this report. The overall influence coefficient, or the normalized uncertainty of RF, is determined by taking the square root of the sum of squares of the individual influence coefficients. The uncertainty of RF is then the product of the overall influence coefficient and the RF. The contribution column quantifies how much each measurement influences the overall uncertainty in RF. The single less than sign indicates that the contribution is between 0.01 and 0.001. The double less than sign, *i.e.* much less than, denotes that the contribution is less than 0.001.

The overall experimental uncertainty in the depleted uranium release fraction was dominated by the uncertainty in just a few key parameters that require additional discussion. The top two contributors are the sample line efficiency, η_{loss} with an overall average contribution of 56% and the average sample pressure, P_{avg} with an overall average contribution of 38%. Other parameters that contributed significantly to the uncertainty are the sampling time, t_{sample}, with a 2% contribution, the flow of gas from the lower chamber into the upper chamber, Δn, with 1%, the sample flow rate, Q, with 1%, and the total mass of fuel rod disrupted by the CSC projectile, m_{tot}, with 1%. Together, the uncertainty in these parameters represents 99% of the average uncertainty in the DU RF determination.

Table 3.2 Error propagation analysis for depleted uranium in Marple 1 impactor for test 3-2A.

Measurement, x_i	Units	Value	Standard uncertainty, u_i	Influence coefficient ($u_i \cdot [(\partial RF/\partial x_i)/RF]$)	Contribution
n_1	mol	3.38	0.09	0.018	< 0.01
Δn	mol	1.92	0.10	0.020	< 0.01
$n_{condense}$	mol	0.23	0.02	0.005	<< 0.01
T_{avg}	K	299.8	2	0.007	< 0.01
m_{tot}	g	26.36	0.5	0.019	< 0.01
Q	m^3/s	3.2E-05	1.6E-07	0.005	<< 0.01
t_{sample}	s	9.0	0.25	0.028	0.02
P_{avg}	Pa	193000	24000	0.124	0.39
$m_{stage,4}$	g	8.16E-05	1.0E-06	0.001	<< 0.01
$\eta_{stage,4}$	--	0.93	0.005	0.000	<< 0.01
$\eta_{loss,4}$	--	0.7	0.15	0.017	< 0.01
$m_{stage,5}$	g	6.81E-04	1.0E-06	0.001	<< 0.01
$\eta_{stage,5}$	--	0.95	0.005	0.004	<< 0.01
$\eta_{loss,5}$	--	0.7	0.15	0.143	0.52
$m_{stage,6}$	g	1.78E-04	1.0E-06	0.001	<< 0.01
$\eta_{stage,6}$	--	0.97	0.005	0.001	<< 0.01
$\eta_{loss,6}$	--	0.7	0.15	0.037	0.03
$m_{stage,7}$	g	3.60E-05	1.0E-06	0.001	<< 0.01
$\eta_{stage,7}$	--	0.98	0.005	0.000	<< 0.01
$\eta_{loss,7}$	--	0.7	0.15	0.007	< 0.01
$m_{stage,8}$	g	4.48E-05	1.0E-06	0.001	<< 0.01
$\eta_{stage,8}$	--	0.99	0.005	0.000	<< 0.01
$\eta_{loss,8}$	--	0.7	0.15	0.009	< 0.01
$m_{stage,9}$	g	6.27E-06	1.0E-06	0.001	<< 0.01
$\eta_{stage,9}$	--	1	0.005	0.000	<< 0.01
$\eta_{loss,9}$	--	0.7	0.15	0.001	<< 0.01
RF	--	0.0133	0.003	0.198	1.00

Uncertainty in the sample pressure measurements contributed significantly to overall uncertainty in RF. In all three of the Phase 3 experiments, four independent Marple sampling systems were used to collect aerosol samples. These systems represented four parallel and hydraulically balanced sample paths from the chamber. Figure 3.3 shows a diagram of one such sampling system setup. The major system components following the sample flow from the chamber are the initial ball valve, the sample gas temperature and pressure measurement, the large particle separator (LPS), the Marple impactor, a HEPA filter, the critical flow orifice and finally another valve that isolates the system from the vacuum source. Each of these Marple sampling systems includes an absolute pressure measurement for independently monitoring the same chamber pressure. Figure 3.4 shows the pressure history measured by the sampling systems in Test 3-5B. Note that all four measured the same initial ambient pressure. Marple 1 and Marple 4 tracked closely, which is the expected behavior. However, Marple 2 and Marple 3 are significantly different. The manufacturer stated error of the instrument is 0.2% of full scale 1.38×10^6 Pa (200

psia), which is a standard uncertainty of 1400 Pa (0.20 psia). For each pressure measurement, the pressure history like those shown in Figure 3.4 were graphically integrated to determine the average sample pressure for the measurement.

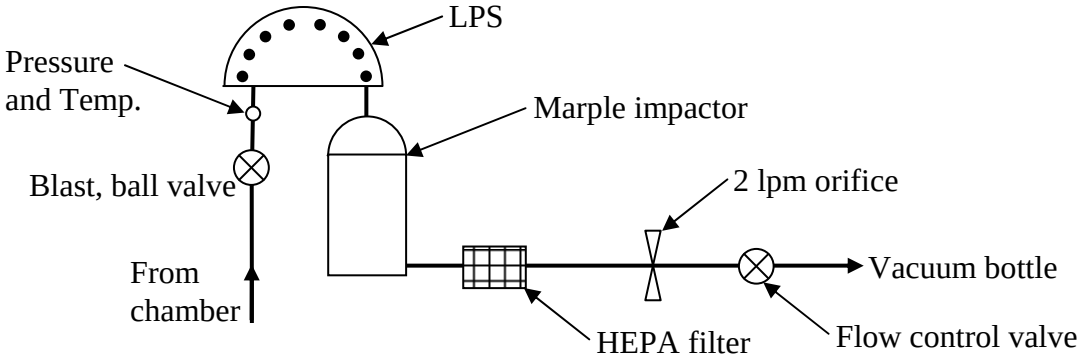

Figure 3.3 Diagram of one aerosol sampling system.

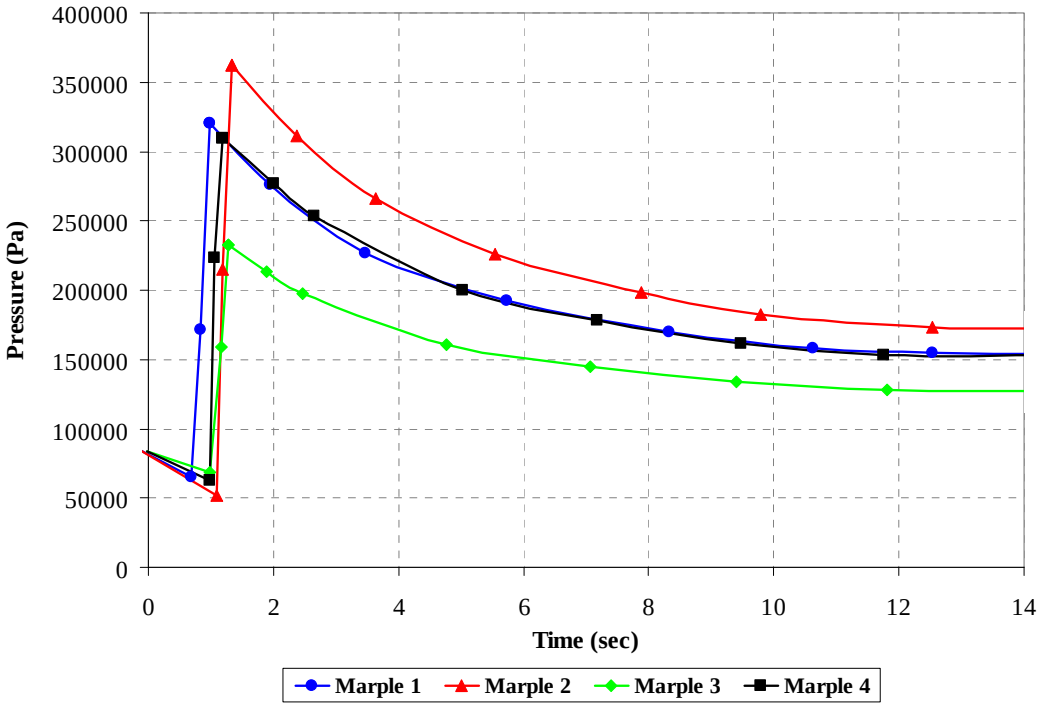

Figure 3.4 Sample line pressures as a function of time for test 3-5B.

The resulting average pressures are shown in Table 3.3 for all Phase 3 testing. There is considerable variability in the four independent measurements for each test. No plausible experimental explanation for different pressures in the sample systems was documented. Therefore, the overall average sample pressure was used to calculate the RF in each sample system, and the standard deviation of the four measurements was used as the standard

uncertainty. Note that the standard uncertainty used was 7 to 23 times greater than the standard uncertainty based on the manufacturer specifications.

Table 3.3 Sample and average pressure measurements for tests 3-2A, 3-5B, and 3-1C.

Test	Marple 1	Marple 2	Marple 3	Marple 4	$P_{test,\,avg}$ (Pa)	u_{Pavg} (Pa)
3-2A	202000	158000	203000	209000	193000	24000
3-5B	210000	240000	163000	208000	205000	32000
3-1C	170000	191000	180000	189000	182000	10000

Uncertainty in sampling time is also significant, contributing 2% to the overall uncertainty. The sampling time was controlled by the two valves shown in Figure 3.3. The first valve encountered was a slow acting electrically actuated ball valve. The second valve is a fast acting electric solenoid valve located between the critical flow orifice and the vacuum source. Both valves need to be open to initiate a steady state sample flow. The relatively large uncertainty in the sample collection time was due to the use of the first valve because it took almost three seconds to fully open and 1 to 1.5 seconds to allow any flow. At time zero both valves are actuated. The second valve opens almost instantly exposing the critical flow orifice and sample system to the vacuum source. The first valve takes one second to allow any flow. Note that in the first second after the valves are actuated the pressure in the sample system drops (see Figure 3.4) from 84,000 to as low as 62,000 Pa (12.2 to 9 psia). Nominally one second after valve activation the first valve finally opens enough to allow flow and the sample system is pressurized to the pressure of the aerosol chamber. Note that there is also considerable variation in the time of flow initiation. About nine seconds later the valves are activated to close. The second valve closes almost instantly stopping flow through the sample system. The first valve takes a second or more to close enough to isolate the sample system and hold the pressure at a constant value. The sampling time for this run was actually 9 seconds, not 10 seconds as assumed by the previous researchers.

The uncertainty in the loss coefficient, η_{loss}, contributes the greatest to the determination of the uncertainty of RF and on average represents 56% of the overall uncertainty. The parameter η_{loss} represents the efficiency with which the aerosols are transported from the aerosol chamber to the Marple impactor (see Figure 3.3). Aerosol losses in the sample line result in a lower η_{loss}. The previous investigators indicated that the mass of aerosols lost in the sample line between the initial ball valve at the top of the aerosol chamber and the LPS was on the order of the mass of aerosols collected in the LPS and Marple impactor combined, which could lead to a doubling of the reported RFs.[5, Section 6.5] Chemical analysis concluded much of the material from the sample line was more likely the larger particles than the smaller particles.[1, Section 3.2] The large aerosol loss in the sample lines was likely due to moisture condensation in the sample lines, a problem acknowledged by the previous investigators but not corrected experimentally (see Section 4.2.1 for discussion on experimental improvements).[1, Section 3.2] The uncertainty of respirable aerosol losses in the sample line to the impactor is large because the magnitude of the loss was not characterized experimentally and therefore can only be based on anecdotal evidence. Assigning a value with uncertainty to this parameter for respirable size aerosols is problematic. The following approach has been taken. The assumption is made that as the aerosol losses increase (*i.e.* loss coefficient decreases), the uncertainty bounds increase up to the physical limit of η_{loss} =

1 (*i.e.* nonphysical loss efficiencies of greater than one are not considered). The resulting relationship between the normalized release fraction uncertainty and assumed η_{loss} is shown in Figure 3.5. Further assuming that all other experimental errors are adequately represented, η_{loss} was reduced, and $u_{\eta loss}$ consequently increased, until experimental error covered the majority of the statistical variation of the data in each of the three test series. The resulting value for η_{loss} is 0.7 ± 0.3 (highlighted blue error bar) and yields a corresponding normalized, expanded RF uncertainty of 0.38, which seems reasonable from the available experimental information.

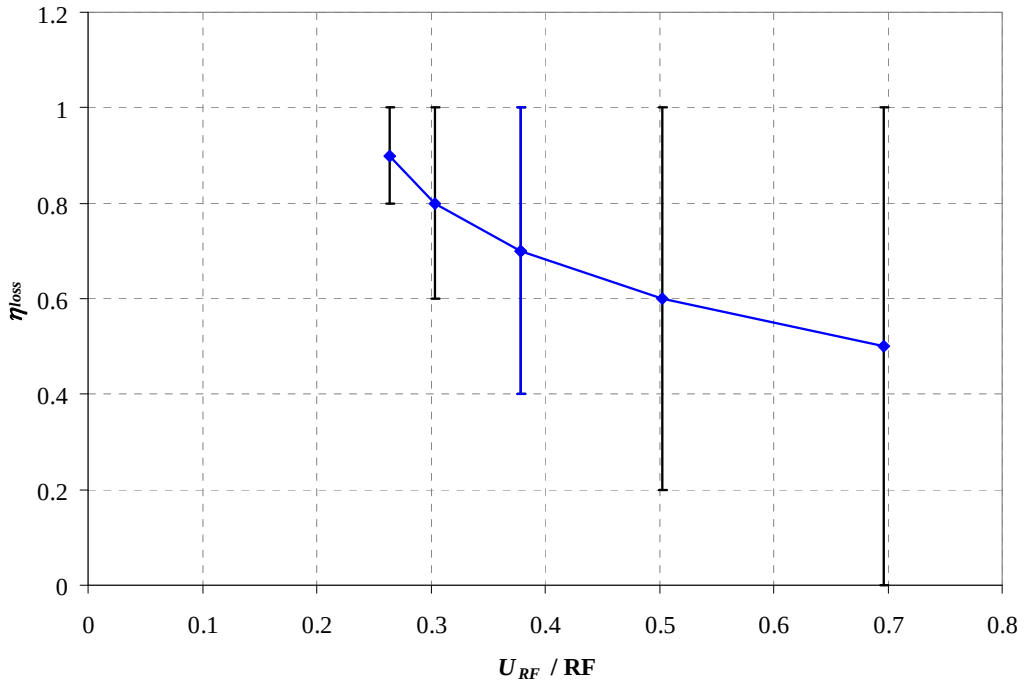

Figure 3.5 Sample line efficiency as a function of the normalized uncertainty in RF.

Figure 3.6 shows the release fraction of depleted uranium from molar (blue diamonds) and volumetric determination (red squares)[1, Table 4.1.1] for tests 3-2A, 3-5B, and 3-1C. Marple impactors 1 through 4 are arranged left to right by test in the plot. The error bars represent the 95% expanded uncertainty based on the experimental error for each impactor and test. The solid lines represent the average value of all RFs for molar (blue) and volumetric determination (red). The dashed lines show the 95% bounds of the sample population based on a *t*-statistic of 2.262 ($t_{0.025, 9}$) for molar (blue) and volumetric determination (red). As discussed previously, the value for η_{loss} was adjusted until the experimental uncertainty was nearly sufficient to explain the large variation in RF within a given test. The exception is between Marple 1 and Marple 4 in test 3-5B. Although not eliminated from the data set, Marple 1 of test 3-5B is a suspected outlier. Tests for outliers in the data set including leverages, Cook's distance, and DFITS did not exclude any samples. The experimental uncertainty was still not sufficient to explain the large variation in RF across test series. Since variability within a test is assumed to be minimized, this lack of accommodation of the data indicates that 1) the experimental uncertainty is underestimated by neglect of an unknown parameter or underestimation of existing parameters and/or 2) the data contain undocumented outliers.

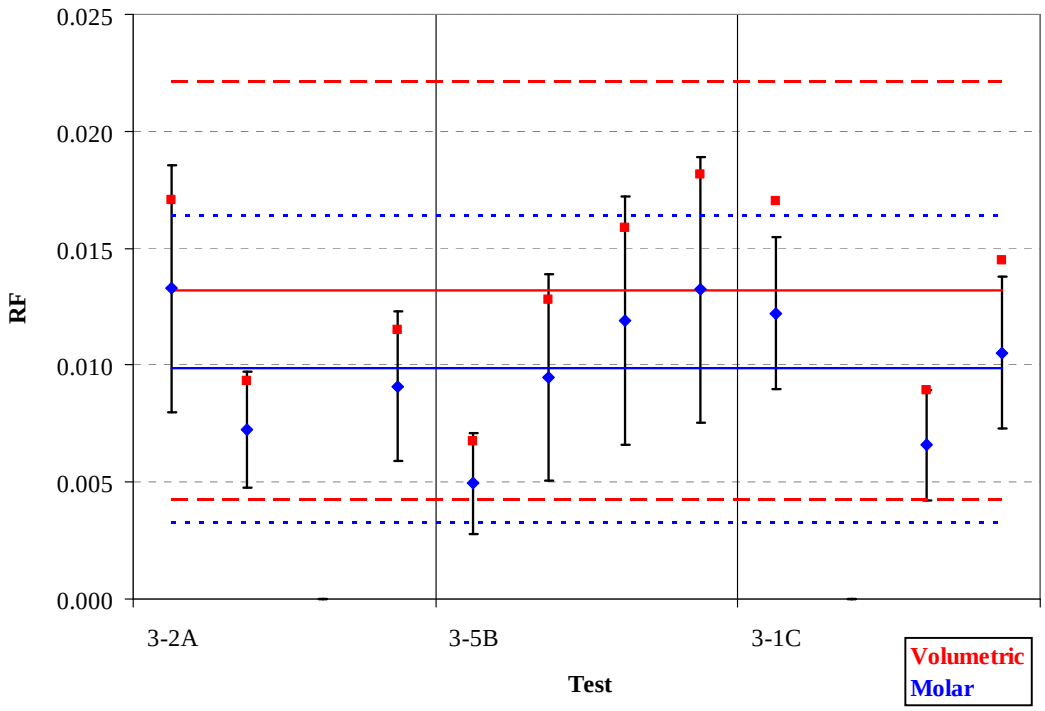

Figure 3.6 Release fraction of depleted uranium for tests 3-2A, 3-5B, and 3-1C.

The statistics and uncertainties for depleted uranium are also presented in Table 3.4. The statistics, including average, standard deviation, and 95% CI, presented for the "Overall" test entry are calculated from the individual Marple impactors of all three tests. These values are the same overall values presented in Table 3.1. The overall average and standard deviations listed for the standard uncertainties were calculated similarly using the values of the individual Marples from all three tests. The overall standard uncertainty for all measurements of depleted uranium RFs is 0.00189. Therefore, the average 95% expanded uncertainty on the experimental measurement is $\mathbf{RF_{DU} = 0.0986 \pm 0.00373}$. Alternatively, the 95% statistical bounds of the data present a more conservative measure of the range in the release fraction of $RF_{DU} = 0.0986 \pm 0.00656$. The magnitude of these confidence intervals in comparison to the experimental measurement brings the validity of any conclusions about this data set into question.

Table 3.4 Release fraction and uncertainties of depleted uranium for tests 3-2A, 3-5B, and 3-1C.

Test	Impactor	RF	u_{RF}	U_{RF}
3-2A	Marple 1	1.33E-02	2.63E-03	5.27E-03
	Marple 2	7.25E-03	1.24E-03	2.48E-03
	Marple 3	--	--	--
	Marple 4	9.10E-03	1.61E-03	3.21E-03
3-5B	Marple 1	4.95E-03	1.07E-03	2.14E-03
	Marple 2	9.48E-03	2.20E-03	4.40E-03
	Marple 3	1.19E-02	2.65E-03	5.30E-03
	Marple 4	1.32E-02	2.84E-03	5.68E-03
3-1C	Marple 1	1.22E-02	1.62E-03	3.25E-03
	Marple 2	--	--	--
	Marple 3	6.58E-03	1.19E-03	2.37E-03
	Marple 4	1.05E-02	1.62E-03	3.25E-03
Overall	Average	**9.86E-03**	1.87E-03	**3.73E-03**
	Std Dev.	2.90E-03	6.61E-04	1.32E-03
	95% CI	**6.56E-03**	--	--
	Avg + 95% CI	1.64E-02	--	--
	Avg - 95% CI	3.29E-03	--	--

3.1.2 Zirconium

3.1.2.1 Statistical Treatment of Test Samples

An ANOVA was conducted for the zirconium RF results from tests 3-2A, 3-5B, and 3-1C. This analysis examines the null hypothesis that the means of each test are equal. The sample populations within each test are assumed to be independent representations of an overall population and normally distributed. If the null hypothesis of the ANOVA is accepted, the test samples are assumed to be from the same overall population and will be analyzed together.

Explicitly, the ANOVA tests the following null hypothesis (H_o) and offers an alternate hypothesis (H_a).

H_o: $\mu_{3\text{-}2A} = \mu_{3\text{-}5B} = \mu_{3\text{-}1C}$

H_a: At least two of the means are not equal.

The ANOVA P-value was determined using MINITAB® 15.1.30.0. The null hypothesis of the ANOVA is accepted with a P-value of 0.125. Therefore, the zirconium RF values from the three tests are treated as samples from a single population for the remainder of this report.

Next, the samples were examined to determine if the data follow a normal or lognormal distribution. Figure 3.7 shows the normal probability plots for the zirconium RF results with 95% confidence intervals. Similarly, Figure 3.8 gives the lognormal probability plot of the same RF data and 95% confidence intervals. Both of these probability tests indicate that either distribution could represent the data with P-values of 0.793 and 0.237 for normal and lognormal, respectively. For ease of analysis, the data will be assumed to follow a normal distribution.

Therefore, the appropriate *t*-distribution statistics will be applied to determine the 95% confidence interval on the overall population.

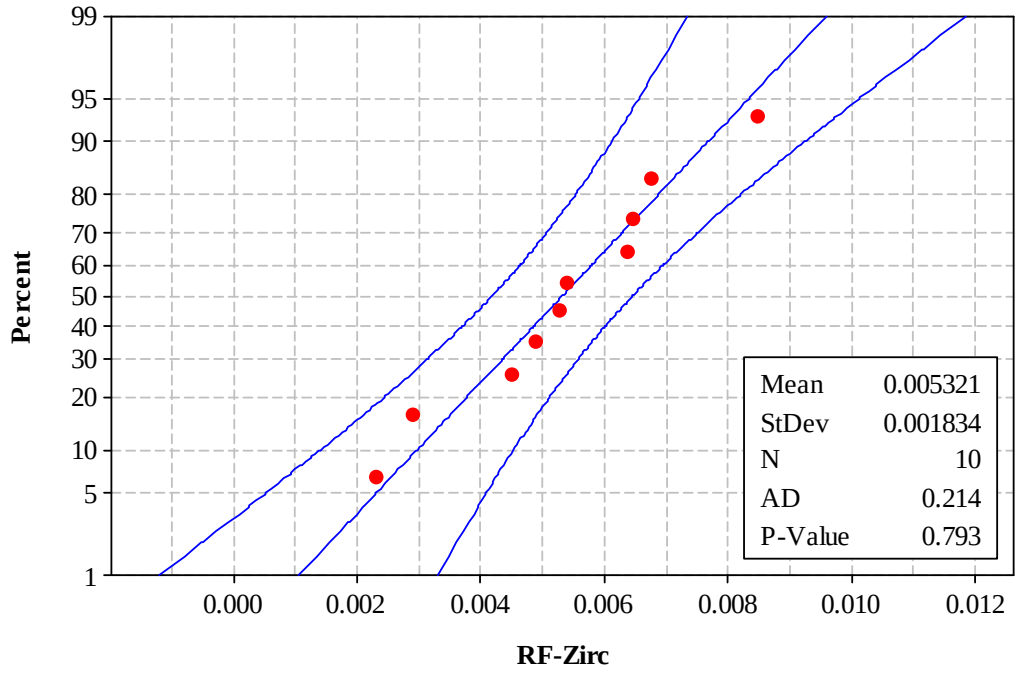

Figure 3.7 Normal probability plot of the zirconium RF values for the Phase 3 tests.

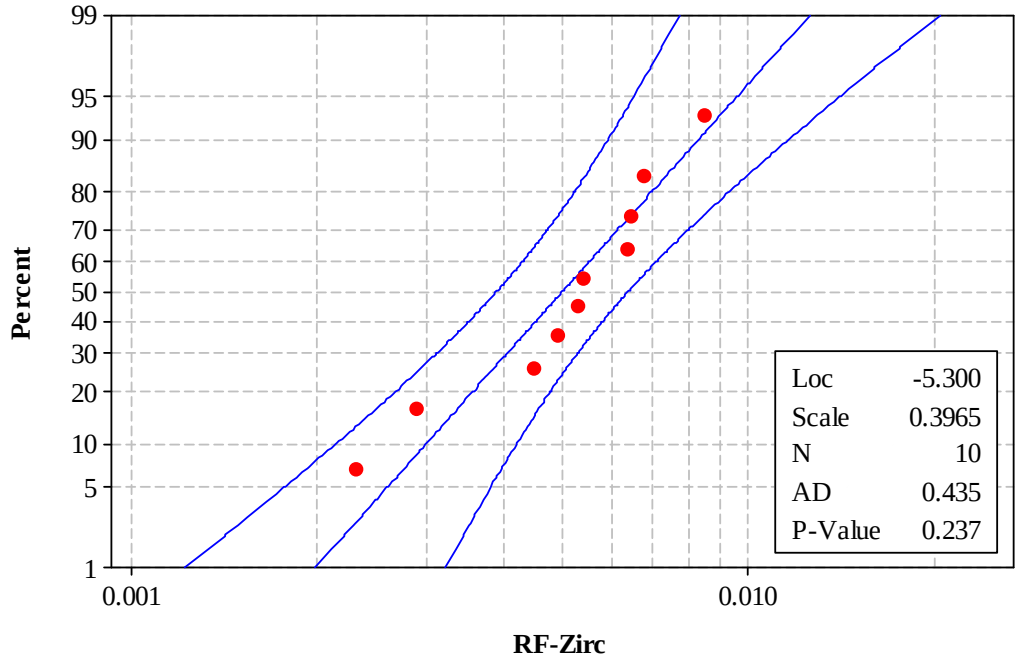

Figure 3.8 Lognormal probability plot of the zirconium RF values for the Phase 3 tests.

Table 3.5 gives the statistical values of all of the Phase 3 tests and an "Overall" entry. The overall values assume that the ANOVA is adequate to group all the Marple samples into one population for analysis. The average of the three tests vary up to 2.71E-3, and the standard deviations vary up to 6.5E-4 between tests. The 95% statistical bounds of the test 3-5B and 3-1C populations predicted by the product of the appropriate *t*-statistic and the standard deviation indicate that the RF varied between negative values (nonphysical) and over twice the reported value. However, combining the samples together as justified in the ANOVA gives a 95% CI of 4.23E-3. Assuming that twelve additional samples may be obtained through additional testing and that the standard deviation does not change appreciably, the overall confidence interval would decrease by a factor of 0.92 due to the decreased value of the *t*-statistic ($t_{0.025,\ 9} = 2.262$ *vs.* $t_{0.025,\ 21} = 2.080$). The standard deviation would also likely change due to an increase in the number of samples but cannot be estimated in the absence of the new data.

Table 3.5 Statistical values of zirconium for tests 3-2A, 3-5B, and 3-1C.

Test	Average	Std Dev.	95% CI	Avg + 95% CI	Avg - 95% CI
3-2A	7.09E-03	1.20E-03	5.18E-03	1.23E-02	1.91E-03
3-5B	4.70E-03	1.85E-03	5.90E-03	1.06E-02	-1.20E-03
3-1C	4.38E-03	1.32E-03	5.67E-03	1.01E-02	-1.29E-03
Overall	5.32E-03	1.83E-03	4.15E-03	9.47E-03	1.17E-03

3.1.2.2 Consideration of Experimental Error

An error propagation analysis (EPA) was performed to determine the uncertainty in the experimentally determined RFs. These error analyses consider the errors, or uncertainties, in the underlying measurements used to determine the release fraction. Table 3.6 gives an example of the error analysis results for Marple 1 of Test 3-2A. These measurements and their associated uncertainties are assumed to behave normally. Again, the 95% expanded uncertainty of each measurement is assumed to equal 2 times the standard uncertainty. The overall influence coefficient, or the normalized uncertainty of RF, is determined by taking the square root of the sum of squares of the individual influence coefficients. The uncertainty of RF is then the product of the overall influence coefficient and the RF. The contribution column quantifies how much each measurement influences the overall uncertainty in RF. The single less than sign indicates that the contribution is between 0.01 and 0.001. The double less than sign, *i.e.* much less than, denotes that the contribution is less than 0.001.

Table 3.6 Error propagation analysis for zirconium in Marple 1 impactor for test 3-2A.

Measurement, x_i	Units	Value	Standard uncertainty, u_i	Influence coefficient ($u_i \cdot [(\partial RF/\partial x_i)/RF]$)	Contribution
n_1	mol	3.38	0.09	0.018	< 0.01
Δn	mol	1.92	0.10	0.020	0.01
$n_{condense}$	mol	0.23	0.02	0.005	<< 0.01
T_{avg}	K	299.8	2	0.007	< 0.01
m_{tot}	g	3.54	0.15	0.042	0.06
Q	m^3/s	3.2E-05	1.6E-07	0.005	<< 0.01
t_{sample}	s	9.0	0.25	0.028	0.02
P_{avg}	Pa	193000	24000	0.124	0.47
$m_{stage,4}$	g	9.68E-06	1.0E-07	0.001	<< 0.01
$\eta_{stage,4}$	--	0.93	0.005	0.001	<< 0.01
$\eta_{loss,4}$	--	0.7	0.15	0.024	0.02
$m_{stage,5}$	g	4.36E-05	1.0E-07	0.001	<< 0.01
$\eta_{stage,5}$	--	0.95	0.005	0.003	<< 0.01
$\eta_{loss,5}$	--	0.7	0.15	0.106	0.35
$m_{stage,6}$	g	1.44E-05	1.0E-07	0.001	<< 0.01
$\eta_{stage,6}$	--	0.97	0.005	0.001	<< 0.01
$\eta_{loss,6}$	--	0.7	0.15	0.034	0.04
$m_{stage,7}$	g	6.44E-06	1.0E-07	0.001	<< 0.01
$\eta_{stage,7}$	--	0.98	0.005	0.000	<< 0.01
$\eta_{loss,7}$	--	0.7	0.15	0.015	< 0.01
$m_{stage,8}$	g	7.93E-06	1.0E-07	0.001	<< 0.01
$\eta_{stage,8}$	--	0.99	0.005	0.000	<< 0.01
$\eta_{loss,8}$	--	0.7	0.15	0.019	0.01
$m_{stage,9}$	g	6.69E-06	1.0E-07	0.001	<< 0.01
$\eta_{stage,9}$	--	1	0.005	0.000	<< 0.01
$\eta_{loss,9}$	--	0.7	0.15	0.016	< 0.01
RF	--	0.0085	0.002	0.180	1.00

Figure 3.9 shows the release fraction of zirconium from molar (blue diamonds) and volumetric determination (red squares)[1, Table 4.1.2] for tests 3-2A, 3-5B, and 3-1C. Marple impactors 1 through 4 are arranged left to right by test in the plot. The error bars represent the 95% confidence interval based on the experimental uncertainty for each impactor and test. The solid lines represent the average value of all RFs for molar (blue) volumetric determination (red). The dashed lines show the 95% bounds of the sample population based on a *t*-statistic of 2.262 ($t_{0.025, 9}$) for molar (blue) volumetric determination (red).

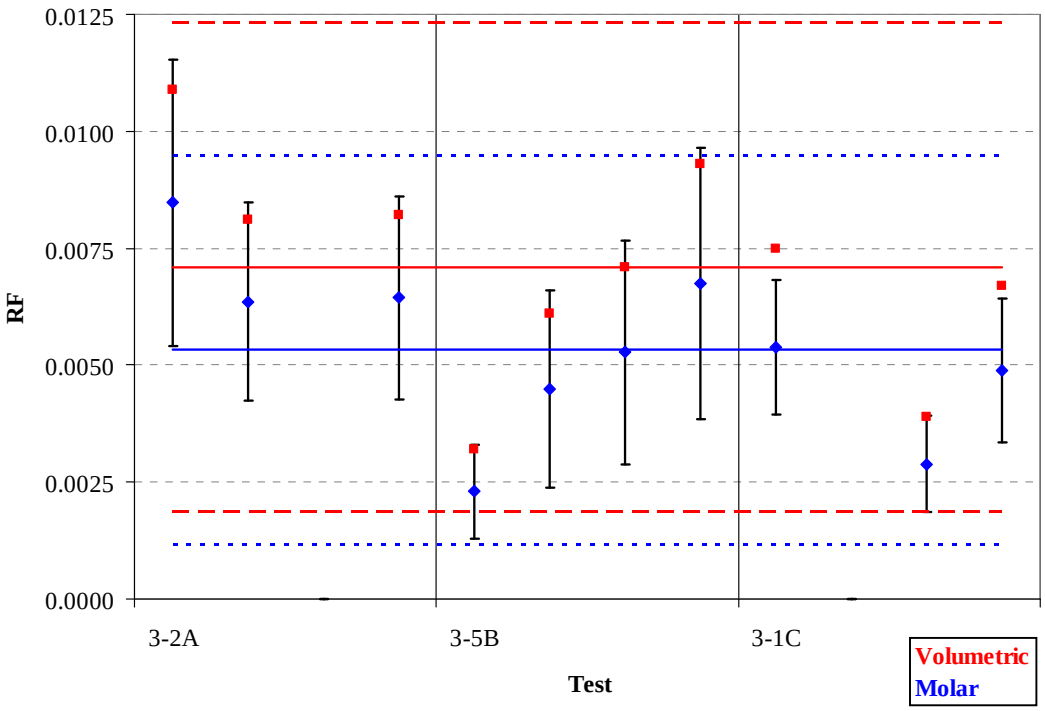

Figure 3.9 Release fraction of zirconium for tests 3-2A, 3-5B, and 3-1C.

The statistics and uncertainties for zirconium are also presented in Table 3.7. The statistics, including average, standard deviation, and 95% CI, presented for the "Overall" test entry are calculated from the individual Marple impactors of all three tests. These values are the same overall values presented in Table 3.5. The overall average and standard deviations listed for the standard uncertainties were calculated similarly using the values of the individual Marples from all three tests. The overall standard uncertainty for all measurements of zirconium RFs is 0.00989. Therefore, the average 95% expanded uncertainty on the experimental measurement is **RF_{Zr} = 0.00532 ± 0.00198**. Alternatively, the 95% statistical bound of the data present a more conservative measure of the range in the release fraction of RF_{Zr} = 0.00532 ± 0.00415. The magnitude of these confidence intervals in comparison to the experimental measurement brings the validity of any conclusions about this data set into question.

Table 3.7 Release fraction and uncertainties of zirconium for tests 3-2A, 3-5B, and 3-1C.

Test	Impactor	RF	u_{RF}	U_{RF}
3-2A	Marple 1	8.48E-03	1.53E-03	3.06E-03
	Marple 2	6.35E-03	1.06E-03	2.12E-03
	Marple 3	--	--	--
	Marple 4	6.44E-03	1.08E-03	2.17E-03
3-5B	Marple 1	2.30E-03	5.04E-04	1.01E-03
	Marple 2	4.48E-03	1.05E-03	2.11E-03
	Marple 3	5.27E-03	1.20E-03	2.39E-03
	Marple 4	6.75E-03	1.46E-03	2.91E-03
3-1C	Marple 1	5.38E-03	7.19E-04	1.44E-03
	Marple 2	--	--	--
	Marple 3	2.89E-03	5.16E-04	1.03E-03
	Marple 4	4.88E-03	7.71E-04	1.54E-03
Overall	Average	**5.32E-03**	9.89E-04	**1.98E-03**
	Std Dev.	1.83E-03	3.58E-04	7.15E-04
	95% CI	**4.15E-03**	--	--
	Avg + 95% CI	9.47E-03	--	--
	Avg - 95% CI	1.17E-03	--	--

3.1.3 Dopants (Cesium and Ruthenium)

3.1.3.1 Consideration of Experimental Error

Similar to depleted uranium and zirconium, the errors in the release fractions of the cesium and ruthenium dopants in test 3-1C were determined using error propagation analysis. These error analyses consider the errors, or uncertainties, in the underlying measurements used to determine the release fraction.

Figure 3.10 shows the release fraction of cesium (left) and ruthenium (right) from molar (blue diamonds) and volumetric determination (red squares)[1, Tables 4.1.3 and 4.1.4] for test 3-1C. Marple impactors 1 through 4 are arranged left to right by element in the plot. The error bars represent the 95% expanded uncertainty based on the experimental error for each impactor and element. The solid lines represent the average values of all RFs for each element. The dashed lines show the 95% bounds of the sample population based on a *t*-statistic of 4.303 ($t_{0.025,\ 2}$) for each element.

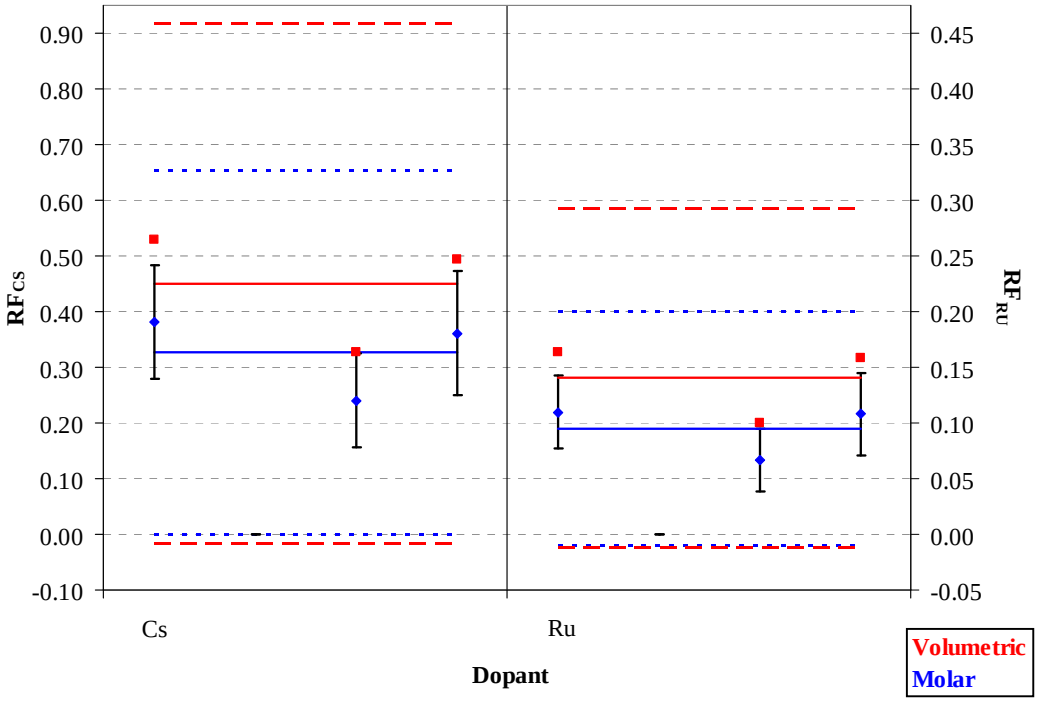

Figure 3.10 Release fraction of cesium (left) and ruthenium (right) dopants for test 3-1C.

The statistics and uncertainties for cesium are presented in Table 3.8. The average of the standard uncertainties for all measurements of cesium RFs is 0.0496. Therefore, the average 95% expanded uncertainty on the experimental measurement is $\mathbf{RF_{Cs} = 0.327 \pm 0.0991}$. Alternatively, the 95% statistical bound of the data present a more conservative measure of the range in the release fraction of $RF_{DU} = 0.327 \pm 0.328$.

The values for ruthenium are presented in Table 3.9. The average of the standard uncertainties for all measurements of ruthenium RFs is 0.0164. Therefore, the average 95% expanded uncertainty on the experimental measurement is $\mathbf{RF_{Ru} = 0.0947 \pm 0.0328}$. Alternatively, the 95% statistical bound of the data present a more conservative measure of the range in the release fraction of $RF_{DU} = 0.0947 \pm 0.108$.

The magnitude of these confidence intervals in comparison to the experimental measurement brings the validity of any conclusions about this data set into question.

Table 3.8 Release fraction and uncertainties of cesium for test 3-1C.

Test	Impactor	RF	u_{RF}	U_{RF}
3-1C	Marple 1	3.88E-01	5.16E-02	1.01E-01
	Marple 2	--	--	--
	Marple 3	2.43E-01	4.27E-02	8.37E-02
	Marple 4	3.68E-01	5.66E-02	1.11E-01
Overall	Average	**3.27E-01**	4.96E-02	**9.91E-02**
	Std Dev.	7.62E-02	6.70E-03	1.34E-02
	95% CI	**3.28E-01**	--	--
	Avg + 95% CI	6.55E-01	--	--
	Avg - 95% CI	-3.36E-04	--	--

Table 3.9 Release fraction and uncertainties of ruthenium for test 3-1C.

Test	Impactor	RF	u_{RF}	U_{RF}
3-1C	Marple 1	1.10E-01	1.64E-02	3.28E-02
	Marple 2	--	--	--
	Marple 3	6.66E-02	1.42E-02	2.84E-02
	Marple 4	1.08E-01	1.86E-02	3.72E-02
Overall	Average	**9.47E-02**	1.64E-02	**3.28E-02**
	Std Dev.	2.44E-02	2.19E-03	4.37E-03
	95% CI	**1.05E-01**	--	--
	Avg + 95% CI	2.00E-01	--	--
	Avg - 95% CI	-1.02E-02	--	--

Phase 2

The Phase 2 testing was conducted using surrogate rods composed of cerium oxide pellets contained within Zircaloy cladding. This section contains statistical analysis of tests 2-5E, 2-5G, 2-6A, 2-6B, 2-8C, 2-8D, 2-9A, 2-9B, 2-10B, 2-10C, and 2-10D for the Ce RF values as presented in Table 4.1.1. of the previous project report.[1] These tests are segregated according to the containment vessel used.

3.1.4 Closed, Double-Chamber Vessel ("Grandma")

Tests 2-5E, 2-5G, 2-6A, 2-6B, 2-8C, and 2-8D were performed using a closed, double-chamber design identified as "Grandma" (see Figure 1.1b) Figure 3.11 shows the average of all samples (red squares) from each test and the 95% confidence interval (dashed black bars) for each test. These confidence intervals do not estimate the experimental uncertainty but instead represent the bounds that contain 95% of the population characterized by the data. The 95% confidence intervals are based on the appropriate *t*-statistic and standard deviation from each test. The 95% confidence interval is not defined for tests 2-5E and 2-5G because only one Marple sample is reported per test. An ANOVA performed on these tests indicates that these samples do not represent data from a single distribution and should not be analyzed together (P-value = 0.000). However, the statistics for the overall data set across tests are included for reference. The solid

line represents the overall average for all tests within the Grandma vessel. The dashed lines represent the 95% confidence interval for the same overall data set with $t_{0.025,\,11} = 2.201$.

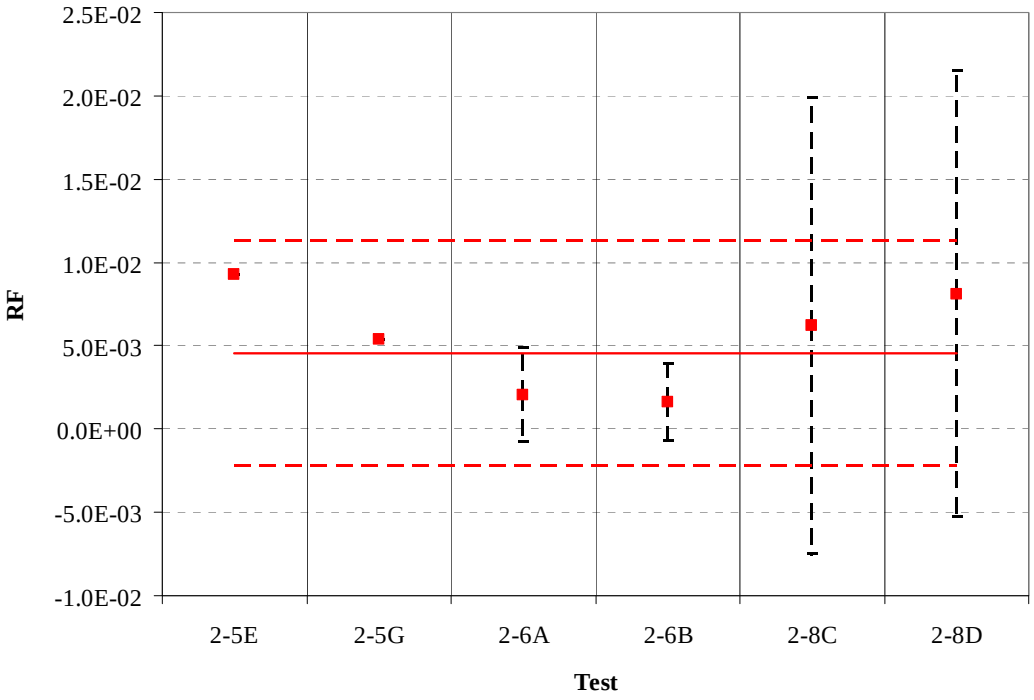

Figure 3.11 Release fraction of cerium from tests 2-5E, 2-5G, 2-6A, 2-6B, 2-8C, and 2-8D.

Table 3.10 gives the release fractions and statistical bounds from the tests conducted with the Grandma vessel. The *t*-statistic used for tests 2-6A and 2-6B was 4.3. The *t*-statistic used for tests 2-8C and 2-8D was 12.7. Statistical bounds below zero are nonphysical but are presented for completeness.

Table 3.10 Release fraction and statistical bounds of cerium for tests 2-5E, 2-5G, 2-6A, 2-6B, 2-8C, and 2-8D.

Test	Average	Std Dev	95% CI	Avg + 95% CI	Avg - 95% CI
2-5E	9.30E-03	--	--	--	--
2-5G	5.39E-03	--	--	--	--
2-6A	2.07E-03	6.49E-04	2.79E-03	4.86E-03	-7.22E-04
2-6B	1.61E-03	5.37E-04	2.31E-03	3.92E-03	-7.05E-04
2-8C	6.23E-03	1.08E-03	1.37E-02	1.99E-02	-7.48E-03
2-8D	8.13E-03	1.05E-03	1.34E-02	2.15E-02	-5.28E-03
Overall	4.54E-03	3.06E-03	6.72E-03	1.13E-02	-2.19E-03

3.1.5 Closed, Double-Chamber Vessel ("Tweety Bird")

Tests 2-9A and 2-9B were performed using a closed, double chamber design specified as "Tweety Bird" (see Figure 1.1a). Figure 3.12 shows the average of all values (red squares) from each test and the 95% confidence interval (dashed black bars) for each test. These confidence intervals do not estimate the experimental uncertainty but instead represent the bounds that

contain 95% of the population characterized by the data. The 95% confidence intervals are based on the appropriate *t*-statistic and standard deviation from each test. An ANOVA performed on these tests indicates that these samples do represent data from a single distribution and should be analyzed together (P-value = 0.509). The solid line represents the overall average for all CeO_2 tests within the Tweety Bird vessel. The dashed lines represent the 95% confidence interval for the same overall data set with $t_{0.025,\,6} = 2.447$.

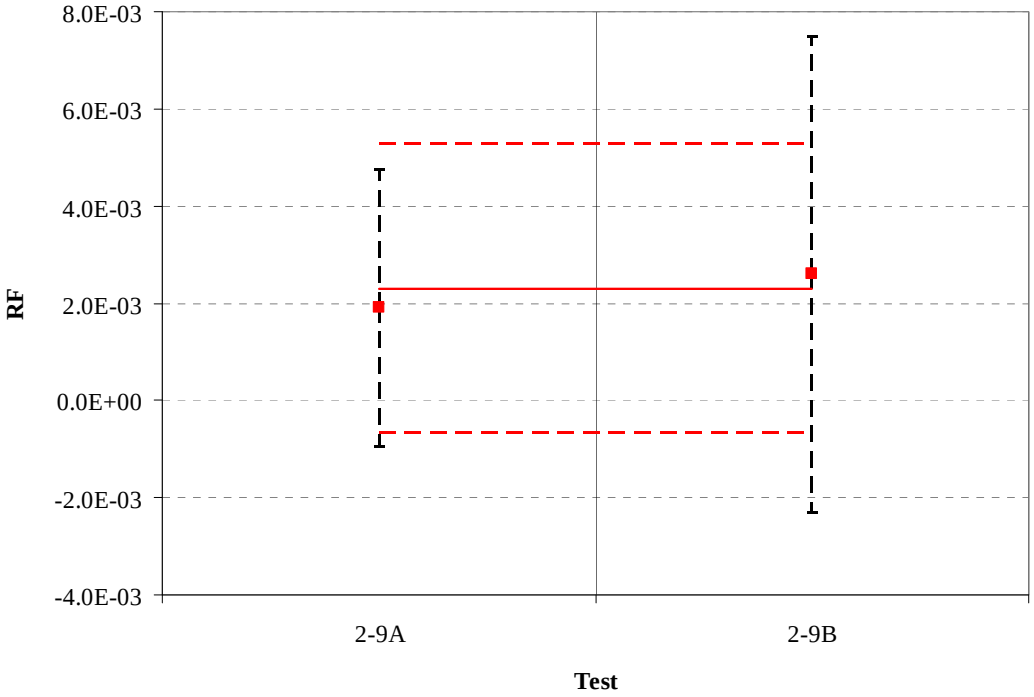

Figure 3.12 Release fraction of cerium from tests 2-9A and 2-9B.

Table 3.11 lists the values plotted in Figure 3.12. The *t*-statistics used in evaluating the 95% CI's in test 2-9A and 2-9B are 4.3 and 3.2, respectively. Statistical bounds below zero are nonphysical but are presented for completeness.

Table 3.11 Release fraction and statistical bounds of cerium for tests 2-9A and 2-9B.

Test	Average	Std Dev	95% CI	Avg + 95% CI	Avg - 95% CI
2-9A	1.91E-03	6.63E-04	2.85E-03	4.77E-03	-9.39E-04
2-9B	2.60E-03	1.54E-03	4.91E-03	7.51E-03	-2.31E-03
Overall	2.31E-03	1.21E-03	2.97E-03	5.27E-03	-6.61E-04

3.1.6 Open, Single-Chamber Vessel

Tests 2-10B, 2-10C, and 2-10D were performed using an open, single-chamber design (see Figure 1.1c). Figure 3.13 shows the average of all Marples (red squares) from each test and the 95% confidence interval (dashed black bars) for each test. These confidence intervals do not estimate the experimental uncertainty but instead represent the bounds that contain 95% of the population characterized by the data. The 95% confidence intervals are based on the appropriate *t*-statistic and standard deviation from each test. An ANOVA performed on these tests indicates

that these samples do not represent data from a single distribution and should not be analyzed together (P-value = 0.004). However, the statistics for the overall data set across tests are included for reference. The solid line represents the overall average for all tests within the open, single-chamber vessel. The dashed lines represent the 95% confidence interval for the same overall data set with $t_{0.025,\,8} = 2.306$.

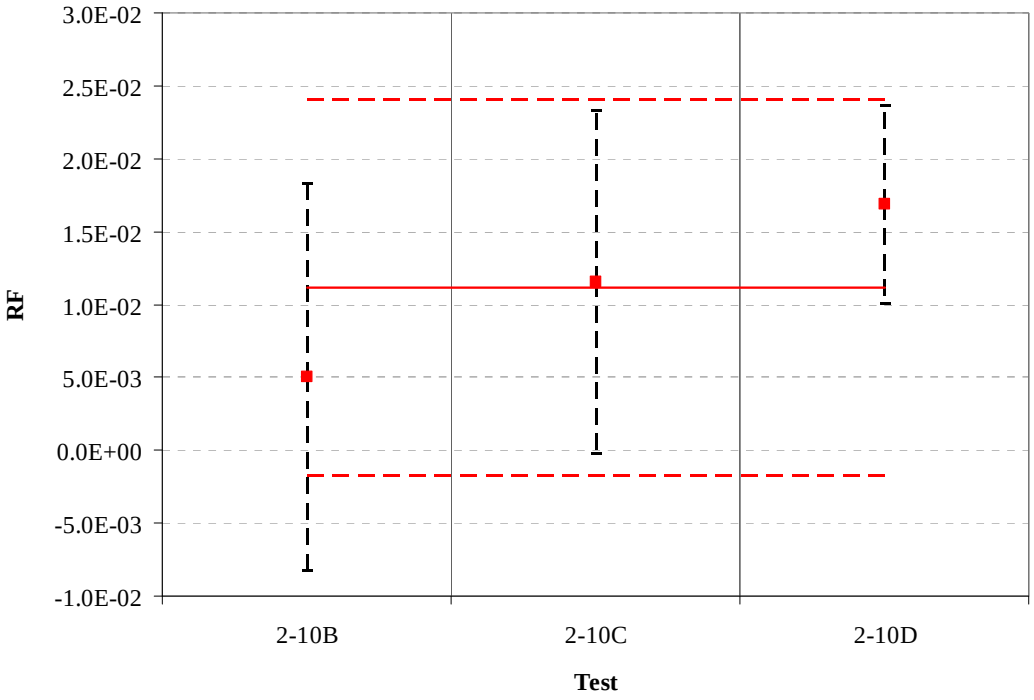

Figure 3.13 Release fraction of cerium from tests 2-10B, 2-10C, and 2-10D.

Table 3.12 gives the release fractions and statistical bounds from the tests conducted with the Grandma vessel. The *t*-statistic used for all tests was 4.3. Statistical bounds below zero are nonphysical but are presented for completeness.

Table 3.12 Release fraction and statistical bounds of cerium for tests 2-10B, 2-10C, and 2-10D.

Test	Average	Std Dev	95% CI	Avg + 95% CI	Avg - 95% CI
2-10B	5.06E-03	3.09E-03	1.33E-02	1.83E-02	-8.22E-03
2-10C	1.16E-02	2.73E-03	1.18E-02	2.33E-02	-1.82E-04
2-10D	1.69E-02	1.58E-03	6.79E-03	2.37E-02	1.01E-02
Overall	1.12E-02	5.58E-03	1.29E-02	2.40E-02	-1.70E-03

3.2 Consideration of Error Propagation on the Spent Fuel Ratio

The resultant uncertainty in the spent fuel ratio (SFR) is estimated in this section. These estimates are based on the results of the error propagation analyses (EPA) because neither the spent fuel nor the experimentally improved DU tests (see Chapter 4) have been conducted. The EPA allows the estimate of the uncertainty in RF based on the known, or assumed, uncertainty of the underlying measurements.

The spent fuel ratio is defined in Equation 3.2. This ratio represents the comparison of respirable particles generated from spent fuel (SF) to those generated from depleted uranium (DU) under identical test conditions.

$$\mathrm{SFR} = \frac{\mathrm{RF_{SF}}}{\mathrm{RF_{DU}}} \tag{3.2}$$

Equation 3.3 gives the relationship between the normalized uncertainty in SFR to the normalized uncertainties in the DU and SF release fractions.

$$\frac{u_{SFR}}{\mathrm{SFR}} = \sqrt{\left(\frac{u_{DU}}{\mathrm{RF_{DU}}}\right)^2 + \left(\frac{u_{SF}}{\mathrm{RF_{SF}}}\right)^2} \tag{3.3}$$

Figure 3.14 graphically represents Equation 3.3. The uncertainties in DU and SF molar-based release fractions are assumed to be equal. This assumption appears to be justified given that the two test series are to be conducted using similar instrumentation and procedures. The red diamond shows the resulting uncertainty in SFR based on the current understanding of uncertainty from the existing data set for DU (see average values of u_{RF} and RF in Table 3.4 where $u_{\mathrm{RF}}/\mathrm{RF} = 0.189$). The 95% expanded uncertainty at these error levels translate to SFR = 1 ± 0.54. By decreasing the uncertainty through experimental improvements, the 95% expanded uncertainty is reduced to SFR = 1 ± 0.13, a factor of 4 improvement. This calculation assumes error reduction in the η_{loss} ($u_{\eta loss} = 0.05$), P_{avg} ($u_{Pavg} = 1400$ Pa), m_{tot} ($u_{\mathrm{mtot}} = 0.05$ g), and t_{sample} ($u_{tsample} = 0.025$ s) measurements. This calculation also assumes a new series of DU experiments would need to be conducted to re-establish $\mathrm{RF_{DU}}$ and u_{DU} as well as the proposed experiments with spent fuel. The next chapter describes how these improvements in measurement error might be achieved.

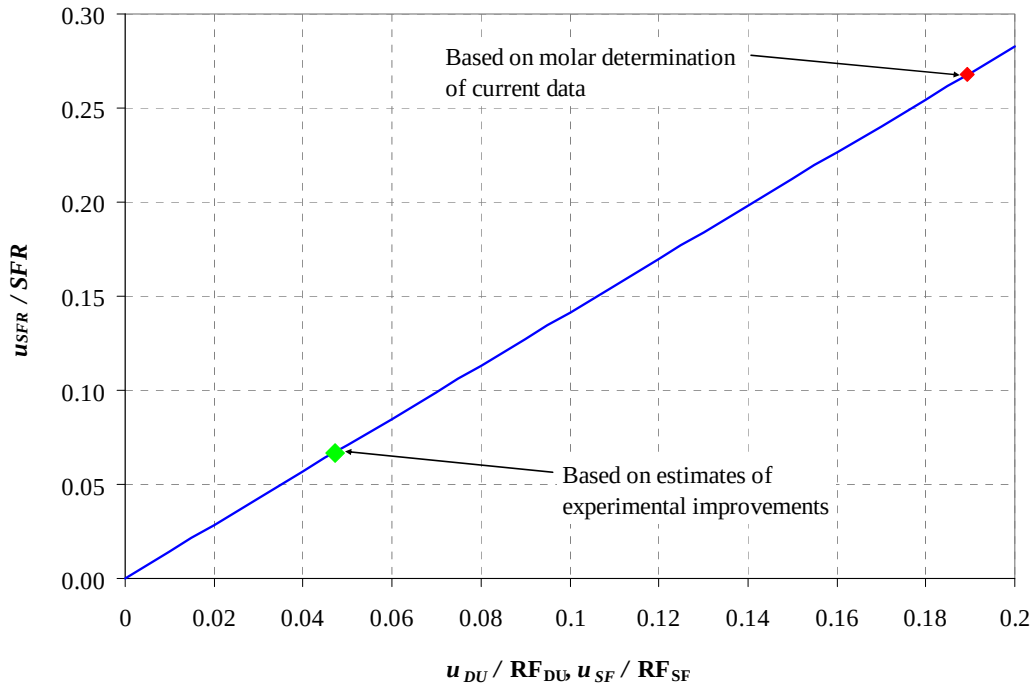

Figure 3.14 **Normalized, standard uncertainty in the spent fuel ratio as a function of normalized, standard uncertainty in release fraction.**

4 IMPLICATIONS FOR FUTURE TESTING

4.1 Parameters of Concern

The error propagation analysis identified the parameters that contribute the most error in the determination of RF. This information can provide guidance for experimental improvements that can most efficiently reduce the overall error. The parameters contributing the most error are the aerosol sample train loss (η_{loss}), the average sample pressure measurement (P_{avg}), the sample collection time (t_{sample}), the number of moles of gas injected into the upper chamber in the pressure equilibration process (Δn), and the total disrupted mass (m_{tot}). Aerosol loss in the sampling system contributes the most error and uncertainty to the determination of RF. This dependence is understandable because these losses were not well characterized but are known to be significant. In light of the error analysis, experimental issues that contribute to the error and uncertainty, along with proposed experimental improvements designed to mitigate the experimental error, are discussed below.

4.2 Experimental Issues and Potential Improvements

4.2.1 Aerosol Loss in Sampling System

An important step in reducing the uncertainty in the sample train would be to perform a calibration of the sample system. The calibration of both the sample train and impactor should be performed using a well-known fluorometric method.[6] In this method, monodisperse oleic acid oil droplets generated with the vibrating orifice aerosol generator are tagged with trace amounts of a fluorescent dye (uranine) and introduced into the sample train and impactor. After the test, the sample train and impactor are disassembled and oleic acid/uranine deposits on various component surfaces are collected and quantified fluorometrically to determine where a given sized particle was captured or lost. The characterization would be performed under ideal ambient conditions. The high temperature and pressure conditions would not be simulated.

The above aerosol loss calibration is only valid for experimental situations where there is no enhanced aerosol loss beyond the aerodynamic losses encountered in a reasonably designed system. During the previously conducted experiments, the aerosol losses in the sample train were exacerbated by two experimental problems. First, the temperature of the chamber and sample train was significantly below the dew point of gas in the upper chamber ($T_{sat} \approx 46$ °C). This would result in moisture condensation in the sample train, which would likely result in significant loss of aerosols. Second, when the valves were opened to initiate gas sampling, the pressure in the upper aerosol chamber was four to seven times greater than the pressure in the sample train. This would result in a pressure shock wave and the initial inflow of gas at sonic velocity likely resulting in the loss of aerosols. During the sample collection time, 2.25E-2 moles of gas are collected. Just before the sample valves are both opened this sample train contains 2.0E-3 moles of gas (or about 9% of the gas sampled) with no aerosols. After the sample valves are opened the sampling system is rapidly pressurized with 7.1E-3 moles of aerosol-laden gas. Due to the rapid pressurization, this gas, which is 32% of the gas sampled, is no longer a representative sample from the aerosol chamber. Therefore, forty percent of the gas sampled was not representative of the gas in the aerosol chamber.

The condensation problem can be solved by heating the vessel and sample train. The dew point of the aerosol chamber gas is estimated to be 46 °C. Heating the chamber and aerosol sampling system to 50 to 55 °C should eliminate condensation. Aerosol loss due to the rapid pressurization of the sample train can be mitigated by pre-pressurizing the sample train to the anticipated pressure of the aerosol chamber at the time of sample collection initiation. Sample collection initiation should be delayed until 15 to 20 seconds after detonation to allow the chamber pressure to reach steady state at slightly above ambient. This delay will allow the matching of the sample train pressure to the chamber pressure with greater certainty and reproducibility. This delay should have little effect on the respirable aerosol concentration but will reduce the concentration of larger aerosols due to settling. Since the spent fuel ratio is defined by the respirable aerosols, the accurate characterization of the respirable aerosol concentration should take precedence over the characterization of larger particles.

4.2.2 Sampling Time

Because the sampling time is short, small errors can have a large effect on the calculated RF value. Valve timing is not sufficient to define the time that a representative sample is flowing through the impactor. Pre-pressurizing the sample system with aerosol free gas is proposed as a method to prevent the violent pressurization of the sample system that likely alters the aerosol concentration of the gas. Sample flow timing should not begin until a representative aerosol sample reaches the impactor. The direct measurement of the sample front arrival at the impactor can be made possible if the sample system is pressurized with helium. Helium has a thermal conductivity that is over five times greater than air so a thermal conductivity sensor installed immediately before the impactor would provide a direct measurement of the sample arrival. Figure 4.1 shows an e2v Inc. technologies thermal conductivity sensor in application of sensing a flowing gas (www.e2v.com). The dimensions AC and AB are just over 8 mm.

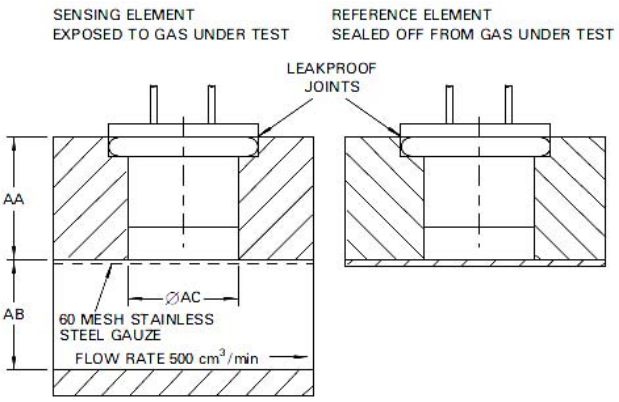

Figure 4.1 Thermal conductivity sensor installation and mounting arrangements.

4.2.3 Influx of Flow from Lower to Upper Chamber (Δ*n* moles)

A major feature of the new molar methodology is that the initial moles of aerosol-laden gas are determined, which allows the determination of the RF even after a significant flow from the aerosol chamber into the bottom chamber. However, the method requires a number of assumptions regarding the energy release of the CSC device, the resulting kinetic energy of the copper jet, and the isentropic expansion of the gas during pressure equilibration, which

introduces some uncertainty. A direct measurement of the number of moles of gas that enter the upper chamber from the bottom chamber during pressure equalization may reduce this uncertainty significantly. A means of accomplishing this is to use the vacuum source bottles for sample gas collection. The CSC reaction produces known amount of carbon dioxide in the bottom chamber that may be used as a tracer to determine the amount of the other gaseous reaction products formed. The atmosphere in the upper test chambers would need to be pure nitrogen to prevent any of the CSC produced particles from forming CO_2. The bottom chamber would be filled with pure argon. A rupture disk between the two chambers and would keep the gases from mixing prematurely. The sample gas in the vacuum bottle would be analyzed for N_2, Ar and CO_2. From these concentration measurements and the moles of N_2 initially charged into the aerosol chamber, a mass balance can determine with certainty the moles of gas into which the aerosols were mixed. If the aerosol chamber is well mixed as assumed, the four gas analyses will be the same within the error of the gas analysis. The only additional assumption would be that none of the nitrogen moved out of the upper chamber before the aerosols were generated and mixed, which is expected to be valid.

Figure 4.2 shows a conceptualization of a double chamber test that incorporates the experimental improvements. Initially, (Figure 4.2a) the bottom chamber is charged with one atmosphere of argon, the top chamber is charged with one atmosphere of nitrogen. A rupture disk keeps the gases separated. The sample train is pressurized with helium to the anticipated chamber pressure at the time of sample collection. A thermal conductivity sensor in the sample system reads the high thermal conductivity of helium. The entire chamber and sample system is heated to 50 °C to prevent moisture condensation. When the CSC is detonated (Figure 4.2b) the jet disintegrates the fuel rodlet releasing aerosols. Combustion products and energy are released into the argon in the bottom chamber. Some combustion products and associated energy are injected into the nitrogen upper chamber. The argon mixture in the bottom chamber reaches a higher temperature and pressure than the nitrogen mixture in the upper chamber. This causes the gas in the bottom chamber to violently flow up into the upper chamber mixing argon and more combustion gases into the aerosol-laden nitrogen (Figure 4.2c). The concentration of aerosols and gases in the upper chamber is established. As the chambers cool, aerosol laden gas flows from the upper chamber into the bottom chamber (Figure 4.2d). This flow does not change the concentration of aerosols or gases in the upper chamber. After the temperatures in the upper and lower chamber equilibrate (~15 seconds) the sample valves are opened. The vacuum in the gas sample bottle draws flow through the impactor. The pressure in the sample system and the aerosol chamber are about equal so there is no catastrophic pressurization of the sample system to compromise the aerosol sample. Aerosol-laden gas is drawn into the sample system and displaces the helium. When the sample gas reaches the impactor, the thermal conductivity sensor senses the lower thermal conductivity of the nitrogen argon mixture which denotes the start time of sampling. Ten seconds later the sample valves are closed. The gas collected in the gas sample bottle is analyzed for nitrogen, argon and carbon dioxide. The carbon dioxide provides a tie to all gaseous combustion products through the reaction stoichiometry. The relative concentrations of N_2, Ar and CO_2 together with the initial amount of N_2 loaded into the aerosol chamber allows the initial moles of aerosol-laden gas to be calculated.

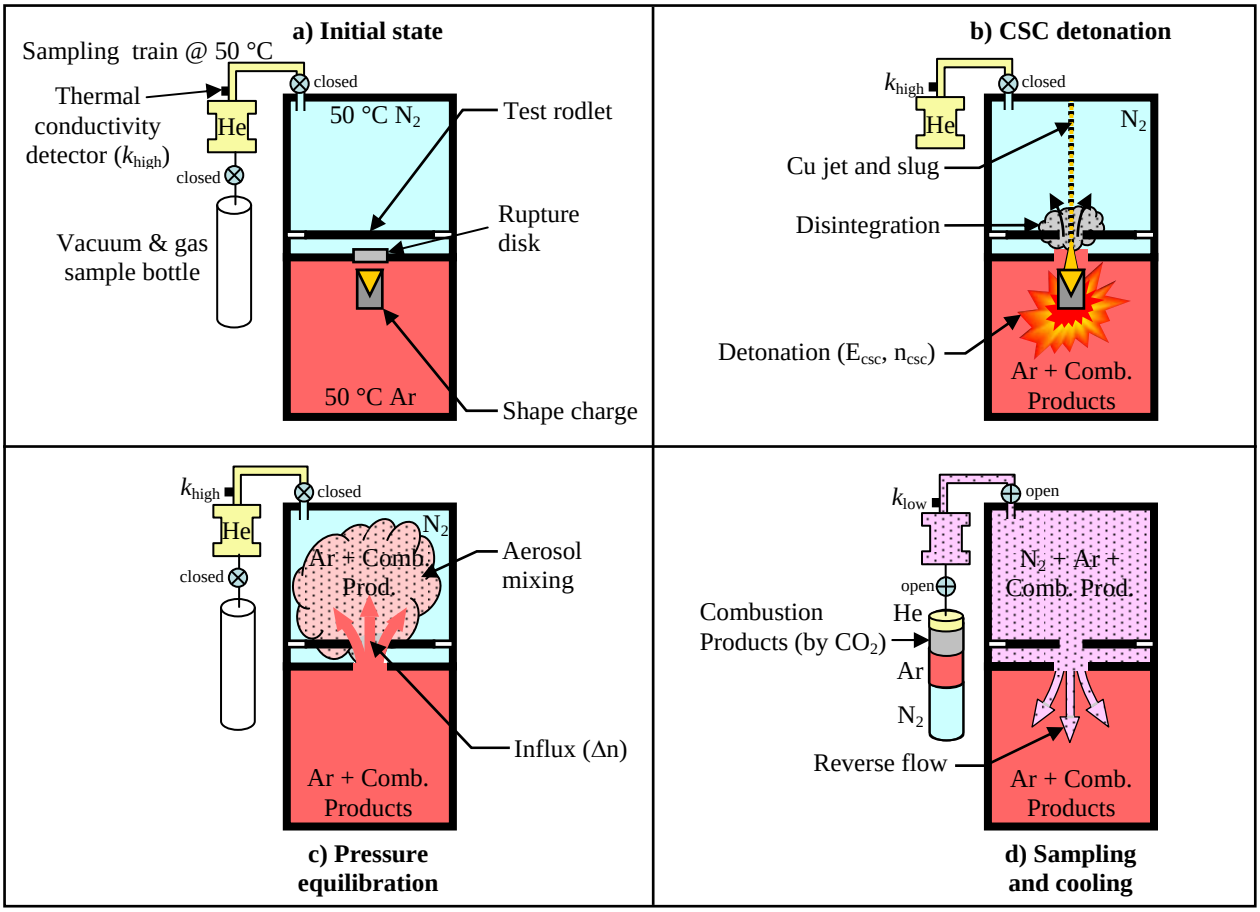

Figure 4.2 **Sequencing and details of an improved experimental setup for measuring RF.**

5 SUMMARY

The overall objective of this project is to provide vital data required to assess the consequences of a terrorist attack on a spent fuel transportation cask. Conical shaped charges (CSC) are capable of damaging a spent fuel transportation cask. In the event of such an attack, the amount of radioactivity that may be released as respirable aerosols is not known with great certainty. To date, the project research has focused on measuring the aerosol release from single short surrogate fuel rodlets subjected to attack by a small CSC device in various aerosol chamber designs. The last series of three experiments tested surrogate fuel rodlets made with depleted uranium oxide ceramic pellets in a specially designed double chamber aerosol containment apparatus. This robust testing apparatus was designed to prevent any radioactive release and allow high level radioactive waste disposal of the entire apparatus following testing of actual spent fuel rodlets as proposed.

DOE and Sandia reviews of the project to date identified a number of issues. The purpose of this supplemental report is to address and document the DOE review comments and resolve the issues identified in the Sandia technical review.

The previous data analysis method determined the aerosols contained in the aerosol chamber at the time of sampling, which required knowledge of the chamber gas temperature. However, the aerosol chamber temperature was not measured. Furthermore, with the double chamber apparatus a significant amount of aerosol-laden gas flows from the upper aerosol chamber into the lower chamber before and during the sample collection period. These aerosols were inherently not counted by the previous methodology.

A more intricate conceptual model has been developed that overcomes the limitation of the previous approach in that the aerosol chamber temperature is not required and the method does not require the assumption that the aerosols are all contained in a single chamber. This method determines the aerosol concentration of the initial moles of aerosol-laden gas by utilizing information about the energy and gaseous release of the explosive device used. Because the new method determines the aerosol concentration of the initial aerosol-laden gas on a molar basis, the method is not affected by the out flow of aerosol laden gas before and during gas sampling.

The respirable fraction (RF) of aerosol release was recalculated for the final three tests conducted with depleted uranium. For each of these tests, at least three (and in one case four) independent aerosol samples were collected (for a total of 10). An analysis of variance indicates that the variance within each test is significantly large to preclude the determination of variation introduced between tests. Therefore, the RF values from the three tests are treated as samples from a single population.

An error propagation analysis (EPA) was performed to determine the uncertainty in the experimentally determined RFs calculated by the molar methodology. These error analyses consider the errors, or uncertainties, in the underlying measurements used to determine the release fraction.

The overall experimental uncertainty in the depleted uranium and zirconium release fractions were dominated by the uncertainty in just a few key parameters. The top two contributors are the

sample line loss efficiency, η_{loss} with an average contribution of 56% and the average sample pressure, P_{avg} with an average contribution of 38%. Other parameters that contributed significantly to the uncertainty are the sampling time, t_{sample}, with a 2% contribution, the flow of gas from the lower chamber into the upper chamber, Δn, with 1%, the sample flow rate, Q, with 1%, and the total mass of fuel rod disrupted by the CSC projectile, m_{tot}, with 1%. Together, the uncertainty in these parameters represent 99% of the average uncertainty in the DU RF determination.

The average RF for depleted uranium was found to be 0.00986 ± 0.00373. This is 34% lower than the 0.0132 value reported previously.[1, Table 4.1.1] The average RF for zirconium was found to be 0.00533 ± 0.00198. This is 33% lower than the 0.0071 value reported previously.[1, Table 4.1.2] The last test conducted included cesium and ruthenium dopants as surrogates for decay products in spent fuel. The average RF for cesium was found to be 0.327 ± 0.0991. This is 38% lower than the 0.450 value reported previously.[1, Table 4.1.3] The average RF for ruthenium was found to be 0.0947 ± 0.0328. This is 48% lower than the 0.141 value reported previously.[1, Table 4.1.4]

The spent fuel ratio (SFR) represents the comparison of respirable particles generated from actual spent fuel to those generated from depleted uranium surrogate under identical test conditions. For purposes of assessing the effects of experimental error on the SFR, it is assumed SFR = 1 and the experimental error is the same for the spent fuel and surrogate rod tests. The 95% expanded uncertainty associated with the previous tests results in SFR = 1 ± 0.54. By decreasing the uncertainty through experimental improvements, the 95% expanded uncertainty is reduced to SFR = 1 ± 0.13, a factor of 4 improvement. The experimental improvements assume error reduction in the η_{loss}, P_{avg}, m_{tot}, and t_{sample} measurements. This calculation also assumes a new series of DU experiments would need to be conducted to re-establish RF_{DU} and u_{DU} as well as the proposed experiments with spent fuel.

A number of experimental improvements have been identified that are expected to significantly reduce experimental uncertainty. Two experimental artifacts of the previously conducted tests are responsible for most of the excessive experimental error encountered and raise serious concerns about the ability to conclusively interpret the resulting data. The largest problem was moisture condensation in the aerosol sample system. Simply heating the chamber and sample system to 50 °C eliminates this problem. The second largest problem was violent pressurization of the aerosol sample system at the initiation of sample collection. The highly turbulent sonic flows coupled with moisture condensation destroyed the representativeness of the aerosol sample initially filling the sample system. The initial amount of gas contained in the sample train represented over 40% of the total sample collected. Waiting until 15 seconds after detonation and pre-pressurizing the sample system with helium will eliminate these problems. Pressurizing with helium will allow a thermal conductivity sensor to signal the arrival of sample gas at the impactor providing a definitive sample collection timing mark. A final experimental improvement allows direct measurement of the initial amount of aerosol laden gas. The bottom chamber would be filled with argon and the upper aerosol chamber filled with nitrogen. The vacuum bottle would be used to collect a gas sample. The gas sample is analyzed for nitrogen, argon and carbon dioxide. This information coupled with the initial amount of nitrogen in the upper chamber and the explosive reaction stoichiometry uniquely defines the initial moles of aerosol laden gas. The proposed experimental improvements would significantly reduce the experimental error and provide a higher level of confidence in the determination of SFR.

The statistical bounds and estimated experimental uncertainty of the data from the previously conducted experiments represent significant fractions of the experimental measurements. Moisture condensation and the pressure shock encountered by the gas sample seriously compromised the integrity of the sample. These serious experimental problems render the previously collected data highly questionable. Continuation of this project to the Phase-4 testing of actual spent fuel must be preceded by the testing of at least the remaining three Phase-3 DUO_2 rodlets using an improved experimental approach such as outlined in this report.

6 REFERENCES

1. Molecke, M.A., J.E. Brockman, M.W. Gregson, M. Steyskal, L.A Klennert, W. Koch, O. Nolte, W. Brücher, G.G. Pretzsch, B.A. Autrusson, and O. Loiseau. Spent Fuel Sabotage Test Program, Characterization of Aerosol Dispersal: Interim Final Report, SAND2007-8070. Sandia National Laboratories. Albuquerque, NM. March 2008.

2. Thrower, A.W. (USDOE – Office of Civilian Radioactive Waste Management). Private Communication – Informal Note to M.A. Molecke and D.R. Miller (Sandia National Laboratories). "Reply to SNL Memo 5-19-08.doc". May 19, 2008.

3. Walpole, R.E. and R.H Myers. Probability and Statistics for Engineers and Scientists, 5th Ed., Englewood Cliffs, NJ: Prentice Hall, 1993.

4. Dorf, R.C., The Engineering Handbook, Chapter 22 – Measurement Errors and Uncertainty, 2nd Ed., Boca Raton, FL: CRC Press, 2005.

5. Molecke, M.A., J.E. Brockman, D.A. Lucero, M. Steyskal, M.W. Gregson, M.C. Billone, T. Burtseva, W. Koch, O. Nolte, G. Pretzsch, W. Brücher, B.A. Autrusson, O. Loiseau. Spent Fuel Sabotage Aerosol Test Program: FY 2005-06 Testing and Aerosol Data Summary, SAND2006-5674. Sandia National Laboratories. Albuquerque, NM. October 2006.

6. Rader, D.J., L.A. Mondy, J.E. Brockman, D.A. Lucero, and K.L. Rubow, "Stage Response Calibration of the Mark III and Marple Personal Cascade Impactor", *Aerosol Sci and Tech*, 14, 1991.

APPENDIX A – DERIVATION OF MOLAR-BASED ANALYSIS

A.1 Release Fraction Calculation Details

$$\mathrm{RF} = \frac{m_{release}}{m_{tot}}$$

RF: release fraction

$m_{release}$: total mass of <10μm aerosols released into aerosol chamber

m_{tot}: total mass of disrupted fuel rod component (DUO_2 ceramic, Zr clad, or dopant) initially present

$m_{release} = C_{aerosols} n_{chamber}$ total mass of <10μm aerosols released into aerosol chamber

$n_{chamber}$: moles of gas in aerosol chamber when aerosols are formed and mixed sometimes refered to as the initial moles of aerosol-laden gas.

$C_{aerosols}$: the concentration of aerosols <10 μm in aerosol chamber (mass of aerosols per mole of gas)

$$C_{aerosols} = \frac{m_{release}}{n_{chamber}} = \frac{m_{collect}}{n_{collect}}$$

$m_{collect}$: mass of <10μm aerosols collected

$n_{collect}$: moles of gas sampled from aerosol chamber (that contained $m_{collect}$)

Assuming the aerosol concentration in the chamber is the same as the aerosol concentration drawn through the aerosol collection system.

$$m_{release} = n_{chamber} \frac{m_{collect}}{n_{collect}}$$

$$m_{collect} = \sum_i \frac{m_{stage,\,i}}{\eta_{stage,\,i} \eta_{loss,\,i}}$$ mass of <10μm aerosols collected

$m_{stage,\,i}$: mass collected on impactor stage *i*

$\eta_{stage,\,i}$: collection efficiency of stage *i*

$\eta_{loss,\,i}$: inlet losses of particles that would have been collected on stage *i*

$$n_{collect} = \frac{P_{avg}\left(Qt_{sample}\right)}{\mathrm{R}T_{avg}}$$ moles of gas sampled from aerosol chamber

Q: ~constant volumetric flow rate through critical flow orifice

P_{avg}: average sample pressure during sample collection ($P(t)$ rapidly dropping)

T_{avg}: average sample temperature during sample collection

t_{sample}: gas sample collection time

R: universal gas constant

$m_{total} = l_{fuel} A_{fuel} \rho_{fuel}$ total mass of disrupted fuel rod initially present

l_{fuel}: length of disrupted fuel rod

A_{fuel}: area of fuel pellet

ρ_{fuel}: density of fuel pellet

Resulting in:

$$\mathrm{RF} = \frac{n_{chamber} \mathrm{R} T_{avg}}{m_{tot} Q t_{sample} P_{avg}} \sum_i \frac{m_{stage,\,i}}{\eta_{stage,\,i} \eta_{loss,\,i}}$$ if mass of disrupted fuel rod is determined by weight

$$\mathrm{RF} = \frac{n_{chamber} \mathrm{R} T_{avg}}{l_{fuel} A_{fuel} \rho_{fuel} Q t_{sample} P_{avg}} \sum_i \frac{m_{stage,\,i}}{\eta_{stage,\,i} \eta_{loss,\,i}}$$ if only the length of disrupted fuel rod is measured

The moles of gas into which the aerosols are dispersed, $n_{chamber}$, can be calculated within the assumptions of the experimental conceptualization discussed above:

Initially:

$$n_1 = \frac{P_i V_1}{\mathrm{R} T_i}$$

$$n_2 = \frac{P_i V_2}{\mathrm{R} T_i}$$

n_1: moles of gas initially in the upper chamber

n_2: moles of gas initially in the lower chamber

P_i: initial chamber pressure (when sealed)

T_i: initial chamber temperature (when sealed)

V_1: volume of upper chamber

V_2: volume of lower chamber

Immediately after CSC detonation:

E_{PV} is the isentropic expansion energy loss to the lower chamber gas and gain to upper chamber gas. E_{PV} is equal to the energy removal required to lower the gas temperature of the initial moles of gas in the lower chamber ($n_2 + n_{csc}$) from $T_{2,\,noPV}$ to T_2 where $T_{2,\,noPV}$ is the gas temperature in the lower chamber with no isentropic expansion cooling.

$$E_{PV} = (n_2 + n_{csc}) c_v T_{2,\,noPV} \left(1 - \left(\frac{P_{eq}}{P_{2,\,noPV}} \right)^{\frac{\gamma - 1}{\gamma}} \right)$$

Where:

c_v: constant-volume, specific heat of gas in chambers (Assumed as c_v = 25.4 J/mol·K – Evaluated @ 1140 K)

n_{csc}: moles of gas released by CSC

γ: specific heat ratio (Assumed as γ = 1.33 – Evaluated @ 1140 K)

$T_{2,noPV}$ is the gas temperature in the lower chamber with no isentropic expansion

$$T_{2,\,noPV} = \frac{E_{csc} - E_{ke}}{(n_2 + n_{csc}) c_v} + T_i$$

E_{csc}: energy release of conical shaped charge (CSC) detonation

E_{ke}: kinetic energy delivered to upper chamber by CSC

$P_{2,\,noPV}$ is the gas pressure in the lower chamber with no isentropic expansion

$$P_{2,\,noPV} = \frac{(n_1 + n_2 + n_{csc}) \mathrm{R} T_{2,\,noPV}}{V_2}$$

P_{eq} is the equilibrium pressure in both upper and lower chambers after energy and gaseous reaction product inputs from the explosive devise.

$$P_{eq} = \frac{(n_1 + n_2 + n_{csc}) \mathrm{R}}{V_1 + V_2} \left(\frac{E_{csc}}{(n_1 + n_2 + n_{csc}) c_v} + T_i \right)$$

Then:

$$T_1 = \frac{\left(E_{ke} - E_{loss} + E_{PV}\right)}{n_1 c_v} + T_i$$

$$T_2 = \frac{E_{csc} - E_{ke} - E_{PV}}{(n_2 + n_{csc})c_v} + T_i$$ (Assumes the gaseous products have the c_v of air)

T_1: post detonation temperature of gas in upper chamber

T_2: post detonation temperature of gas in lower chamber

E_{loss}: kinetic energy loss to wall impact (does not heat the gas)

n_1: initial moles of gas in upper chamber

n_2: initial moles of gas in lower chamber

After pressure equalization:

$$\frac{P_{eq}V_1}{(n_1 + \Delta n)T_{mix}} = \frac{P_{eq}V_2}{(n_2 + n_{csc} - \Delta n)T_2}$$

$$T_{mix} = \frac{n_1}{n_1 + \Delta n}T_1 + \frac{\Delta n}{n_1 + \Delta n}T_2$$

$$P_{eq} = \frac{(n_1 + \Delta n)\mathrm{R}T_{mix}}{V_1}$$

Where

Δn: moles of gas that moved from the lower chamber into the upper chamber to equilibrate pressure

T_{mix}: temperature of gas in the upper chamber after Δn moles of gas from the lower chamber at T_2 mixed with the gas in the upper chamber at T_1

Combining and solving for Δn yields

$$\Delta n = \frac{V_1(n_2 + n_{csc})T_2 - V_2 n_1 T_1}{T_2(V_2 + V_1)}$$

which can be generalized using the relationships for T_1, T_2, n_1, and n_2 to yield:

$$\Delta n = \frac{V_1\left[\frac{(E_{csc} - E_{ke} - E_{PV})}{c_V} + T_i \cdot n_{csc}\right] - V_2\frac{\left(E_{ke} - E_{loss} + E_{PV}\right)}{c_V}}{\left[\frac{(E_{csc} - E_{ke} - E_{PV})/c_V}{\left(\frac{P_i V_2}{RT_i}\right) + n_{csc}} + T_i\right]\left(V_2 + V_1\right)}$$

The gaseous water produced by the explosive reaction requires special treatment in order to account for condensation. The dew point of the gas in the upper chamber is calculated to be 319 K (assuming initial dry air) and the average sample temperature was measured to be 296 K so water likely condensed in the sample train. In order to account for this, the moles of gas in the upper chamber, $n_{chamber}$, must also be corrected by the moles of water that could condense:

$n_{chamber} = n_1 + \Delta n - n_{cond}$

$n_{chamber}$: moles of gas in upper aerosol chamber when aerosols are formed and mixed

n_{cond}: moles of water that would be condensed by cooling the gas to the average sample temperature.

$$n_{cond} = \Delta n \frac{n_{H2O}}{n_2 + n_{csc}} - \left(n_1 + \Delta n\right)\frac{P_{sat}}{P_{avg}}$$

n_{H_2O} : moles of H_2O produced by explosive

P_{sat} : partial pressure of water in saturated sample stream at T_{avg} and P_{avg}

Release fraction parameter discussion

V_1 & V_2: Volume of the upper and lower chambers. These parameters are of vital importance in determining the moles of gas into which the aerosols were dispersed. These volumes are best determined by direct measurement such as measuring the mass of water required to fill the chambers. 2000 kg floor scales are available with resolution of 0.5 kg (or +/- 0.5 liter). If the volume is determined by dimensional drawings, the tolerance on the large steel components is +/- 1/8" leading to a volume error of +/- 2 liters. Dimensional drawings of the most recently used double chamber apparatus were obtained from the fabrication vendor and are shown in Drawings A1 and A2.

E_{csc}: Total energy of detonation of the CSC. This is the product of 5339 J/g (+/- 1 J/g) and 72.5 g (+/- 0.5 g) of explosive used. The energy release assumes negligible combustion of the carbon aerosols produced as advised by the explosives SME Will Wente. The validity of the assumption is supported by the production of copious amounts of carbon black with each detonation. However, when conducted with an atmosphere of air there is 10% excess O_2 present for

complete carbon particle oxidation. Conducting these experiments in a nitrogen atmosphere would eliminate this uncertainty.

E_{ke}: Kinetic energy injected into upper chamber in the form of a fast moving projectile. The projectile hits and fragments the target fuel rod. The fragmentation process heats the fragments which in turn heat the gas. About half of this energy is assumed to heat the gas in the upper chamber in this manner. The other half is assumed lost to the stop block

E_{loss}: Amount of kinetic energy lost to the stop block. Assumed to be half the KE with an error of the same magnitude,

E_{PV}: The isentropic expansion energy loss to the lower chamber gas and gain to upper chamber gas.

n_{csc}: Total moles of gas produced by the CSC detonation. This is determined by the composition and mass of the explosive both of which are well characterized.

n_{cond}: Moles of water that would be condensed by cooling the gas to the average sample temperature. The gaseous products of the explosive reaction are 40% water vapor and there is uncertainty in knowing the fate of water vapor in the previous experiments. The calculation scheme outlined above predicts a dew point of 46 C in the aerosol chamber but the gas sample temperature was measured to be 23 C which is likely the temperature of the massive, unheated chamber walls. Moisture must have condensed on the walls of the chamber and sampling train. Operating the experiment with the chamber and sample train heated to 50 C would eliminate this problem.

P_i, T_i: Initial pressure and temperature of the gas in the chambers when the chamber was sealed. These measurements were not documented for the previous experiments so assumption of room temperature is needed.

P_{avg}, T_{avg}: Average pressure and temperature of the sample gas drawn through the impactors. The pressure was dropping rapidly during sampling which requires integration of the P(t) curve. Since the data files were not located, the integration was done graphically.

t_{sample}: Time duration for sampling. Sampling was controlled by the data acquisition system via two control valves. The downstream "impactor" control valve was fast acting but the upstream "detonation ball valve" required 3 seconds to fully open. The use of the slow acting ball valve to initiate sampling introduces considerable uncertainty in the sample time.

m_{tot}: Total mass of fuel rod component (*e.g.* U, Zr, Cs or Ru) disrupted by the CSC projectile. Typically determined by before and after weight measurements. For the spent fuel experiments, post weight measurement will not be possible. The amount of rod disrupted will be determined by x-ray imaging.

$m_{stage,i}$: Mass of target component (*e.g.* U, Zr, Cs or Ru) collected on stage *i*. Determined chemically by complete acid digestion and ICP/MS analysis. Precision and accuracy of method well defined. Some blank measurements available.

$\eta_{stage,i}$: Aerosol collection efficiency of stage *i*. Well characterized by impactor manufacturer.

$\eta_{loss,i}$: Inlet sampling efficiency factor for the sample train (tubing, valves, LPS) leading up to the impactor stages. This factor accounts for particles that would have been collected on a stage had they not been lost before reaching the impactor. This parameter is difficult to determine. The inlet loss for Marple impactor with cowl but without the visor has been determined. The inlet was 100% efficient for particles 4 μm and smaller and 95% efficient for 10 μm particles. However, the cowl inlet is designed for open air sampling. The inline inlet used in these experiments is significantly different and with 34.5 inches of 3/8" tubing used to transfer the sample to the impactor, losses are likely greater. The previous investigators suggested losses of up to 50%. Condensation in the sample lines would of course exasperate the problem. The only way to get a realistic handle on this parameter is to measure it.

A.2 Previous Analytic Approach with Corrections

The previous calculation can be improved by correcting the input information such as the chamber volume and sampling time. The calculation can be further improved by correcting the model to represent the physics of the experiment better such as correcting the gas volumes in the chamber and sample so they are on the same temperature and pressure basis and accounting for known aerosol losses in the sample train and impactor. Further correction is not practical. The model still inherently assumes all of the aerosols are generated and contained in a single chamber without possibility of loss. Essentially, the method calculates the aerosols contained in the aerosol chamber at the time of sampling. With the double chamber apparatus a significant amount of aerosol laden gas flows from the upper aerosol chamber into the lower chamber. These lost aerosols are inherently not counted by the previous methodology.

$$\mathrm{RF}_{\mathrm{corrected}} = \frac{T_{avg}}{T_{chamber}} \frac{V_1}{m_{tot} Q t_{sample}} \sum_i \frac{m_{stage,\,i}}{\eta_{stage,\,i} \eta_{loss,\,i}} = \frac{T_{avg}}{T_{chamber}} \frac{V_1}{V_{sample}} \frac{\sum_i \frac{m_{stage,\,i}}{\eta_{stage,\,i} \eta_{loss,\,i}}}{m_{tot}}$$

V_1 = 99.1 liters

$T_{chamber} \approx 600$ K

$P_{avg} = 1.93 \times 10^5$ Pa

$T_{avg} = 299.8$ K

Q = 1.920 lpm = 0.0320 lps

$t_{sample} = 8.99$ sec

$m_{tot} = 26{,}360$ mg

$\sum_i m_{stage,\,i} = 1.0276$ mg

$\eta_{stage,\,i} = 0.955$

$\eta_{loss,\,i} = 0.7$

$RF_{corrected} = 0.0100$

The corrected RF for the previous methodology is 25% lower than the RF calculated by the new methodology. This is due to the flow of aerosol-laden gas from the upper chamber into the lower chamber prior to and during aerosol sampling.

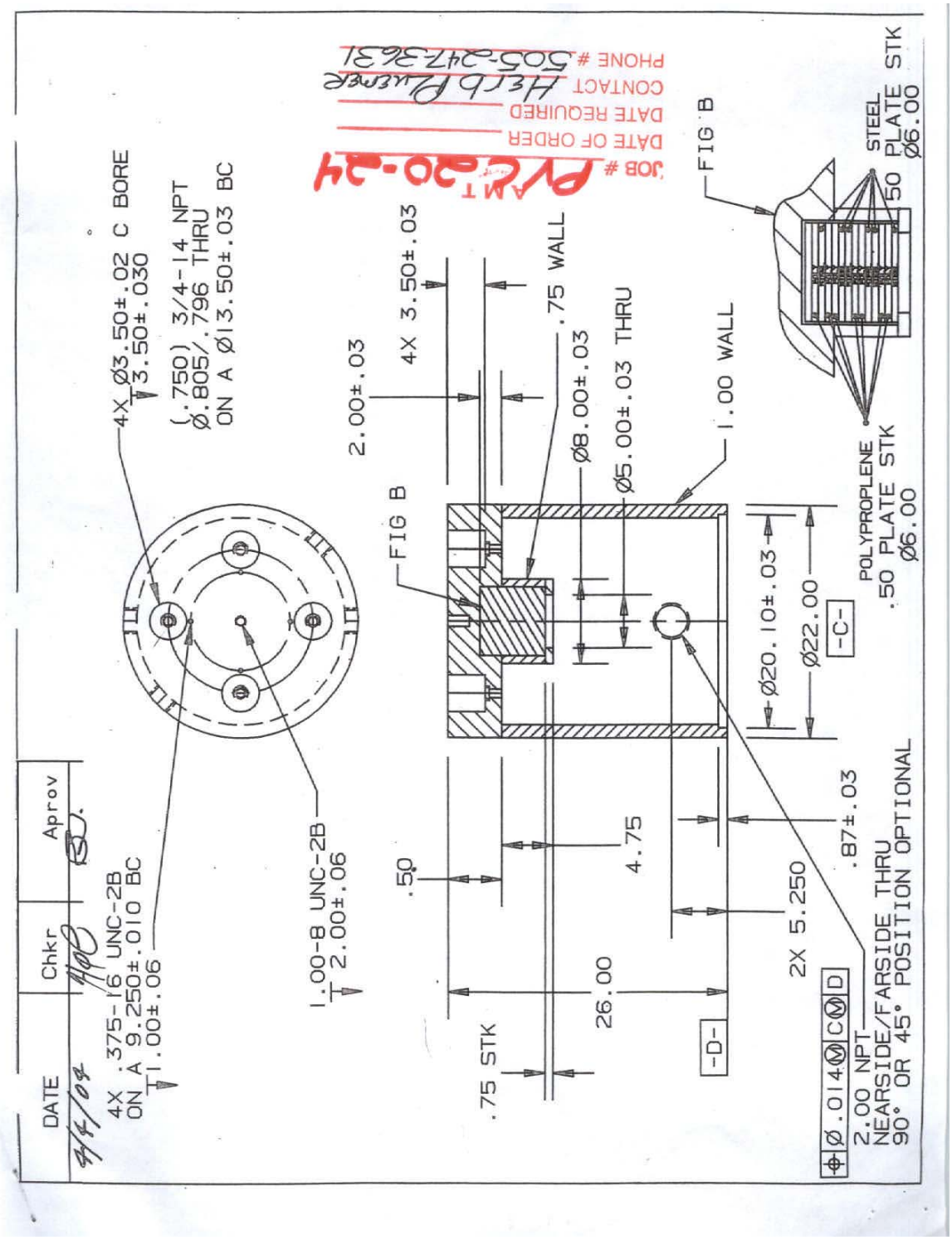

Drawing A.1 Drawing of the upper aerosol chamber of the spent fuel apparatus.

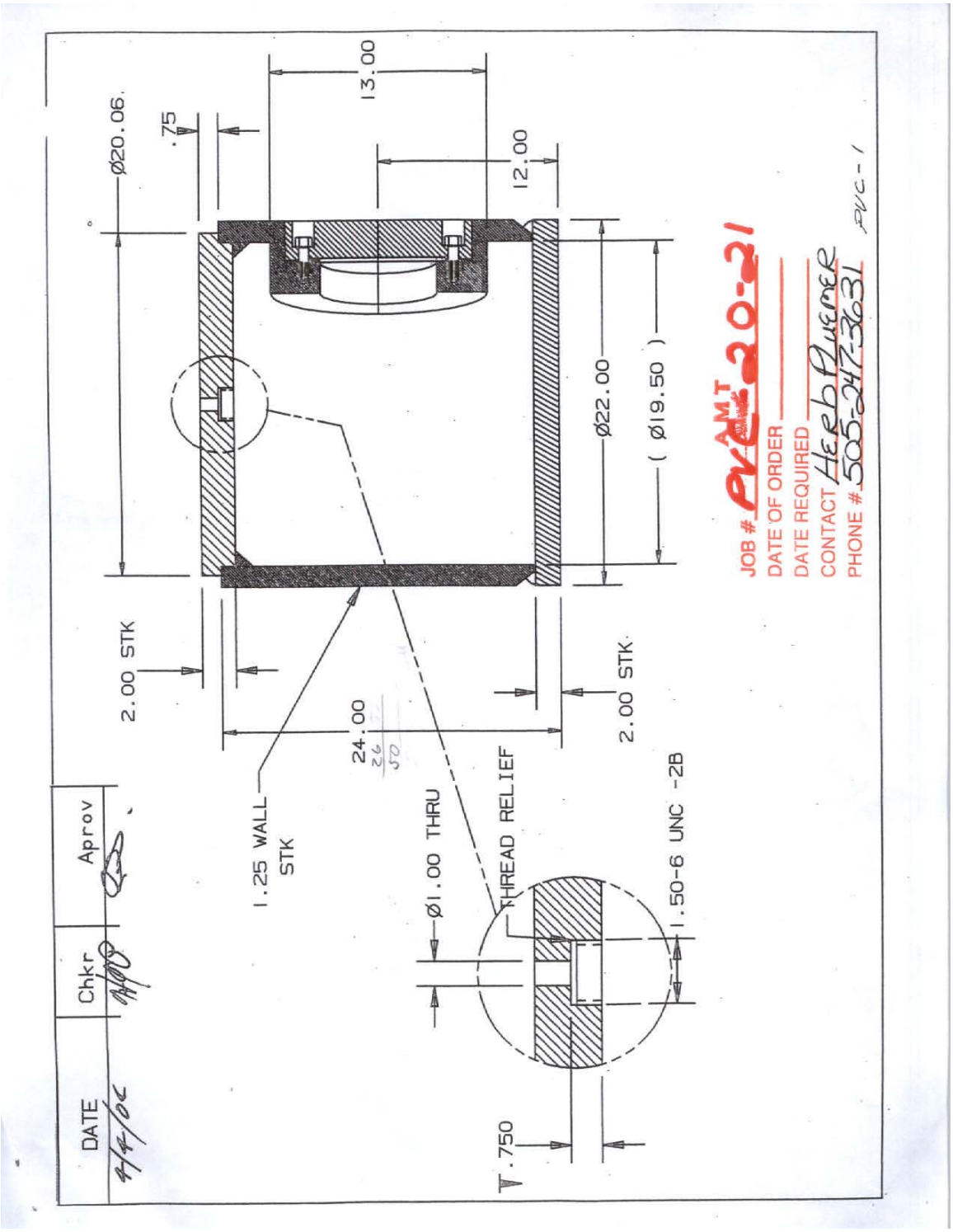

Drawing A.2 Drawing of the lower explosive chamber of the spent fuel apparatus.

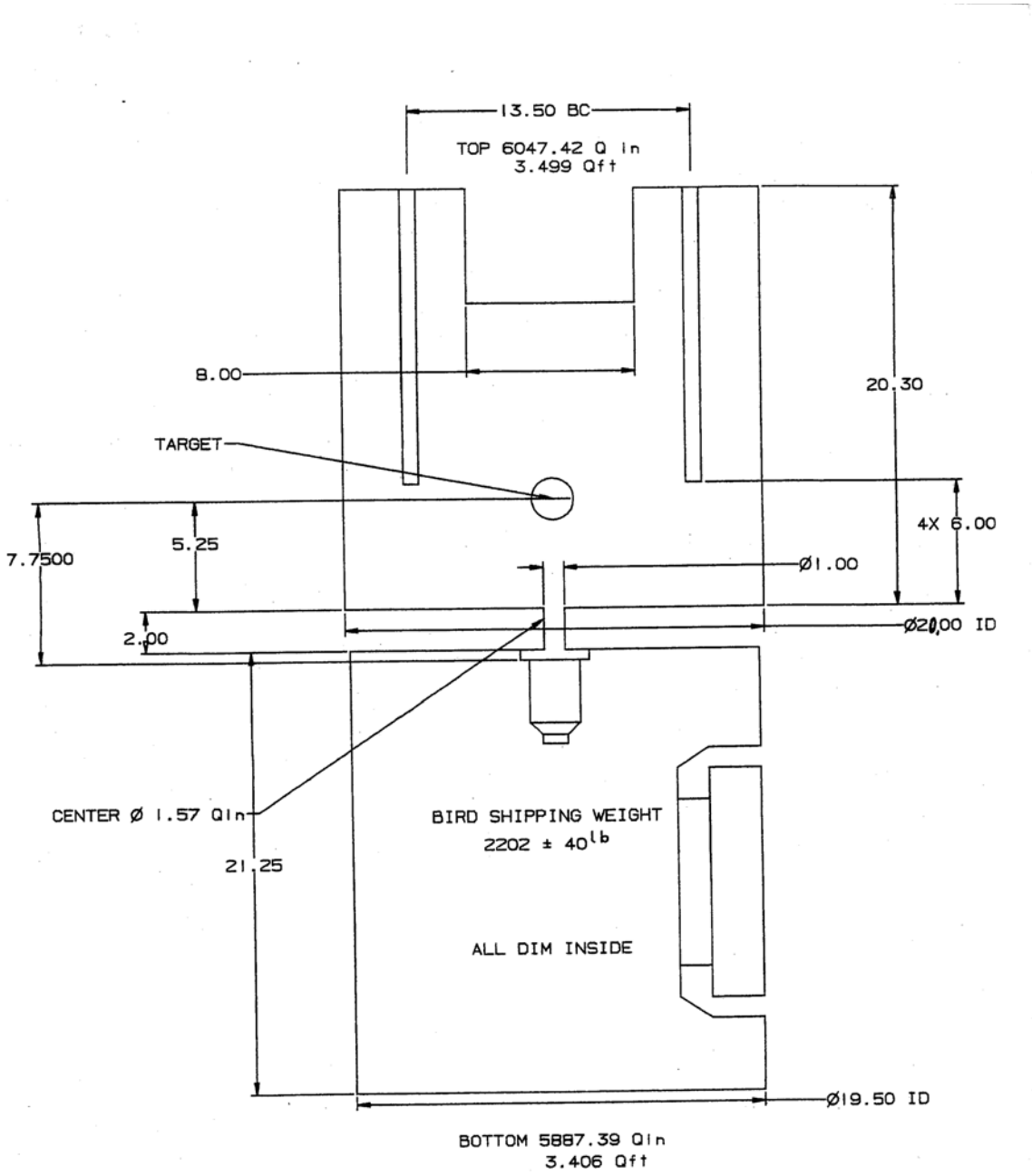

Drawing A.3 Internal dimensions and CAD volume analysis of the spent fuel apparatus.

This page intentionally blank

APPENDIX B – ERROR PROPAGATION ANALYSIS

The error and uncertainty inherent to an experimental result are critical to the accurate interpretation of the data. Therefore, the uncertainties in the experimental measurements are estimated in this section. Results of this analysis are given, followed by a general description of the method used and a brief explanation of the source of each reported measurement uncertainty.

The overall standard uncertainty of an indirect measurement y, dependent on N indirect measurements x_i, is defined in Equation B.1. The standard uncertainty associated with an indirect measurement is analogous to the standard deviation of a statistical population.

$$u^2 = \sum_{i=1}^{N} \left(\frac{\partial y}{\partial x_i} u_i \right)^2 \qquad \text{B.1}$$

Here, u is used to define the standard uncertainty of a measurement.

The expanded uncertainty U is reported in this appendix and defines the bounds that include 95% of the possible data. The expanded uncertainty is usually defined as some multiple of the standard uncertainty. For purposes of this report, all uncertainty measurements are assumed to behave according to a normal distribution. Therefore, Equation B.2 shows the definition of the expanded uncertainty as used in the following sections for a 95% confidence interval, where the factor of 1.96 has been rounded to a value of 2.

$$U = 2 \cdot u \qquad \text{B.2}$$

B.1 Formulation of Uncertainty in Respirable Fraction

The uncertainty in the respirable fraction was determined using error propagation analysis (EPA). Eqaution B.3 gives the relationship of the release fraction to the underlying measurements. A number of these quantities were not directly measured but were estimated based on constitutive relationships or informed guesses. These quantities include Δn, n_{cond}, and η_{loss}.

$$\mathrm{RF} = \frac{\left(n_1 + \Delta n - n_{cond}\right) \mathrm{R} T_{avg}}{m_{tot} Q t_{sample} P_{avg}} \sum_i \frac{m_{stage,\,i}}{\eta_{stage,\,i} \eta_{loss,\,i}} \qquad \text{B.3}$$

Table B.1 summarizes the values used to determine the overall uncertainty of the respirable fraction. Entries with an asterisk were calculated from secondary error analyses. All uncertainty values are explained in more detail in the listed sections.

Table B.1 Measurement uncertainties for RF.

Measurement, x_i	**Standard Uncertainty, u_i**	**Section Containing Explanation**
Initial chamber moles, n_1	0.09 moles	B.1.1
Influx of moles, Δn	0.10 moles	B.1.2
Moles of H_2O condensate, n_{cond}	0.02 moles	B.1.3
Average sample temperature, T_{avg}	2 K	B.1.4
Disrupted rod mass, m_{tot}	0.5 g (DU), 0.15 g (Zr), 5E-5 g (Cs, Ru)	B.1.5
Sample flow rate, Q	7.5E-8 – 1.0E-6 m^3/s	B.1.6
Sample time, t_{sample}	0.25 s	B.1.7
Average test pressure, P_{avg}	1.0E4 – 3.2E4 Pa	B.1.8
Stage mass, $m_{stage,\,i}$	1.0E-6 g (DU), 1.0E-7 g (Zr), 1.3E-8 g (Cs), 5.0E-8 g (Ru)	B.1.9
Stage efficiency coefficient, $\eta_{stage,\,i}$	0.005	B.1.10
Inlet efficiency coefficient, $\eta_{loss,\,i}$	0.15	B.1.11

B.1.1 Uncertainty in Initial Chamber Moles, n_1

The initial moles in the upper chamber are calculated using the ideal gas law from the initial pressure, initial temperature, and chamber volume. The measurement uncertainties are listed for each of these parameters in Table B.2. The uncertainty in moles of the lower chamber were calculated in the same manner.

Table B.2 Measurement uncertainties for n_1.

Measurement, x_i	**Standard Uncertainty, u_i**	**Section Containing Explanation**
Initial chamber pressure, P_i	1400 Pa	B.1.1.1
Initial chamber temperature, T_i	2 K	B.1.1.2
Chamber volume, V_1	0.002 m^3	B.1.1.3

B.1.1.1 Uncertainty in Initial Chamber Pressure

The expanded uncertainty in the initial chamber pressure was taken as the manufacturer's stated limit of ±0.2% of full scale, or 2800 Pa. The standard uncertainty is half this amount, or 1400 Pa.

B.1.1.2 Uncertainty in Initial Chamber Temperature

The initial chamber temperature was assumed to be the average of the four thermocouples in the Marple sample trains. The sample temperatures were measured using a K-type thermocouples, which have a generally-accepted, expanded uncertainty of 2.2 K. A more conservative estimate of the standard uncertainty of 2 K was chosen for these error estimates. This higher uncertainty accounts for system variations and error inherent to the device.

B.1.1.3 Uncertainty in Chamber Volume

The chamber volume was calculated from drawings obtained from the manufacturer. The manufacturer indicated that the critical dimensions in the drawings were accurate to within ±3.175 mm (0.125 in.). Because no as-built drawings or other documentation pertaining to the accuracy of the chamber dimensions were found, the dimensions were assumed to be accurate to within twice this amount. This dimensional uncertainty translates to an expanded uncertainty of ±0.004 m^3. This calculation also applies to the lower chamber volume, V_2.

B.1.2 Uncertainty in Influx of Moles, Δn

The influx of moles from the lower chamber was calculated according the equation outlined in Appendix A on page 43 of this report. The measurement uncertainties are listed for each of the underlying parameters in Table B.3.

Table B.3 Measurement uncertainties for Δn.

Measurement, x_i	**Standard Uncertainty, u_i**	**Section Containing Explanation**
Chamber volume, V_1	0.002 m^3	B.1.1.3
Chamber volume, V_2	0.002 m^3	B.1.1.3
CSC explosive energy, E_{csc}	1340 J	B.1.2.1
CSC kinetic energy, E_{ke}	10,700 J	B.1.2.2
Flow work energy, E_{PV}	7,000 J	B.1.2.3
Initial chamber pressure, P_i	1400 Pa	B.1.1.1
Initial chamber temperature, T_i	2 K	B.1.1.2
Moles of combustion gas, n_{csc}	10,000 – 32,000 Pa	B.1.2.4

B.1.2.1 Uncertainty in Conical Shape Charge Explosive Energy

The expanded uncertainty in the explosive energy released by the CSC is based on the uncertainty in the weight of the explosive of ±0.5 g. This amount translates to ±2,770 J, which is twice the standard uncertainty.

B.1.2.2 Uncertainty in Conical Shape Charge Kinetic Energy

The kinetic energy of the copper jet emanating from CSC is estimated from the mass of the copper and earlier measurements of the jet velocity. Because the kinetic energy is not well known, the expanded uncertainty was assigned such that the value could range from zero to twice the estimated value (*i.e.* the standard uncertainty was set to one half the value of the kinetic energy).

B.1.2.3 Uncertainty in Flow Work Energy

The standard uncertainty in the flow work energy was assumed to be one quarter the calculated value. The 95% confidence interval of the flow work was then 0.5 to 1.5 times E_{PV}.

B.1.2.4 Uncertainty in Moles of Combustion Gas

The uncertainty in the moles of gas from combustion of the explosives were determined from stoichiometry and the expanded uncertainty in the mass of the explosives, ±0.5 g. The uncertainty in mass translates to a standard uncertainty of 0.003 moles in the combustion gases.

B.1.3 Uncertainty in Moles of Condensate, n_{cond}

The moles of condensate was calculated according the equation outlined in Appendix A on page 43 of this report. The measurement uncertainties are listed for each of the underlying parameters in Table B.4.

Table B.4 Measurement uncertainties for n_{cond}.

Measurement, x_i	**Standard Uncertainty, u_i**	**Section Containing Explanation**
Influx of moles, Δn	0.110 moles	B.1.2
Moles H_2O, n_{H2O}	0.001 moles	B.1.3.1
Initial upper chamber moles, n_1	0.091 moles	B.1.1
Initial lower chamber moles, n_2	0.090 moles	B.1.1
Moles of combustion gas, n_{csc}	0.003 moles	B.1.2.4
Saturation pressure, P_{sat}	400 Pa	B.1.3.2
Average chamber pressure, P_{avg}	2 K	B.1.8

B.1.3.1 Uncertainty in Moles of Water from Combustion

The uncertainty in the moles of water produced from the combustion of the explosives was determined from stoichiometry and the expanded uncertainty in the mass of the explosives, ±0.5 g. The uncertainty in mass translates to a standard uncertainty of 0.001 moles in the water produced from combustion.

B.1.3.2 Uncertainty in the Saturation Pressure of Water

The saturation pressure of water was calculated using the following equation from Bolton (1980). This equation is accurate to within 0.3% for the temperatures in degrees Celsius of -35 to 35 °C. However, the uncertainty in the saturation pressure was taken from the propagated error from the average chamber temperature, which was 2 K. The resulting standard uncertainty in the saturation pressure was 400 Pa.

$$P_{sat} = 611.2 \cdot e^{(17.67 \cdot [T/(T+243.5)])}$$

B.1.4 Uncertainty in Average Sample Temperature, T_{avg}

The average sample temperature was determined by numerically integrating the temperature history of the each Marple and averaging these values together for each test. The error associated with the numerical integration was insignificant compared to the error of the thermocouples of 2 K, which is the same as reported in B.1.1.2.

B.1.5 Uncertainty in Disrupted Rod Mass, m_{tot}

The total mass of fuel rod component (*e.g.* U, Zr, Cs or Ru) disrupted by the CSC projectile as determined by before and after weight and length measurement of the test rodlet. The weight measurement was only made for tests 3-5B and 3-1C. The mass of disrupted uranium was reported to a precision of 0.1 g, but the expanded uncertainty was taken as 1 g (standard uncertainty = 0.5 g) due to the discrepancies in the test records and documentation. The disrupted mass of Zr was based on a length measurement. The standard uncertainty of 0.15 g is based on a standard uncertainty of 1 mm in the length measurement. The standard uncertainty of the initial mass of Cs and Ru is half the reported precision of the initial mass of 0.1 mg.

B.1.6 Uncertainty in Sample Flow Rate, Q

The volumetric flow rate through each sample system was controlled by a critical flow orifice. Each orifice was calibrated with a bubble flow meter a number of times including just before a test. The critical flow should be independent of gas pressure and only weakly dependent on the gas temperature. However, the various calibrations demonstrated considerable variability. The variability is due to temperature and pressure dependence of the gas flow through the bubble meter. Thus, variation in atmospheric pressure and ambient temperature will affect the bubble meter reading. Unfortunately, atmospheric pressure and ambient temperature were not recorded. The standard uncertainty of the critical flow rate was taken as the standard deviation of all the flow calibrations made for a given orifice as recorded in the project lab book.

B.1.7 Uncertainty in Sample Time, t_{sample}

The relatively large uncertainty in the sample collection time was due to the use of a control valve that took almost three seconds to fully open and 1 to 1.5 seconds to allow any flow. The use of this slow acting valve resulted in the actual sample time being a full second less than assumed by the original investigators. The variability of the valve opening was about 0.5 seconds so the standard uncertainty was taken as 0.25 seconds.

B.1.8 Uncertainty in Average Test Pressure, P_{avg}

The average sample pressure was determined by numerically integrating the pressure history of the each Marple and averaging these values together for each test. The error associated with the numerical integration was insignificant compared to the standard deviation of the four Marple values in each test. The standard deviation was also much larger than the manufacturer's stated uncertainty of 0.2% of full scale. The standard uncertainty was assumed to be the standard deviation of the four Marples from each test.

B.1.9 Uncertainty in Stage Mass, $m_{stage,\,i}$

The uncertainty in stage mass was determined by the typical quantitation limit of the inductively coupled plasma mass spectroscopy (ICP-MS) chemical analysis. The quantitation limit is the lowest level at which the elemental species may be accurately and reproducibly quantitated. For the uranium analysis, the worst case quantitation limit realized in Test 3-5B was used for all.

B.1.10 Uncertainty in Stage Efficiency Coefficient, $\eta_{stage,\,i}$

The stage efficiency was based on Rader *et al*. where the stage response was determined for the same Marple impactor but with the cowl inlet rather than the inline inlet. An empirical correlation to the data had an average deviation of 0.5%. To account for the use of this

correlation with the inline inlet rather than the cowl inlet, the standard uncertainty was assumed to be twice this value.

B.1.11 Uncertainty in Inlet Efficiency Coefficient, $\eta_{loss,\,i}$

The uncertainty of respirable aerosol losses in the sample line to the impactor was not characterized experimentally and therefore can only be based on anecdotal evidence. In determining the standard uncertainty, the assumption is made that as the aerosol losses increase (*i.e.* loss coefficient decreases), the uncertainty bounds increase up to the physical limit of 100% collection efficiency (*i.e.* nonphysical loss efficiencies of greater than one are not considered). Further assuming that all other experimental errors are adequately represented, η_{loss} was reduced, and $u_{\eta loss}$ consequently increased, until experimental error covered the majority of the statistical variation of the data in each of the three test series.

B.2 Uncertainty Tables for All Measurements

The following tables contain the uncertainty values used to calculate the experimental uncertainty in RF for all elements. The contribution column gives the fraction that each component contributes to the overall uncertainty. The single less than sign indicates that the contribution is between 0.01 and 0.001. The double less than sign, *i.e.* much less than, denotes that the contribution is less than 0.001.

B.2.1 Depleted Uranium

Table B.5 Error propagation analysis of depleted uranium in Marple 1 impactor for test 3-2A.

Measurement, x_i	Units	Value	Standard uncertainty, u_i	Influence coefficient ($u_i \cdot [(\partial RF/\partial x_i)/RF]$)	Contribution
n_1	mol	3.38	0.09	0.018	< 0.01
Δn	mol	1.92	0.10	0.020	< 0.01
n_{cond}	mol	0.23	0.02	0.005	<< 0.01
T_{avg}	K	299.8	2	0.007	< 0.01
m_{tot}	g	26.36	0.5	0.019	< 0.01
Q	m^3/s	3.2E-05	1.6E-07	0.005	<< 0.01
t_{sample}	s	9.0	0.25	0.028	0.02
P_{avg}	Pa	193000	24000	0.124	0.39
$m_{stage,4}$	g	8.16E-05	1.0E-06	0.001	<< 0.01
$\eta_{stage,4}$	--	0.93	0.005	0.000	<< 0.01
$\eta_{loss,4}$	--	0.7	0.15	0.017	< 0.01
$m_{stage,5}$	g	6.81E-04	1.0E-06	0.001	<< 0.01
$\eta_{stage,5}$	--	0.95	0.005	0.004	<< 0.01
$\eta_{loss,5}$	--	0.7	0.15	0.143	0.52
$m_{stage,6}$	g	1.78E-04	1.0E-06	0.001	<< 0.01
$\eta_{stage,6}$	--	0.97	0.005	0.001	<< 0.01
$\eta_{loss,6}$	--	0.7	0.15	0.037	0.03
$m_{stage,7}$	g	3.60E-05	1.0E-06	0.001	<< 0.01
$\eta_{stage,7}$	--	0.98	0.005	0.000	<< 0.01
$\eta_{loss,7}$	--	0.7	0.15	0.007	< 0.01
$m_{stage,8}$	g	4.48E-05	1.0E-06	0.001	<< 0.01
$\eta_{stage,8}$	--	0.99	0.005	0.000	<< 0.01
$\eta_{loss,8}$	--	0.7	0.15	0.009	< 0.01
$m_{stage,9}$	g	6.27E-06	1.0E-06	0.001	<< 0.01
$\eta_{stage,9}$	--	1	0.005	0.000	<< 0.01
$\eta_{loss,9}$	--	0.7	0.15	0.001	<< 0.01
RF	--	0.0133	0.003	0.198	1.00

Table B.6 Error propagation analysis of depleted uranium in Marple 2 impactor for test 3-2A.

Measurement, x_i	Units	Value	Standard uncertainty, u_i	Influence coefficient ($u_i \cdot [(\partial RF/\partial x_i)/RF]$)	Contribution
n_1	mol	3.38	0.09	0.018	0.01
Δn	mol	1.92	0.10	0.020	0.01
n_{cond}	mol	0.23	0.02	0.005	<< 0.01
T_{avg}	K	299.8	2	0.007	< 0.01
m_{tot}	g	26.36	0.5	0.019	0.01
Q	m^3/s	2.8E-05	7.5E-08	0.003	<< 0.01
t_{sample}	s	9.0	0.25	0.028	0.03
P_{avg}	Pa	193000	24000	0.124	0.52
$m_{stage,4}$	g	1.24E-05	1.0E-06	0.002	<< 0.01
$\eta_{stage,4}$	--	0.93	0.005	0.000	<< 0.01
$\eta_{loss,4}$	--	0.7	0.15	0.006	< 0.01
$m_{stage,5}$	g	1.71E-04	1.0E-06	0.002	<< 0.01
$\eta_{stage,5}$	--	0.95	0.005	0.002	<< 0.01
$\eta_{loss,5}$	--	0.7	0.15	0.076	0.20
$m_{stage,6}$	g	1.18E-04	1.0E-06	0.002	<< 0.01
$\eta_{stage,6}$	--	0.97	0.005	0.001	<< 0.01
$\eta_{loss,6}$	--	0.7	0.15	0.052	0.09
$m_{stage,7}$	g	1.24E-04	1.0E-06	0.002	<< 0.01
$\eta_{stage,7}$	--	0.98	0.005	0.001	<< 0.01
$\eta_{loss,7}$	--	0.7	0.15	0.053	0.10
$m_{stage,8}$	g	5.63E-05	1.0E-06	0.002	<< 0.01
$\eta_{stage,8}$	--	0.99	0.005	0.001	<< 0.01
$\eta_{loss,8}$	--	0.7	0.15	0.024	0.02
$m_{stage,9}$	g	8.09E-06	1.0E-06	0.002	<< 0.01
$\eta_{stage,9}$	--	1	0.005	0.000	<< 0.01
$\eta_{loss,9}$	--	0.7	0.15	0.003	<< 0.01
RF	--	0.0072	0.001	0.171	1.00

Table B.7 Error propagation analysis of depleted uranium in Marple 4 impactor for test 3-2A.

Measurement, x_i	Units	Value	Standard uncertainty, u_i	Influence coefficient ($u_i \cdot [(\partial RF/\partial x_i)/RF]$)	Contribution
n_1	mol	3.38	0.09	0.018	0.01
Δn	mol	1.92	0.10	0.020	0.01
n_{cond}	mol	0.23	0.02	0.005	<< 0.01
T_{avg}	K	299.8	2	0.007	< 0.01
m_{tot}	g	26.36	0.5	0.019	0.01
Q	m^3/s	2.9E-05	1.8E-07	0.006	< 0.01
t_{sample}	s	9.0	0.25	0.028	0.02
P_{avg}	Pa	193000	24000	0.124	0.49
$m_{stage,4}$	g	7.61E-05	1.0E-06	0.002	<< 0.01
$\eta_{stage,4}$	--	0.93	0.005	0.001	<< 0.01
$\eta_{loss,4}$	--	0.7	0.15	0.027	0.02
$m_{stage,5}$	g	2.98E-04	1.0E-06	0.002	<< 0.01
$\eta_{stage,5}$	--	0.95	0.005	0.002	<< 0.01
$\eta_{loss,5}$	--	0.7	0.15	0.102	0.33
$m_{stage,6}$	g	1.32E-04	1.0E-06	0.002	<< 0.01
$\eta_{stage,6}$	--	0.97	0.005	0.001	<< 0.01
$\eta_{loss,6}$	--	0.7	0.15	0.044	0.06
$m_{stage,7}$	g	8.23E-05	1.0E-06	0.002	<< 0.01
$\eta_{stage,7}$	--	0.98	0.005	0.001	<< 0.01
$\eta_{loss,7}$	--	0.7	0.15	0.027	0.02
$m_{stage,8}$	g	3.81E-05	1.0E-06	0.002	<< 0.01
$\eta_{stage,8}$	--	0.99	0.005	0.000	<< 0.01
$\eta_{loss,8}$	--	0.7	0.15	0.013	< 0.01
$m_{stage,9}$	g	6.31E-06	1.0E-06	0.002	<< 0.01
$\eta_{stage,9}$	--	1	0.005	0.000	<< 0.01
$\eta_{loss,9}$	--	0.7	0.15	0.002	<< 0.01
RF	--	0.0091	0.002	0.176	1.00

Table B.8 Error propagation analysis of depleted uranium in Marple 1 impactor for test 3-5B.

Measurement, x_i	Units	Value	Standard uncertainty, u_i	Influence coefficient ($u_i \cdot [(\partial RF/\partial x_i)/RF]$)	Contribution
n_1	mol	3.40	0.09	0.018	< 0.01
Δn	mol	1.92	0.10	0.020	< 0.01
n_{cond}	mol	0.25	0.02	0.004	<< 0.01
T_{avg}	K	296.2	2	0.007	<< 0.01
m_{tot}	g	26.36	0.5	0.019	< 0.01
Q	m^3/s	3.1E-05	2.4E-07	0.008	< 0.01
t_{sample}	s	9.0	0.25	0.028	0.02
P_{avg}	Pa	205000	32000	0.156	0.52
$m_{stage,4}$	g	4.99E-05	1.0E-06	0.003	<< 0.01
$\eta_{stage,4}$	--	0.93	0.005	0.001	<< 0.01
$\eta_{loss,4}$	--	0.7	0.15	0.027	0.02
$m_{stage,5}$	g	2.52E-04	1.0E-06	0.002	<< 0.01
$\eta_{stage,5}$	--	0.95	0.005	0.003	<< 0.01
$\eta_{loss,5}$	--	0.7	0.15	0.134	0.38
$m_{stage,6}$	g	8.42E-05	1.0E-06	0.002	<< 0.01
$\eta_{stage,6}$	--	0.97	0.005	0.001	<< 0.01
$\eta_{loss,6}$	--	0.7	0.15	0.044	0.04
$m_{stage,7}$	g	5.83E-06	1.0E-06	0.002	<< 0.01
$\eta_{stage,7}$	--	0.98	0.005	0.000	<< 0.01
$\eta_{loss,7}$	--	0.7	0.15	0.003	<< 0.01
$m_{stage,8}$	g	1.02E-05	1.0E-06	0.002	<< 0.01
$\eta_{stage,8}$	--	0.99	0.005	0.000	<< 0.01
$\eta_{loss,8}$	--	0.7	0.15	0.005	<< 0.01
$m_{stage,9}$	g	3.44E-06	1.0E-06	0.002	<< 0.01
$\eta_{stage,9}$	--	1	0.005	0.000	<< 0.01
$\eta_{loss,9}$	--	0.7	0.15	0.002	<< 0.01
RF	--	0.0049	0.001	0.217	1.00

Table B.9 Error propagation analysis of depleted uranium in Marple 2 impactor for test 3-5B.

Measurement, x_i	Units	Value	Standard uncertainty, u_i	Influence coefficient ($u_i \cdot [(\partial RF/\partial x_i)/RF]$)	Contribution
n_1	mol	3.40	0.09	0.018	< 0.01
Δn	mol	1.92	0.10	0.020	< 0.01
n_{cond}	mol	0.25	0.02	0.004	<< 0.01
T_{avg}	K	296.2	2	0.007	<< 0.01
m_{tot}	g	26.36	0.5	0.019	< 0.01
Q	m^3/s	3.0E-05	5.4E-07	0.018	< 0.01
t_{sample}	s	9.0	0.25	0.028	0.01
P_{avg}	Pa	205000	32000	0.156	0.45
$m_{stage,4}$	g	5.76E-05	1.0E-06	0.001	<< 0.01
$\eta_{stage,4}$	--	0.93	0.005	0.000	<< 0.01
$\eta_{loss,4}$	--	0.7	0.15	0.017	< 0.01
$m_{stage,5}$	g	5.61E-04	1.0E-06	0.001	<< 0.01
$\eta_{stage,5}$	--	0.95	0.005	0.004	<< 0.01
$\eta_{loss,5}$	--	0.7	0.15	0.162	0.49
$m_{stage,6}$	g	8.33E-05	1.0E-06	0.001	<< 0.01
$\eta_{stage,6}$	--	0.97	0.005	0.001	<< 0.01
$\eta_{loss,6}$	--	0.7	0.15	0.024	0.01
$m_{stage,7}$	g	1.83E-05	1.0E-06	0.001	<< 0.01
$\eta_{stage,7}$	--	0.98	0.005	0.000	<< 0.01
$\eta_{loss,7}$	--	0.7	0.15	0.005	<< 0.01
$m_{stage,8}$	g	1.83E-05	1.0E-06	0.001	<< 0.01
$\eta_{stage,8}$	--	0.99	0.005	0.000	<< 0.01
$\eta_{loss,8}$	--	0.7	0.15	0.005	<< 0.01
$m_{stage,9}$	g	4.85E-06	1.0E-06	0.001	<< 0.01
$\eta_{stage,9}$	--	1	0.005	0.000	<< 0.01
$\eta_{loss,9}$	--	0.7	0.15	0.001	<< 0.01
RF	--	0.0095	0.002	0.232	1.00

Table B.10 Error propagation analysis of depleted uranium in Marple 3 impactor for test 3-5B.

Measurement, x_i	Units	Value	Standard uncertainty, u_i	Influence coefficient ($u_i \cdot [(\partial RF/\partial x_i)/RF]$)	Contribution
n_1	mol	3.40	0.09	0.018	< 0.01
Δn	mol	1.92	0.10	0.020	< 0.01
n_{cond}	mol	0.25	0.02	0.004	<< 0.01
T_{avg}	K	296.2	2	0.007	<< 0.01
m_{tot}	g	26.36	0.5	0.019	< 0.01
Q	m^3/s	2.9E-05	9.5E-07	0.032	0.02
t_{sample}	s	9.0	0.25	0.028	0.02
P_{avg}	Pa	205000	32000	0.156	0.49
$m_{stage,4}$	g	5.99E-05	1.0E-06	0.001	<< 0.01
$\eta_{stage,4}$	--	0.93	0.005	0.000	<< 0.01
$\eta_{loss,4}$	--	0.7	0.15	0.014	< 0.01
$m_{stage,5}$	g	6.02E-04	1.0E-06	0.001	<< 0.01
$\eta_{stage,5}$	--	0.95	0.005	0.003	<< 0.01
$\eta_{loss,5}$	--	0.7	0.15	0.142	0.41
$m_{stage,6}$	g	1.61E-04	1.0E-06	0.001	<< 0.01
$\eta_{stage,6}$	--	0.97	0.005	0.001	<< 0.01
$\eta_{loss,6}$	--	0.7	0.15	0.037	0.03
$m_{stage,7}$	g	6.32E-05	1.0E-06	0.001	<< 0.01
$\eta_{stage,7}$	--	0.98	0.005	0.000	<< 0.01
$\eta_{loss,7}$	--	0.7	0.15	0.014	< 0.01
$m_{stage,8}$	g	2.19E-05	1.0E-06	0.001	<< 0.01
$\eta_{stage,8}$	--	0.99	0.005	0.000	<< 0.01
$\eta_{loss,8}$	--	0.7	0.15	0.005	<< 0.01
$m_{stage,9}$	g	4.75E-06	1.0E-06	0.001	<< 0.01
$\eta_{stage,9}$	--	1	0.005	0.000	<< 0.01
$\eta_{loss,9}$	--	0.7	0.15	0.001	<< 0.01
RF	--	0.0119	0.003	0.222	1.00

Table B.11 Error propagation analysis of depleted uranium in Marple 4 impactor for test 3-5B.

Measurement, x_i	Units	Value	Standard uncertainty, u_i	Influence coefficient ($u_i \cdot [(\partial RF/\partial x_i)/RF]$)	Contribution
n_1	mol	3.40	0.09	0.018	< 0.01
Δn	mol	1.92	0.10	0.020	< 0.01
n_{cond}	mol	0.25	0.02	0.004	<< 0.01
T_{avg}	K	296.2	2	0.007	<< 0.01
m_{tot}	g	26.36	0.5	0.019	< 0.01
Q	m^3/s	2.8E-05	1.4E-07	0.005	<< 0.01
t_{sample}	s	9.0	0.25	0.028	0.02
P_{avg}	Pa	205000	32000	0.156	0.53
$m_{stage,4}$	g	6.21E-05	1.0E-06	0.001	<< 0.01
$\eta_{stage,4}$	--	0.93	0.005	0.000	<< 0.01
$\eta_{loss,4}$	--	0.7	0.15	0.014	< 0.01
$m_{stage,5}$	g	6.02E-04	1.0E-06	0.001	<< 0.01
$\eta_{stage,5}$	--	0.95	0.005	0.003	<< 0.01
$\eta_{loss,5}$	--	0.7	0.15	0.132	0.38
$m_{stage,6}$	g	1.85E-04	1.0E-06	0.001	<< 0.01
$\eta_{stage,6}$	--	0.97	0.005	0.001	<< 0.01
$\eta_{loss,6}$	--	0.7	0.15	0.040	0.03
$m_{stage,7}$	g	6.07E-05	1.0E-06	0.001	<< 0.01
$\eta_{stage,7}$	--	0.98	0.005	0.000	<< 0.01
$\eta_{loss,7}$	--	0.7	0.15	0.013	< 0.01
$m_{stage,8}$	g	6.54E-05	1.0E-06	0.001	<< 0.01
$\eta_{stage,8}$	--	0.99	0.005	0.000	<< 0.01
$\eta_{loss,8}$	--	0.7	0.15	0.014	< 0.01
$m_{stage,9}$	g	8.66E-06	1.0E-06	0.001	<< 0.01
$\eta_{stage,9}$	--	1	0.005	0.000	<< 0.01
$\eta_{loss,9}$	--	0.7	0.15	0.002	<< 0.01
RF	--	0.0132	0.003	0.214	1.00

Table B.12 Error propagation analysis of depleted uranium in Marple 1 impactor for test 3-1C.

Measurement, x_i	Units	Value	Standard uncertainty, u_i	Influence coefficient ($u_i \cdot [(\partial RF/\partial x_i)/RF]$)	Contribution
n_1	mol	3.38	0.09	0.018	0.02
Δn	mol	1.92	0.10	0.020	0.02
n_{cond}	mol	0.25	0.02	0.004	<< 0.01
T_{avg}	K	296.2	2	0.007	< 0.01
m_{tot}	g	28.38	0.5	0.018	0.02
Q	m^3/s	3.6E-05	1.0E-06	0.028	0.04
t_{sample}	s	10.0	0.25	0.025	0.04
P_{avg}	Pa	182000	10000	0.053	0.16
$m_{stage,4}$	g	5.62E-05	1.0E-06	0.001	<< 0.01
$\eta_{stage,4}$	--	0.93	0.005	0.000	<< 0.01
$\eta_{loss,4}$	--	0.7	0.15	0.010	< 0.01
$m_{stage,5}$	g	7.70E-05	1.0E-06	0.001	<< 0.01
$\eta_{stage,5}$	--	0.95	0.005	0.000	<< 0.01
$\eta_{loss,5}$	--	0.7	0.15	0.014	0.01
$m_{stage,6}$	g	5.14E-04	1.0E-06	0.001	<< 0.01
$\eta_{stage,6}$	--	0.97	0.005	0.002	<< 0.01
$\eta_{loss,6}$	--	0.7	0.15	0.089	0.45
$m_{stage,7}$	g	2.43E-04	1.0E-06	0.001	<< 0.01
$\eta_{stage,7}$	--	0.98	0.005	0.001	<< 0.01
$\eta_{loss,7}$	--	0.7	0.15	0.042	0.10
$m_{stage,8}$	g	2.77E-04	1.0E-06	0.001	<< 0.01
$\eta_{stage,8}$	--	0.99	0.005	0.001	<< 0.01
$\eta_{loss,8}$	--	0.7	0.15	0.047	0.13
$m_{stage,9}$	g	7.89E-05	1.0E-06	0.001	<< 0.01
$\eta_{stage,9}$	--	1	0.005	0.000	<< 0.01
$\eta_{loss,9}$	--	0.7	0.15	0.013	< 0.01
RF	--	0.0122	0.002	0.133	1.00

Table B.13 Error propagation analysis of depleted uranium in Marple 3 impactor for test 3-1C.

Measurement, x_i	Units	Value	Standard uncertainty, u_i	Influence coefficient ($u_i \cdot [(\partial RF/\partial x_i)/RF]$)	Contribution
n_1	mol	3.38	0.09	0.018	0.01
Δn	mol	1.92	0.10	0.020	0.01
n_{cond}	mol	0.25	0.02	0.004	<< 0.01
T_{avg}	K	296.2	2	0.007	< 0.01
m_{tot}	g	28.38	0.5	0.018	< 0.01
Q	m^3/s	3.6E-05	9.3E-07	0.026	0.02
t_{sample}	s	10.0	0.25	0.025	0.02
P_{avg}	Pa	182000	10000	0.053	0.09
$m_{stage,4}$	g	1.45E-05	1.0E-06	0.002	<< 0.01
$\eta_{stage,4}$	--	0.93	0.005	0.000	<< 0.01
$\eta_{loss,4}$	--	0.7	0.15	0.005	<< 0.01
$m_{stage,5}$	g	4.89E-04	1.0E-06	0.002	<< 0.01
$\eta_{stage,5}$	--	0.95	0.005	0.004	<< 0.01
$\eta_{loss,5}$	--	0.7	0.15	0.159	0.78
$m_{stage,6}$	g	1.31E-04	1.0E-06	0.001	<< 0.01
$\eta_{stage,6}$	--	0.97	0.005	0.001	<< 0.01
$\eta_{loss,6}$	--	0.7	0.15	0.042	0.05
$m_{stage,7}$	g	1.09E-05	1.0E-06	0.001	<< 0.01
$\eta_{stage,7}$	--	0.98	0.005	0.000	<< 0.01
$\eta_{loss,7}$	--	0.7	0.15	0.003	<< 0.01
$m_{stage,8}$	g	1.32E-05	1.0E-06	0.001	<< 0.01
$\eta_{stage,8}$	--	0.99	0.005	0.000	<< 0.01
$\eta_{loss,8}$	--	0.7	0.15	0.004	<< 0.01
$m_{stage,9}$	g	2.36E-06	1.0E-06	0.001	<< 0.01
$\eta_{stage,9}$	--	1	0.005	0.000	<< 0.01
$\eta_{loss,9}$	--	0.7	0.15	0.001	<< 0.01
RF	--	0.0066	0.001	0.180	1.00

Table B.14 Error propagation analysis of depleted uranium in Marple 4 impactor for test 3-1C.

Measurement, x_i	Units	Value	Standard uncertainty, u_i	Influence coefficient ($u_i \cdot [(\partial RF/\partial x_i)/RF]$)	Contribution
n_1	mol	3.38	0.09	0.018	0.01
Δn	mol	1.92	0.10	0.020	0.02
n_{cond}	mol	0.25	0.02	0.004	<< 0.01
T_{avg}	K	296.2	2	0.007	< 0.01
m_{tot}	g	28.38	0.5	0.018	0.01
Q	m^3/s	3.6E-05	6.4E-07	0.018	0.01
t_{sample}	s	10.0	0.25	0.025	0.03
P_{avg}	Pa	182000	10000	0.053	0.12
$m_{stage,4}$	g	1.01E-04	1.0E-06	0.001	<< 0.01
$\eta_{stage,4}$	--	0.93	0.005	0.001	<< 0.01
$\eta_{loss,4}$	--	0.7	0.15	0.021	0.02
$m_{stage,5}$	g	6.20E-04	1.0E-06	0.001	<< 0.01
$\eta_{stage,5}$	--	0.95	0.005	0.003	<< 0.01
$\eta_{loss,5}$	--	0.7	0.15	0.128	0.68
$m_{stage,6}$	g	2.19E-04	1.0E-06	0.001	<< 0.01
$\eta_{stage,6}$	--	0.97	0.005	0.001	<< 0.01
$\eta_{loss,6}$	--	0.7	0.15	0.044	0.08
$m_{stage,7}$	g	4.89E-05	1.0E-06	0.001	<< 0.01
$\eta_{stage,7}$	--	0.98	0.005	0.000	<< 0.01
$\eta_{loss,7}$	--	0.7	0.15	0.010	< 0.01
$m_{stage,8}$	g	4.42E-05	1.0E-06	0.001	<< 0.01
$\eta_{stage,8}$	--	0.99	0.005	0.000	<< 0.01
$\eta_{loss,8}$	--	0.7	0.15	0.009	< 0.01
$m_{stage,9}$	g	1.39E-05	1.0E-06	0.001	<< 0.01
$\eta_{stage,9}$	--	1	0.005	0.000	<< 0.01
$\eta_{loss,9}$	--	0.7	0.15	0.003	<< 0.01
RF	--	0.0105	0.002	0.154	1.00

B.2.1 Zirconium

Table B.15 Error propagation analysis of zirconium in Marple 1 impactor for test 3-2A.

Measurement, x_i	Units	Value	Standard uncertainty, u_i	Influence coefficient ($u_i \cdot [(\partial RF/\partial x_i)/RF]$)	Contribution
n_1	mol	3.38	0.09	0.018	< 0.01
Δn	mol	1.92	0.10	0.020	0.01
n_{cond}	mol	0.23	0.02	0.005	<< 0.01
T_{avg}	K	299.8	2	0.007	< 0.01
m_{tot}	g	3.54	0.15	0.042	0.06
Q	m^3/s	3.2E-05	1.6E-07	0.005	<< 0.01
t_{sample}	s	9.0	0.25	0.028	0.02
P_{avg}	Pa	193000	24000	0.124	0.47
$m_{stage,4}$	g	9.68E-06	1.0E-07	0.001	<< 0.01
$\eta_{stage,4}$	--	0.93	0.005	0.001	<< 0.01
$\eta_{loss,4}$	--	0.7	0.15	0.024	0.02
$m_{stage,5}$	g	4.36E-05	1.0E-07	0.001	<< 0.01
$\eta_{stage,5}$	--	0.95	0.005	0.003	<< 0.01
$\eta_{loss,5}$	--	0.7	0.15	0.106	0.35
$m_{stage,6}$	g	1.44E-05	1.0E-07	0.001	<< 0.01
$\eta_{stage,6}$	--	0.97	0.005	0.001	<< 0.01
$\eta_{loss,6}$	--	0.7	0.15	0.034	0.04
$m_{stage,7}$	g	6.44E-06	1.0E-07	0.001	<< 0.01
$\eta_{stage,7}$	--	0.98	0.005	0.000	<< 0.01
$\eta_{loss,7}$	--	0.7	0.15	0.015	< 0.01
$m_{stage,8}$	g	7.93E-06	1.0E-07	0.001	<< 0.01
$\eta_{stage,8}$	--	0.99	0.005	0.000	<< 0.01
$\eta_{loss,8}$	--	0.7	0.15	0.019	0.01
$m_{stage,9}$	g	6.69E-06	1.0E-07	0.001	<< 0.01
$\eta_{stage,9}$	--	1	0.005	0.000	<< 0.01
$\eta_{loss,9}$	--	0.7	0.15	0.016	< 0.01
RF	--	0.0085	0.002	0.180	1.00

Table B.16 Error propagation analysis of zirconium in Marple 2 impactor for test 3-2A.

Measurement, x_i	Units	Value	Standard uncertainty, u_i	Influence coefficient ($u_i \cdot [(\partial RF/\partial x_i)/RF]$)	Contribution
n_1	mol	3.38	0.09	0.018	0.01
Δn	mol	1.92	0.10	0.020	0.01
n_{cond}	mol	0.23	0.02	0.005	<< 0.01
T_{avg}	K	299.8	2	0.007	< 0.01
m_{tot}	g	3.54	0.15	0.042	0.06
Q	m^3/s	2.8E-05	7.5E-08	0.003	<< 0.01
t_{sample}	s	9.0	0.25	0.028	0.03
P_{avg}	Pa	193000	24000	0.124	0.55
$m_{stage,4}$	g	4.84E-06	1.0E-07	0.002	<< 0.01
$\eta_{stage,4}$	--	0.93	0.005	0.000	<< 0.01
$\eta_{loss,4}$	--	0.7	0.15	0.019	0.01
$m_{stage,5}$	g	1.74E-05	1.0E-07	0.002	<< 0.01
$\eta_{stage,5}$	--	0.95	0.005	0.002	<< 0.01
$\eta_{loss,5}$	--	0.7	0.15	0.066	0.15
$m_{stage,6}$	g	1.05E-05	1.0E-07	0.002	<< 0.01
$\eta_{stage,6}$	--	0.97	0.005	0.001	<< 0.01
$\eta_{loss,6}$	--	0.7	0.15	0.039	0.05
$m_{stage,7}$	g	1.15E-05	1.0E-07	0.002	<< 0.01
$\eta_{stage,7}$	--	0.98	0.005	0.001	<< 0.01
$\eta_{loss,7}$	--	0.7	0.15	0.042	0.06
$m_{stage,8}$	g	7.57E-06	1.0E-07	0.002	<< 0.01
$\eta_{stage,8}$	--	0.99	0.005	0.001	<< 0.01
$\eta_{loss,8}$	--	0.7	0.15	0.028	0.03
$m_{stage,9}$	g	6.04E-06	1.0E-07	0.002	<< 0.01
$\eta_{stage,9}$	--	1	0.005	0.001	<< 0.01
$\eta_{loss,9}$	--	0.7	0.15	0.022	0.02
RF	--	0.0064	0.001	0.167	1.00

Table B.17 Error propagation analysis of zirconium in Marple 4 impactor for test 3-2A.

Measurement, x_i	Units	Value	Standard uncertainty, u_i	Influence coefficient ($u_i \cdot [(\partial RF/\partial x_i)/RF]$)	Contribution
n_1	mol	3.38	0.09	0.018	0.01
Δn	mol	1.92	0.10	0.020	0.01
n_{cond}	mol	0.23	0.02	0.005	<< 0.01
T_{avg}	K	299.8	2	0.007	< 0.01
m_{tot}	g	3.54	0.15	0.042	0.06
Q	m^3/s	2.9E-05	1.8E-07	0.006	< 0.01
t_{sample}	s	9.0	0.25	0.028	0.03
P_{avg}	Pa	193000	24000	0.124	0.54
$m_{stage,4}$	g	8.30E-06	1.0E-07	0.002	<< 0.01
$\eta_{stage,4}$	--	0.93	0.005	0.001	<< 0.01
$\eta_{loss,4}$	--	0.7	0.15	0.030	0.03
$m_{stage,5}$	g	2.10E-05	1.0E-07	0.002	<< 0.01
$\eta_{stage,5}$	--	0.95	0.005	0.002	<< 0.01
$\eta_{loss,5}$	--	0.7	0.15	0.075	0.20
$m_{stage,6}$	g	1.03E-05	1.0E-07	0.002	<< 0.01
$\eta_{stage,6}$	--	0.97	0.005	0.001	<< 0.01
$\eta_{loss,6}$	--	0.7	0.15	0.036	0.05
$m_{stage,7}$	g	8.54E-06	1.0E-07	0.002	<< 0.01
$\eta_{stage,7}$	--	0.98	0.005	0.001	<< 0.01
$\eta_{loss,7}$	--	0.7	0.15	0.030	0.03
$m_{stage,8}$	g	6.64E-06	1.0E-07	0.002	<< 0.01
$\eta_{stage,8}$	--	0.99	0.005	0.001	<< 0.01
$\eta_{loss,8}$	--	0.7	0.15	0.023	0.02
$m_{stage,9}$	g	5.75E-06	1.0E-07	0.002	<< 0.01
$\eta_{stage,9}$	--	1	0.005	0.000	<< 0.01
$\eta_{loss,9}$	--	0.7	0.15	0.020	0.01
RF	--	0.0064	0.001	0.168	1.00

Table B.18 Error propagation analysis of zirconium in Marple 1 impactor for test 3-5B.

Measurement, x_i	Units	Value	Standard uncertainty, u_i	Influence coefficient ($u_i \cdot [(\partial RF/\partial x_i)/RF]$)	Contribution
n_1	mol	3.40	0.09	0.018	< 0.01
Δn	mol	1.92	0.10	0.020	< 0.01
n_{cond}	mol	0.25	0.02	0.004	<< 0.01
T_{avg}	K	296.2	2	0.007	<< 0.01
m_{tot}	g	3.8	0.15	0.039	0.03
Q	m^3/s	3.1E-05	2.4E-07	0.008	< 0.01
t_{sample}	s	9.0	0.25	0.028	0.02
P_{avg}	Pa	205000	32000	0.156	0.51
$m_{stage,4}$	g	2.93E-06	1.0E-07	0.004	<< 0.01
$\eta_{stage,4}$	--	0.93	0.005	0.001	<< 0.01
$\eta_{loss,4}$	--	0.7	0.15	0.024	0.01
$m_{stage,5}$	g	1.68E-05	1.0E-07	0.004	<< 0.01
$\eta_{stage,5}$	--	0.95	0.005	0.003	<< 0.01
$\eta_{loss,5}$	--	0.7	0.15	0.132	0.36
$m_{stage,6}$	g	6.08E-06	1.0E-07	0.004	<< 0.01
$\eta_{stage,6}$	--	0.97	0.005	0.001	<< 0.01
$\eta_{loss,6}$	--	0.7	0.15	0.047	0.05
$m_{stage,7}$	g	4.21E-07	1.0E-07	0.004	<< 0.01
$\eta_{stage,7}$	--	0.98	0.005	0.000	<< 0.01
$\eta_{loss,7}$	--	0.7	0.15	0.003	<< 0.01
$m_{stage,8}$	g	7.74E-07	1.0E-07	0.004	<< 0.01
$\eta_{stage,8}$	--	0.99	0.005	0.000	<< 0.01
$\eta_{loss,8}$	--	0.7	0.15	0.006	<< 0.01
$m_{stage,9}$	g	2.70E-07	1.0E-07	0.004	<< 0.01
$\eta_{stage,9}$	--	1	0.005	0.000	<< 0.01
$\eta_{loss,9}$	--	0.7	0.15	0.002	<< 0.01
RF	--	0.0023	0.001	0.219	1.00

Table B.19 Error propagation analysis of zirconium in Marple 2 impactor for test 3-5B.

Measurement, x_i	Units	Value	Standard uncertainty, u_i	Influence coefficient ($u_i \cdot [(\partial RF/\partial x_i)/RF]$)	Contribution
n_1	mol	3.40	0.09	0.018	< 0.01
Δn	mol	1.92	0.10	0.020	< 0.01
n_{cond}	mol	0.25	0.02	0.004	<< 0.01
T_{avg}	K	296.2	2	0.007	<< 0.01
m_{tot}	g	3.8	0.15	0.039	0.03
Q	m^3/s	3.0E-05	5.4E-07	0.018	< 0.01
t_{sample}	s	9.0	0.25	0.028	0.01
P_{avg}	Pa	205000	32000	0.156	0.44
$m_{stage,4}$	g	3.42E-06	1.0E-07	0.002	<< 0.01
$\eta_{stage,4}$	--	0.93	0.005	0.000	<< 0.01
$\eta_{loss,4}$	--	0.7	0.15	0.015	< 0.01
$m_{stage,5}$	g	3.84E-05	1.0E-07	0.002	<< 0.01
$\eta_{stage,5}$	--	0.95	0.005	0.004	<< 0.01
$\eta_{loss,5}$	--	0.7	0.15	0.163	0.48
$m_{stage,6}$	g	5.86E-06	1.0E-07	0.002	<< 0.01
$\eta_{stage,6}$	--	0.97	0.005	0.001	<< 0.01
$\eta_{loss,6}$	--	0.7	0.15	0.024	0.01
$m_{stage,7}$	g	1.22E-06	1.0E-07	0.002	<< 0.01
$\eta_{stage,7}$	--	0.98	0.005	0.000	<< 0.01
$\eta_{loss,7}$	--	0.7	0.15	0.005	<< 0.01
$m_{stage,8}$	g	1.36E-06	1.0E-07	0.002	<< 0.01
$\eta_{stage,8}$	--	0.99	0.005	0.000	<< 0.01
$\eta_{loss,8}$	--	0.7	0.15	0.006	<< 0.01
$m_{stage,9}$	g	4.71E-07	1.0E-07	0.002	<< 0.01
$\eta_{stage,9}$	--	1	0.005	0.000	<< 0.01
$\eta_{loss,9}$	--	0.7	0.15	0.002	<< 0.01
RF	--	0.0045	0.001	0.235	1.00

Table B.20 Error propagation analysis of zirconium in Marple 3 impactor for test 3-5B.

Measurement, x_i	Units	Value	Standard uncertainty, u_i	Influence coefficient ($u_i \cdot [(\partial RF/\partial x_i)/RF]$)	Contribution
n_1	mol	3.40	0.09	0.018	< 0.01
Δn	mol	1.92	0.10	0.020	< 0.01
n_{cond}	mol	0.25	0.02	0.004	<< 0.01
T_{avg}	K	296.2	2	0.007	<< 0.01
m_{tot}	g	3.8	0.15	0.039	0.03
Q	m^3/s	2.9E-05	9.5E-07	0.032	0.02
t_{sample}	s	9.0	0.25	0.028	0.01
P_{avg}	Pa	205000	32000	0.156	0.47
$m_{stage,4}$	g	3.36E-06	1.0E-07	0.002	<< 0.01
$\eta_{stage,4}$	--	0.93	0.005	0.000	<< 0.01
$\eta_{loss,4}$	--	0.7	0.15	0.013	< 0.01
$m_{stage,5}$	g	3.92E-05	1.0E-07	0.002	<< 0.01
$\eta_{stage,5}$	--	0.95	0.005	0.004	<< 0.01
$\eta_{loss,5}$	--	0.7	0.15	0.145	0.41
$m_{stage,6}$	g	1.09E-05	1.0E-07	0.002	<< 0.01
$\eta_{stage,6}$	--	0.97	0.005	0.001	<< 0.01
$\eta_{loss,6}$	--	0.7	0.15	0.039	0.03
$m_{stage,7}$	g	2.74E-06	1.0E-07	0.002	<< 0.01
$\eta_{stage,7}$	--	0.98	0.005	0.000	<< 0.01
$\eta_{loss,7}$	--	0.7	0.15	0.010	< 0.01
$m_{stage,8}$	g	1.66E-06	1.0E-07	0.002	<< 0.01
$\eta_{stage,8}$	--	0.99	0.005	0.000	<< 0.01
$\eta_{loss,8}$	--	0.7	0.15	0.006	<< 0.01
$m_{stage,9}$	g	4.57E-07	1.0E-07	0.002	<< 0.01
$\eta_{stage,9}$	--	1	0.005	0.000	<< 0.01
$\eta_{loss,9}$	--	0.7	0.15	0.002	<< 0.01
RF	--	0.0053	0.001	0.227	1.00

Table B.21 Error propagation analysis of zirconium in Marple 4 impactor for test 3-5B.

Measurement, x_i	Units	Value	Standard uncertainty, u_i	Influence coefficient ($u_i \cdot [(\partial RF/\partial x_i)/RF]$)	Contribution
n_1	mol	3.40	0.09	0.018	< 0.01
Δn	mol	1.92	0.10	0.020	< 0.01
n_{cond}	mol	0.25	0.02	0.004	<< 0.01
T_{avg}	K	296.2	2	0.007	<< 0.01
m_{tot}	g	3.8	0.15	0.039	0.03
Q	m^3/s	2.8E-05	1.4E-07	0.005	<< 0.01
t_{sample}	s	9.0	0.25	0.028	0.02
P_{avg}	Pa	205000	32000	0.156	0.52
$m_{stage,4}$	g	4.15E-06	1.0E-07	0.001	<< 0.01
$\eta_{stage,4}$	--	0.93	0.005	0.000	<< 0.01
$\eta_{loss,4}$	--	0.7	0.15	0.013	< 0.01
$m_{stage,5}$	g	4.34E-05	1.0E-07	0.001	<< 0.01
$\eta_{stage,5}$	--	0.95	0.005	0.003	<< 0.01
$\eta_{loss,5}$	--	0.7	0.15	0.129	0.36
$m_{stage,6}$	g	1.39E-05	1.0E-07	0.001	<< 0.01
$\eta_{stage,6}$	--	0.97	0.005	0.001	<< 0.01
$\eta_{loss,6}$	--	0.7	0.15	0.041	0.04
$m_{stage,7}$	g	4.63E-06	1.0E-07	0.001	<< 0.01
$\eta_{stage,7}$	--	0.98	0.005	0.000	<< 0.01
$\eta_{loss,7}$	--	0.7	0.15	0.013	< 0.01
$m_{stage,8}$	g	5.42E-06	1.0E-07	0.001	<< 0.01
$\eta_{stage,8}$	--	0.99	0.005	0.000	<< 0.01
$\eta_{loss,8}$	--	0.7	0.15	0.016	< 0.01
$m_{stage,9}$	g	9.41E-07	1.0E-07	0.001	<< 0.01
$\eta_{stage,9}$	--	1	0.005	0.000	<< 0.01
$\eta_{loss,9}$	--	0.7	0.15	0.003	<< 0.01
RF	--	0.0067	0.001	0.216	1.00

Table B.22 Error propagation analysis of zirconium in Marple 1 impactor for test 3-1C.

Measurement, x_i	Units	Value	Standard uncertainty, u_i	Influence coefficient ($u_i \cdot [(\partial RF/\partial x_i)/RF]$)	Contribution
n_1	mol	3.38	0.09	0.018	0.02
Δn	mol	1.92	0.10	0.020	0.02
n_{cond}	mol	0.25	0.02	0.004	<< 0.01
T_{avg}	K	296.2	2	0.007	< 0.01
m_{tot}	g	4.19	0.15	0.036	0.07
Q	m^3/s	3.6E-05	1.0E-06	0.028	0.04
t_{sample}	s	10.0	0.25	0.025	0.03
P_{avg}	Pa	182000	10000	0.053	0.16
$m_{stage,4}$	g	3.08E-06	1.0E-07	0.001	<< 0.01
$\eta_{stage,4}$	--	0.93	0.005	0.000	<< 0.01
$\eta_{loss,4}$	--	0.7	0.15	0.009	< 0.01
$m_{stage,5}$	g	4.91E-06	1.0E-07	0.001	<< 0.01
$\eta_{stage,5}$	--	0.95	0.005	0.000	<< 0.01
$\eta_{loss,5}$	--	0.7	0.15	0.013	< 0.01
$m_{stage,6}$	g	3.00E-05	1.0E-07	0.001	<< 0.01
$\eta_{stage,6}$	--	0.97	0.005	0.002	<< 0.01
$\eta_{loss,6}$	--	0.7	0.15	0.080	0.36
$m_{stage,7}$	g	1.67E-05	1.0E-07	0.001	<< 0.01
$\eta_{stage,7}$	--	0.98	0.005	0.001	<< 0.01
$\eta_{loss,7}$	--	0.7	0.15	0.044	0.11
$m_{stage,8}$	g	2.00E-05	1.0E-07	0.001	<< 0.01
$\eta_{stage,8}$	--	0.99	0.005	0.001	<< 0.01
$\eta_{loss,8}$	--	0.7	0.15	0.052	0.15
$m_{stage,9}$	g	6.44E-06	1.0E-07	0.001	<< 0.01
$\eta_{stage,9}$	--	1	0.005	0.000	<< 0.01
$\eta_{loss,9}$	--	0.7	0.15	0.017	0.02
RF	--	0.0054	0.001	0.134	1.00

Table B.23 Error propagation analysis of zirconium in Marple 3 impactor for test 3-1C.

Measurement, x_i	Units	Value	Standard uncertainty, u_i	Influence coefficient ($u_i \cdot [(\partial RF/\partial x_i)/RF]$)	Contribution
n_1	mol	3.38	0.09	0.018	0.01
Δn	mol	1.92	0.10	0.020	0.01
n_{cond}	mol	0.25	0.02	0.004	<< 0.01
T_{avg}	K	296.2	2	0.007	< 0.01
m_{tot}	g	4.19	0.15	0.036	0.04
Q	m^3/s	3.6E-05	9.3E-07	0.026	0.02
t_{sample}	s	10.0	0.25	0.025	0.02
P_{avg}	Pa	182000	10000	0.053	0.09
$m_{stage,4}$	g	1.00E-06	1.0E-07	0.002	<< 0.01
$\eta_{stage,4}$	--	0.93	0.005	0.000	<< 0.01
$\eta_{loss,4}$	--	0.7	0.15	0.005	<< 0.01
$m_{stage,5}$	g	3.05E-05	1.0E-07	0.002	<< 0.01
$\eta_{stage,5}$	--	0.95	0.005	0.004	<< 0.01
$\eta_{loss,5}$	--	0.7	0.15	0.153	0.74
$m_{stage,6}$	g	9.37E-06	1.0E-07	0.002	<< 0.01
$\eta_{stage,6}$	--	0.97	0.005	0.001	<< 0.01
$\eta_{loss,6}$	--	0.7	0.15	0.046	0.07
$m_{stage,7}$	g	7.93E-07	1.0E-07	0.002	<< 0.01
$\eta_{stage,7}$	--	0.98	0.005	0.000	<< 0.01
$\eta_{loss,7}$	--	0.7	0.15	0.004	<< 0.01
$m_{stage,8}$	g	9.60E-07	1.0E-07	0.002	<< 0.01
$\eta_{stage,8}$	--	0.99	0.005	0.000	<< 0.01
$\eta_{loss,8}$	--	0.7	0.15	0.005	<< 0.01
$m_{stage,9}$	g	2.31E-07	1.0E-07	0.002	<< 0.01
$\eta_{stage,9}$	--	1	0.005	0.000	<< 0.01
$\eta_{loss,9}$	--	0.7	0.15	0.001	<< 0.01
RF	--	0.0029	0.001	0.179	1.00

Table B.24 Error propagation analysis of zirconium in Marple 4 impactor for test 3-1C.

Measurement, x_i	Units	Value	Standard uncertainty, u_i	Influence coefficient ($u_i \cdot [(\partial RF/\partial x_i)/RF]$)	Contribution
n_1	mol	3.38	0.09	0.018	0.01
Δn	mol	1.92	0.10	0.020	0.02
n_{cond}	mol	0.25	0.02	0.004	<< 0.01
T_{avg}	K	296.2	2	0.007	< 0.01
m_{tot}	g	4.19	0.15	0.036	0.05
Q	m^3/s	3.6E-05	6.4E-07	0.018	0.01
t_{sample}	s	10.0	0.25	0.025	0.03
P_{avg}	Pa	182000	10000	0.053	0.11
$m_{stage,4}$	g	5.88E-06	1.0E-07	0.001	<< 0.01
$\eta_{stage,4}$	--	0.93	0.005	0.000	<< 0.01
$\eta_{loss,4}$	--	0.7	0.15	0.018	0.01
$m_{stage,5}$	g	4.29E-05	1.0E-07	0.001	<< 0.01
$\eta_{stage,5}$	--	0.95	0.005	0.003	<< 0.01
$\eta_{loss,5}$	--	0.7	0.15	0.129	0.67
$m_{stage,6}$	g	1.48E-05	1.0E-07	0.001	<< 0.01
$\eta_{stage,6}$	--	0.97	0.005	0.001	<< 0.01
$\eta_{loss,6}$	--	0.7	0.15	0.044	0.08
$m_{stage,7}$	g	3.43E-06	1.0E-07	0.001	<< 0.01
$\eta_{stage,7}$	--	0.98	0.005	0.000	<< 0.01
$\eta_{loss,7}$	--	0.7	0.15	0.010	< 0.01
$m_{stage,8}$	g	3.45E-06	1.0E-07	0.001	<< 0.01
$\eta_{stage,8}$	--	0.99	0.005	0.000	<< 0.01
$\eta_{loss,8}$	--	0.7	0.15	0.010	< 0.01
$m_{stage,9}$	g	1.19E-06	1.0E-07	0.001	<< 0.01
$\eta_{stage,9}$	--	1	0.005	0.000	<< 0.01
$\eta_{loss,9}$	--	0.7	0.15	0.003	<< 0.01
RF	--	0.0049	0.001	0.158	1.00

B.2.1 Cesium

Table B.25 Error propagation analysis of cesium in Marple 1 impactor for test 3-1C.

Measurement, x_i	Units	Value	Standard uncertainty, u_i	Influence coefficient ($u_i \cdot [(\partial RF/\partial x_i)/RF]$)	Contribution
n_1	mol	3.38	0.09	0.018	0.02
Δn	mol	1.92	0.10	0.020	0.02
n_{cond}	mol	0.25	0.02	0.004	<< 0.01
T_{avg}	K	296.2	2	0.007	< 0.01
m_{tot}	g	0.0173	0.00005	0.003	<< 0.01
Q	m^3/s	3.6E-05	1.0E-06	0.028	0.04
t_{sample}	s	10.0	0.25	0.025	0.04
P_{avg}	Pa	182000	10000	0.053	0.16
$m_{stage,4}$	g	4.65E-07	1.3E-08	0.001	<< 0.01
$\eta_{stage,4}$	--	0.93	0.005	0.000	<< 0.01
$\eta_{loss,4}$	--	0.7	0.15	0.004	< 0.01
$m_{stage,5}$	g	8.96E-07	1.3E-08	0.001	<< 0.01
$\eta_{stage,5}$	--	0.95	0.005	0.000	<< 0.01
$\eta_{loss,5}$	--	0.7	0.15	0.008	< 0.01
$m_{stage,6}$	g	9.62E-06	1.3E-08	0.001	<< 0.01
$\eta_{stage,6}$	--	0.97	0.005	0.002	<< 0.01
$\eta_{loss,6}$	--	0.7	0.15	0.088	0.43
$m_{stage,7}$	g	4.95E-06	1.3E-08	0.001	<< 0.01
$\eta_{stage,7}$	--	0.98	0.005	0.001	<< 0.01
$\eta_{loss,7}$	--	0.7	0.15	0.045	0.11
$m_{stage,8}$	g	5.87E-06	1.3E-08	0.001	<< 0.01
$\eta_{stage,8}$	--	0.99	0.005	0.001	<< 0.01
$\eta_{loss,8}$	--	0.7	0.15	0.052	0.15
$m_{stage,9}$	g	1.93E-06	1.3E-08	0.001	<< 0.01
$\eta_{stage,9}$	--	1	0.005	0.000	<< 0.01
$\eta_{loss,9}$	--	0.7	0.15	0.017	0.02
RF	--	0.3809	0.051	0.133	1.00

Table B.26 Error propagation analysis of cesium in Marple 3 impactor for test 3-1C.

Measurement, x_i	Units	Value	Standard uncertainty, u_i	Influence coefficient ($u_i \cdot [(\partial RF/\partial x_i)/RF]$)	Contribution
n_1	mol	3.38	0.09	0.018	0.01
Δn	mol	1.92	0.10	0.020	0.01
n_{cond}	mol	0.25	0.02	0.004	<< 0.01
T_{avg}	K	296.2	2	0.007	< 0.01
m_{tot}	g	0.0173	0.00005	0.003	<< 0.01
Q	m^3/s	3.6E-05	9.3E-07	0.026	0.02
t_{sample}	s	10.0	0.25	0.025	0.02
P_{avg}	Pa	182000	10000	0.053	0.09
$m_{stage,4}$	g	2.97E-07	1.3E-08	0.001	<< 0.01
$\eta_{stage,4}$	--	0.93	0.005	0.000	<< 0.01
$\eta_{loss,4}$	--	0.7	0.15	0.004	<< 0.01
$m_{stage,5}$	g	1.06E-05	1.3E-08	0.001	<< 0.01
$\eta_{stage,5}$	--	0.95	0.005	0.004	<< 0.01
$\eta_{loss,5}$	--	0.7	0.15	0.155	0.77
$m_{stage,6}$	g	3.10E-06	1.3E-08	0.001	<< 0.01
$\eta_{stage,6}$	--	0.97	0.005	0.001	<< 0.01
$\eta_{loss,6}$	--	0.7	0.15	0.045	0.06
$m_{stage,7}$	g	2.78E-07	1.3E-08	0.001	<< 0.01
$\eta_{stage,7}$	--	0.98	0.005	0.000	<< 0.01
$\eta_{loss,7}$	--	0.7	0.15	0.004	<< 0.01
$m_{stage,8}$	g	3.60E-07	1.3E-08	0.001	<< 0.01
$\eta_{stage,8}$	--	0.99	0.005	0.000	<< 0.01
$\eta_{loss,8}$	--	0.7	0.15	0.005	<< 0.01
$m_{stage,9}$	g	8.70E-08	1.3E-08	0.001	<< 0.01
$\eta_{stage,9}$	--	1	0.005	0.000	<< 0.01
$\eta_{loss,9}$	--	0.7	0.15	0.001	<< 0.01
RF	--	0.2402	0.042	0.176	1.00

Table B.27 Error propagation analysis of cesium in Marple 4 impactor for test 3-1C.

Measurement, x_i	Units	Value	Standard uncertainty, u_i	Influence coefficient ($u_i \cdot [(\partial RF/\partial x_i)/RF]$)	Contribution
n_1	mol	3.38	0.09	0.018	0.01
Δn	mol	1.92	0.10	0.020	0.02
n_{cond}	mol	0.25	0.02	0.004	<< 0.01
T_{avg}	K	296.2	2	0.007	< 0.01
m_{tot}	g	0.0173	0.00005	0.003	<< 0.01
Q	m^3/s	3.6E-05	6.4E-07	0.018	0.01
t_{sample}	s	10.0	0.25	0.025	0.03
P_{avg}	Pa	182000	10000	0.053	0.12
$m_{stage,4}$	g	1.20E-06	1.3E-08	0.001	<< 0.01
$\eta_{stage,4}$	--	0.93	0.005	0.000	<< 0.01
$\eta_{loss,4}$	--	0.7	0.15	0.012	< 0.01
$m_{stage,5}$	g	1.30E-05	1.3E-08	0.001	<< 0.01
$\eta_{stage,5}$	--	0.95	0.005	0.003	<< 0.01
$\eta_{loss,5}$	--	0.7	0.15	0.128	0.69
$m_{stage,6}$	g	4.91E-06	1.3E-08	0.001	<< 0.01
$\eta_{stage,6}$	--	0.97	0.005	0.001	<< 0.01
$\eta_{loss,6}$	--	0.7	0.15	0.048	0.10
$m_{stage,7}$	g	1.18E-06	1.3E-08	0.001	<< 0.01
$\eta_{stage,7}$	--	0.98	0.005	0.000	<< 0.01
$\eta_{loss,7}$	--	0.7	0.15	0.011	< 0.01
$m_{stage,8}$	g	1.18E-06	1.3E-08	0.001	<< 0.01
$\eta_{stage,8}$	--	0.99	0.005	0.000	<< 0.01
$\eta_{loss,8}$	--	0.7	0.15	0.011	< 0.01
$m_{stage,9}$	g	4.56E-07	1.3E-08	0.001	<< 0.01
$\eta_{stage,9}$	--	1	0.005	0.000	<< 0.01
$\eta_{loss,9}$	--	0.7	0.15	0.004	<< 0.01
RF	--	0.3611	0.056	0.154	1.00

B.2.1 Ruthenium

Table B.28 Error propagation analysis of ruthenium in Marple 1 impactor for test 3-1C.

Measurement, x_i	Units	Value	Standard uncertainty, u_i	Influence coefficient ($u_i \cdot [(\partial RF/\partial x_i)/RF]$)	Contribution
n_1	mol	3.38	0.09	0.018	0.01
Δn	mol	1.92	0.10	0.020	0.02
n_{cond}	mol	0.25	0.02	0.004	<< 0.01
T_{avg}	K	296.2	2	0.007	< 0.01
m_{tot}	g	0.0049	0.00005	0.010	< 0.01
Q	m^3/s	3.6E-05	1.0E-06	0.028	0.03
t_{sample}	s	10.0	0.25	0.025	0.03
P_{avg}	Pa	182000	10000	0.053	0.13
$m_{stage,4}$	g	4.80E-08	5.0E-08	0.027	0.03
$\eta_{stage,4}$	--	0.93	0.005	0.000	<< 0.01
$\eta_{loss,4}$	--	0.7	0.15	0.006	< 0.01
$m_{stage,5}$	g	8.80E-08	5.0E-08	0.027	0.03
$\eta_{stage,5}$	--	0.95	0.005	0.000	<< 0.01
$\eta_{loss,5}$	--	0.7	0.15	0.010	< 0.01
$m_{stage,6}$	g	8.27E-07	5.0E-08	0.026	0.03
$\eta_{stage,6}$	--	0.97	0.005	0.002	<< 0.01
$\eta_{loss,6}$	--	0.7	0.15	0.092	0.38
$m_{stage,7}$	g	4.00E-07	5.0E-08	0.026	0.03
$\eta_{stage,7}$	--	0.98	0.005	0.001	<< 0.01
$\eta_{loss,7}$	--	0.7	0.15	0.044	0.09
$m_{stage,8}$	g	4.49E-07	5.0E-08	0.026	0.03
$\eta_{stage,8}$	--	0.99	0.005	0.001	<< 0.01
$\eta_{loss,8}$	--	0.7	0.15	0.049	0.11
$m_{stage,9}$	g	1.22E-07	5.0E-08	0.025	0.03
$\eta_{stage,9}$	--	1	0.005	0.000	<< 0.01
$\eta_{loss,9}$	--	0.7	0.15	0.013	< 0.01
RF	--	0.1097	0.016	0.150	1.00

Table B.29 Error propagation analysis of ruthenium in Marple 3 impactor for test 3-1C.

Measurement, x_i	Units	Value	Standard uncertainty, u_i	Influence coefficient ($u_i \cdot [(\partial RF/\partial x_i)/RF]$)	Contribution
n_1	mol	3.38	0.09	0.018	< 0.01
Δn	mol	1.92	0.10	0.020	< 0.01
n_{cond}	mol	0.25	0.02	0.004	<< 0.01
T_{avg}	K	296.2	2	0.007	< 0.01
m_{tot}	g	0.0049	0.00005	0.010	< 0.01
Q	m^3/s	3.6E-05	9.3E-07	0.026	0.01
t_{sample}	s	10.0	0.25	0.025	0.01
P_{avg}	Pa	182000	10000	0.053	0.06
$m_{stage,4}$	g	5.00E-09	5.0E-08	0.044	0.04
$\eta_{stage,4}$	--	0.93	0.005	0.000	<< 0.01
$\eta_{loss,4}$	--	0.7	0.15	0.001	<< 0.01
$m_{stage,5}$	g	8.91E-07	5.0E-08	0.044	0.04
$\eta_{stage,5}$	--	0.95	0.005	0.004	<< 0.01
$\eta_{loss,5}$	--	0.7	0.15	0.166	0.61
$m_{stage,6}$	g	2.45E-07	5.0E-08	0.043	0.04
$\eta_{stage,6}$	--	0.97	0.005	0.001	<< 0.01
$\eta_{loss,6}$	--	0.7	0.15	0.045	0.04
$m_{stage,7}$	g	4.00E-09	5.0E-08	0.042	0.04
$\eta_{stage,7}$	--	0.98	0.005	0.000	<< 0.01
$\eta_{loss,7}$	--	0.7	0.15	0.001	<< 0.01
$m_{stage,8}$	g	9.00E-09	5.0E-08	0.042	0.04
$\eta_{stage,8}$	--	0.99	0.005	0.000	<< 0.01
$\eta_{loss,8}$	--	0.7	0.15	0.002	<< 0.01
$m_{stage,9}$	g	0.00E+00	5.0E-08	0.041	0.04
$\eta_{stage,9}$	--	1	0.005	0.000	<< 0.01
$\eta_{loss,9}$	--	0.7	0.15	0.000	<< 0.01
RF	--	0.0666	0.014	0.214	1.00

Table B.30 Error propagation analysis of ruthenium in Marple 4 impactor for test 3-1C.

Measurement, x_i	Units	Value	Standard uncertainty, u_i	Influence coefficient ($u_i \cdot [(\partial RF/\partial x_i)/RF]$)	Contribution
n_1	mol	3.38	0.09	0.018	0.01
Δn	mol	1.92	0.10	0.020	0.01
n_{cond}	mol	0.25	0.02	0.004	<< 0.01
T_{avg}	K	296.2	2	0.007	< 0.01
m_{tot}	g	0.0049	0.00005	0.010	< 0.01
Q	m^3/s	3.6E-05	6.4E-07	0.018	0.01
t_{sample}	s	10.0	0.25	0.025	0.02
P_{avg}	Pa	182000	10000	0.053	0.10
$m_{stage,4}$	g	1.26E-07	5.0E-08	0.028	0.03
$\eta_{stage,4}$	--	0.93	0.005	0.000	<< 0.01
$\eta_{loss,4}$	--	0.7	0.15	0.015	< 0.01
$m_{stage,5}$	g	1.16E-06	5.0E-08	0.027	0.02
$\eta_{stage,5}$	--	0.95	0.005	0.003	<< 0.01
$\eta_{loss,5}$	--	0.7	0.15	0.135	0.61
$m_{stage,6}$	g	4.05E-07	5.0E-08	0.027	0.02
$\eta_{stage,6}$	--	0.97	0.005	0.001	<< 0.01
$\eta_{loss,6}$	--	0.7	0.15	0.046	0.07
$m_{stage,7}$	g	7.60E-08	5.0E-08	0.026	0.02
$\eta_{stage,7}$	--	0.98	0.005	0.000	<< 0.01
$\eta_{loss,7}$	--	0.7	0.15	0.009	< 0.01
$m_{stage,8}$	g	7.10E-08	5.0E-08	0.026	0.02
$\eta_{stage,8}$	--	0.99	0.005	0.000	<< 0.01
$\eta_{loss,8}$	--	0.7	0.15	0.008	< 0.01
$m_{stage,9}$	g	1.20E-08	5.0E-08	0.026	0.02
$\eta_{stage,9}$	--	1	0.005	0.000	<< 0.01
$\eta_{loss,9}$	--	0.7	0.15	0.001	<< 0.01
RF	--	0.1079	0.019	0.172	1.00

DISTRIBUTION

U.S. Dept. of Energy, NNSA (4)
Sandia Site Office
MS-0184 P.O. Box 5400
Albuquerque, NM 87185-5400
Patty Wagner
Kevin T. Gray
John Cormier
Michael J. Brown

U.S. Dept. of Energy, NNSA (2)
Office of International Safeguards
1000 Independence Ave., SW
Washington, DC 20585
Ronald C. Cherry, NA-243
Russell S. Hibbs, NA-243

U.S. Department of Energy, OCRWM (5)
1000 Independence Ave., SW
Washington, DC 20585
Gary Lanthrum, RW-10
Alex Thrower, RW-10
Lee Finewood, RW-10
David W. Crawford, RW-15
Jay M. Thompson, RW-15

U.S. Department of Energy (1)
1000 Independence Ave., SW
Washington, DC 20585
Diana D. Clark, GC-53

U.S. Nuclear Regulatory Commission (6)
Washington, DC 20555-0001
D. Helton, RES, MS C4A07M
F.I. Young, OIP, MS O4-E21
G. Bjorkman, NMSS, MS E3-D2M
R.E. Einziger, NMSS, MS E3-D2M
S. Bush-Goddard, RES, MS C3A07M
L. Thompson, NMSS, MS E3-D2M

Robert E. Luna, Consultant (1)
10025 Barrinson NE
Albuquerque, NM 87111

Institut de Radioprotection et de Surete (4)
Nucleaire, IRSN/DEND/SATE, BP17
92262 Fontenay-aux-Roses Cedex, France
Bruno Autrusson
Pierre Funk
Jerome Joly
Olivier Loiseau

Gesellschaft für Anlagen- und (1)
Reaktorsicherheit (GRS) mbH
Kurfuerstendamm 200
10719 Berlin, Germany
Gunter Pretzsch

Gesellschaft für Anlagen- und (1)
Reaktorsicherheit (GRS) mbH
Schwertnergasse 1
50667 Köln, Germany
Wenzel Brücher

Fraunhofer-Institut für Toxikologie und (2)
Experimentelle Medizin, ITEM
Nikolai-Fuchs-Str. 1
D-30625 Hannover, Germany
Wolfgang Koch
Oliver Nolte

Japan Nuclear Energy Safety Org. (1)
Fujita Kanko Toranomon Bldg 3-17-1
Toranomon, Minato-ku
Tokyo 105-0001, Japan
Nagao Ogawa

Argonne National Laboratory (2)
Energy Technology Div., Bldg 212
9700 S. Cass Ave
Argonne, IL 60439-3838
Mike C. Billone
Tatiana Burtseva

Sandia Internal:

6774, MS 0747 E.R. Lindgren (4)
6774, MS 0747 S.G. Durbin (4)
1380, MS 1145 P.S. Raglin
1382, MS 1146 D. Wheeler
1386, MS 1143 W.R. Strong
1384, MS 1146 D.W. Vehar
1383, MS 1141 J. Dahl
1383, MS 1141 R.L. Coats
1383, MS 1141 M.W. Gregson
1384, MS 1146 K.O. Reil
1532, MS 0825 J.E. Brockmann
2554, MS 1455 L.M.G. Minier
2554, MS 1454 W. Wente
6417, MS 0791 L.A. Klennert
6760, MS 0736 M.C. Walck
6771, MS 1136 G.E. Rochau
6765, MS 0718 D.R. Miller
6765, MS 0718 R.H. Yoshimura
6774, MS 0747 K.B. Sorenson
9536, MS 0899 Technical Library (-)
(electronic copy)


Sandia National Laboratories